

Parametric Design and Optimization of an Upright of a Formula SAE car

Shubhankar Sudesh Kaisare

Thesis submitted to the faculty of the Virginia Polytechnic Institute and State University in
partial fulfillment of the requirements for the degree of

Master of Science
In
Mechanical Engineering

Robert L. West, Chair
Robert. A. Canfield
Pinar Acar

April 24th, 2024
Blacksburg, Virginia

Keywords: Parametric Design Optimization, Finite Element Analysis(FEA), Response Surface
Methodology.

Parametric Design and Optimization of an Upright of a Formula SAE car

Shubhankar Sudesh Kaisare

Abstract

The success of any racing car hinges on three key factors: its speed, handling, and reliability. In a highly competitive environment where lap times are extremely tight, even slight variations in components can significantly affect performance and, consequently, lap times. At the heart of a race car's performance lies the upright—a critical component of its suspension system. The upright serves to link the suspension arms to the wheels, effectively transmitting steering and braking forces to the suspension setup. Achieving optimal performance requires finding the right balance between lightweight design and ample stiffness, crucial for maintaining precise steering geometry and overall vehicle dynamics, especially under intense loads.

Furthermore, there is a need to explore the system of structural optimization and seamlessly integrate Finite Element (FE) Models into the mathematical optimization process. This thesis explores a technique for parametric structural optimization utilizing finite element analysis and response surfaces to minimize the weight of the upright. Various constraints such as frequency, stress, displacement, and fatigue are taken into consideration during this optimization process.

A parametric finite element model of the upright was designed, along with the mathematical formulation of the optimization problem as a nonlinear programming problem, based on the design objectives and suspension geometry. By conducting parameter sensitivity analysis, three design variables were chosen from a pool of five, and response surfaces were constructed to represent the constraints and objective function to be used to solve the optimization problem using Sequential Quadratic Programming (SQP).

To streamline the process of parameter sensitivity analysis and response surface development, a Python scripting procedure was employed to automate the finite element job analysis and results extraction. The optimized upright design resulted in overall weight reduction of 25.3% from the maximum weight design of the parameterized upright.

Parametric Design and Optimization of an Upright of a Formula SAE car

Shubhankar Sudesh Kaisare

General Audience Abstract

The success of any racing car depends on three key factors: its speed, handling and reliability. In a highly competitive environment where lap times are extremely tight, even slight variations in components can significantly affect performance and consequently, lap times. At the heart of a race car's performance lies the upright—a critical component of its suspension system. The upright serves to link the suspension arms to the wheels, effectively transmitting steering and braking forces to the suspension setup. To achieve the best performance, upright must be as light as possible but it needs to be strong enough to ensure that the car is predictable when turning in a corner or while braking.

Additionally, there is a need to explore methods of structural optimization and integrate finite element analysis seamlessly into the optimization process. Finite element analysis (FEA) is the use of part models, simulations, and calculations to predict and understand how an object might behave under certain physical conditions. This thesis examines a technique for optimizing the upright by designing it with numerous adjustable features for testing and then utilizing response surfaces to minimize its weight. Throughout this process, factors such as vibration, stress, deformation, and fatigue are carefully considered.

A detailed parametric finite element model of the upright was developed, alongside the formulation of the optimization problem as a nonlinear programming problem, based on the objectives of the design and the geometry of the suspension. Through rigorous testing of parameters for optimization potential, design variables are selected for optimization. Response surfaces were then constructed to represent the constraints and objective function necessary to solve the optimization problem using Sequential Quadratic Programming (SQP).

To enhance the efficiency of this process, a Python script was created to handle specific tasks within the finite element solver. This automation streamlined the analysis of the finite element model and the extraction of results. Ultimately, the optimized design of the upright yielded a 25.3% reduction in weight compared to its maximum weight configuration.

Acknowledgement

I extend my heartfelt thanks to Dr. Robert West, my academic advisor and committee chair, for his priceless mentorship during my pursuit of a master's degree. His expertise in the fields of finite element analysis and structural optimization, along with the courses he instructed, were of immense benefit to my research work. I am also thankful to Dr. Robert A. Canfield and Dr. Pinar Acar for their contributions as committee members. The courses taught by them provided the fundamental knowledge for my research work. Additionally, I thank Ram Suraj for his assistance in learning Abaqus software and python scripting, which were invaluable resources during my research.

I express my deep gratitude to my parents for their constant love and support during my master's journey and beyond. Their encouragement was pivotal in my accomplishments. Lastly, I extend my appreciation to all my friends, especially those at University Terrace, for supporting me during challenging times and helping me navigate through my master's program.

Table of Contents

List of Tables	viii
List of Figures.....	x
Chapter 1 Introduction.....	1
1.1 Overview and Statement of Need	1
1.2 Hypothesis Statement	2
1.3 Research Goals	2
1.4 Scope	3
1.5 Thesis Outline.....	4
Chapter 2 Literature Review	5
2.1 Double Wishbone Suspension System	5
2.2 Upright and some of the examples.	7
2.3 Structural Optimization Methods.....	9
2.4 Sequential Quadratic Programming (SQP) process.....	11
Chapter 3 Design Inputs.....	13
3.1 Suspension Linkage Points.....	13
3.2 Design Objectives.....	14
Chapter 4 Upright Finite Element (FE) Model	16
4.1 Upright FE Model Data Flow.....	16
4.2 Upright Model Part and Assembly Description.....	16
4.2.1 Dominant Mechanics Identification of Upright.....	16
4.2.2 Initial Assembly Model of Upright	18
4.2.3 Final Upright Parametric Model.....	21
4.3 Upright Material and Section Properties.....	24

4.4	<i>Step Manager</i>	26
4.5	<i>Upright Assembly Joint Interactions</i>	27
4.5.1	General Surface to Surface Interaction.....	27
4.5.2	TIE constraints.....	29
4.6	<i>Loads and Boundary Conditions</i>	30
4.6.1	Defining Loads	30
4.6.2	Defining Boundary Conditions.....	32
4.7	<i>Meshing and Element Selection</i>	34
4.7.1	Mesh and Element Types for Upright Part.....	34
4.7.2	Mesh and Element Type for Bearings	36
4.8	<i>Job Creation</i>	37
Chapter 5 Mathematical formulation of the Optimization Problem		38
Chapter 6 Parameter selection for optimization		42
6.1	<i>Upright Baseline Model Chosen for Parameter Sensitivity Analysis</i>	42
6.2	<i>Design Parameters Chosen for the Analysis</i>	43
6.3	<i>Script for creating job files and extracting output.</i>	45
6.3.1	Job file Creation for Parameter Sensitivity Analysis.....	45
6.3.2	Results Extraction for Parameter Sensitivity Analysis.....	47
6.4	<i>Parameter Sensitivity Analysis Results</i>	48
6.4.1	Vertical Ribs Thickness Sensitivity Results.....	50
6.4.2	Primary Angular Ribs Thickness Sensitivity Results.....	52
6.4.3	Secondary Angular Ribs Thickness Sensitivity Results.....	54
6.4.4	Secondary Angular Ribs Angle Sensitivity Results	57
6.4.5	Primary Angular Ribs Angle Changer Sensitivity Results.....	59
6.5	<i>Final Design Parameters Chosen</i>	62
Chapter 7 Response Surface Development.....		64
7.1	<i>Overall Procedure of Response Surface Development</i>	64

7.1.1	Three-Level Factorial Design	65
7.1.2	Output extraction for all combinations of the design variables	66
7.1.3	Response Surface Development	67
7.1.4	R ² value determination of the response surfaces	68
7.2	<i>Response Surfaces for Stress, Displacement, Natural Frequency and Weight</i>	69
7.3	<i>Fatigue Life Constraint Deletion</i>	74
Chapter 8	Results after Optimization	77
8.1	<i>Final Optimization Problem</i>	77
8.2	<i>Optimization Results</i>	78
Chapter 9	Summary, Conclusions, and Recommendations	83
9.1	<i>Summary</i>	83
9.2	<i>Conclusions</i>	84
9.3	<i>Recommendations</i>	86
9.3.1	Considering the joints characteristics	86
9.3.2	Improving the script used for conducting parameter sensitivity analysis and response surface development	86
9.3.3	Testing more design variables in the upright.....	87
9.3.4	Response Surface Development	87
References		89
Appendix		91
A)	Mesh convergence study	91

List of Tables

Table 3-1. Suspension Linkages Outboard Points [6]	13
Table 4-1. Coordinate system change description.	20
Table 4-2. Final upright assembly parts description.	24
Table 4-3. Comparison of results between <i>Initial upright model</i> and <i>Final upright model</i>	24
Table 4-4. Materials tested for upright.	25
Table 4-5. Static General Step Parameters.	26
Table 4-6. Surface to surface interaction contact properties.	28
Table 4-7. Interaction and constraints summary.	29
Table 4-8. Load case for a quasi-static single load.	31
Table 4-9. Summary of boundary conditions on upright.	33
Table 4-10. Quantitative mesh convergence study for fundamental natural frequency.	35
Table 4-11. Number of nodes and elements in parts of upright.	37
Table 5-1. Optimization problem variable description.	40
Table 5-2. Stress and displacement points in the upright.	41
Table 6-1. Comparison of interactions results.	43
Table 6-2. Design parameters to be tested.	43
Table 6-3. Outputs and percentage change in outputs for varying vertical rib thickness.	50
Table 6-4. Sensitivity of outputs for varying vertical rib thickness.	50
Table 6-5. Curve fit coefficients of outputs for varying vertical rib thickness.	51
Table 6-6. Outputs and percentage change in outputs for varying primary angular rib thickness.	52
Table 6-7. Sensitivity of outputs for varying primary angular rib thickness.	53
Table 6-8. Curve fit coefficients of outputs for varying primary angular rib thickness.	54
Table 6-9. Outputs and percentage change in outputs for varying secondary angular rib thickness.	55
Table 6-10. Sensitivity of outputs for varying secondary angular rib thickness.	55
Table 6-11. Curve fit coefficients of outputs for varying secondary angular rib thickness.	56
Table 6-12. Outputs and percentage change in outputs for varying secondary angular rib angles.	57
Table 6-13. Sensitivity of outputs for varying secondary angular rib angles.	58

Table 6-14. Curve fit coefficients of outputs for varying secondary angular rib angles.	59
Table 6-15. Outputs and percentage change in outputs for varying primary angular ribs angle changer values.....	60
Table 6-16. Sensitivity of outputs for varying primary angular ribs angle changer values.....	60
Table 6-17. Curve fit coefficients of outputs for varying primary angular rib angle changer values.	61
Table 7-1. Three level factorial design for final design variables.	66
Table 7-2. Response surface coefficients for different stress points equations.	70
Table 7-3. Adjusted Coefficient of determination values of different stress points equations.....	70
Table 7-4. Corner Scenario Loads Value.....	74
Table 7-5. Brown Miller fatigue life evaluation for Corner Maneuver cycle.....	76
Table 8-1. Description of variables of the final optimization problem.....	78
Table 8-2. Final Optimization Results	79
Table 8-3. Comparison of outputs for the final optimized design variables.....	81

List of Figures

Figure 2-1. Camber description.	6
Figure 2-2. Double wishbone suspension system setup[2].	6
Figure 2-3. SLA suspension system setup [6].	7
Figure 3-1. Front right suspension system view[6].	13
Figure 3-2. SAE car coordinate system[6].	14
Figure 3-3. Corner Maneuver Loading Scenario.	15
Figure 4-1. DFD of Upright FE model creation.	16
Figure 4-2. Upright for a double wishbone suspension setup[2].	17
Figure 4-3. 1D beam approximation of upright.	18
Figure 4-4. Assembly model of initial upright.	19
Figure 4-5. Extrude Sketch of First Upright Design.	20
Figure 4-6. Assembly Model of Final Upright.	21
Figure 4-7. Asymmetric tapers in <i>Final upright model</i>	22
Figure 4-8. New features in <i>Final upright model</i>	23
Figure 4-9. Material and section properties given to upright.	25
Figure 4-10. Tie constraint and General Surface to Surface interaction distinction.	28
Figure 4-11. Interactions and constraints summary in <i>Final upright model</i>	30
Figure 4-12. Sequence of loading for a corner.	31
Figure 4-13. Forces at wheel center vs time.	32
Figure 4-14. Moments at wheel center vs time.	32
Figure 4-15. Loads and boundary conditions on <i>Final upright model</i>	33
Figure 4-16. Qualitative mesh convergence study for fundamental natural frequency.	35
Figure 4-17. Meshed upright part with partitioning.	36
Figure 4-18. Bearing part meshed model.	37
Figure 5-1. DFD of the optimization process.	39
Figure 5-2. Stress and displacement points in the upright.	41
Figure 6-1. Sizing design variables.	44
Figure 6-2. Shape design variables.	44
Figure 6-3. DFD for <i>input_file_creator</i> module.	46
Figure 6-4. DFD for <i>odbextractor</i> module.	47

Figure 6-5. Flowchart for ' <i>PSanalysis</i> ' script.....	48
Figure 6-6. Qualitative analysis plot of varying vertical rib thicknesses.....	51
Figure 6-7. Qualitative analysis plot of varying primary angular rib thicknesses.....	53
Figure 6-8. Qualitative analysis plot of varying secondary angular rib thicknesses.	56
Figure 6-9. Qualitative analysis plot of varying secondary angular ribs angles.....	58
Figure 6-10. Qualitative analysis plot of varying primary angular ribs angle changer values.	61
Figure 6-11. Final parameters selected for optimization.	63
Figure 7-1. DFD of process of response surface development.	64
Figure 7-2. Three-level factorial design graphical representation.	65
Figure 7-3. Contour Plots for varying x_1 and x_2	71
Figure 7-4. Contour plots for varying x_1 and x_3	72
Figure 7-5. Contour plots for varying x_2 and x_3	72
Figure 8-1. Objective function history.....	79
Figure 8-2. Constraint value history.	81

Chapter 1 Introduction

1.1 Overview and Statement of Need

The success of any racing vehicle hinges on achieving the fastest lap times and ensuring it remains predictable and reliable for the driver. Given the tight competition where lap times are incredibly close, even minor variations in the components can significantly impact performance and, consequently, lap times.

Central to the performance of the race car is the upright, a pivotal component in the vehicle's suspension setup. The upright connects the suspension arms to the chassis, effectively transmitting steering and braking loads from the suspension system to the chassis. To optimize performance, the upright must strike a balance between being lightweight and sufficiently stiff, crucial for maintaining steering geometry and overall vehicle dynamics, particularly under extreme loads[3].

The rigidity of the upright is instrumental in isolating changes in suspension springs and dampers, simplifying suspension setup and tuning. However, achieving low weight without compromising stiffness is challenging. Additionally, with the brake caliper mounted on the upright, it becomes a structure for transferring braking forces and moments to the suspension system. Ensuring the car's predictability and reliability necessitates designing the upright to withstand varying loads over the course of a race, guarding against fatigue failure.

Given these complex design challenges, optimizing the upright design becomes imperative to meet constraints while minimizing weight. In the context of a Formula SAE car, reducing weight by even small percentages can shave off fractions of a second that could be the decisive factor in overall performance. While previous research has explored upright optimization, existing approaches often lack the use of a nonlinear mathematical formulation of the problem to tackle optimization directly.

Also, there is a need to continuously work into the development of the structural optimization system framework and there needs to be an understanding of how parametric models should be created and how variables could be selected to have the most impact for the optimization problem.

This thesis aims to address these shortcomings by providing tools to develop a parametric finite element model of the upright, incorporating several adjustable features. Through non-linear programming formulation for optimization and response surfaces to visualize the impact of these

features on stress, displacement, natural frequency, and fatigue, this research endeavors to optimize the upright design effectively by selecting the three best design variables for optimization from a pool of five.

1.2 Hypothesis Statement

In this thesis a parametric finite element model of the upright is created with numerous adjustable features. Further mathematical formulation of the optimization problem is created for an upright for three design variables. To select the three most sensitive and acceptable parameters for optimization, parameter sensitivity analysis is conducted. A python script named *PSanalysis* is used which extracts the stress, displacement, and first natural frequency for different samples of a parameter to perform the sensitivity analysis. Further a curve fit analytical function is evaluated which is used to evaluate the sensitivities to determine whether the parameter is relevant as a design variable for optimization or not.

After the parameter selection the response surfaces for stress, displacement, first natural frequency and number of cycles to fatigue failure are evaluated using a second order two factor interaction model and three level factorial design. A python script named *RSanalysis* uses similar functions to the *PSanalysis* script but instead of extraction for single parameter change, *RSanalysis* results extraction for three parameter change is included.

The optimization problem is solved using Sequential Quadratic Programming (SQP), using the response surfaces for the objective function and constraints. The results from the optimal solution produced by the response surfaces for the objective function and constraints are compared with the results produced by the finite element model.

1.3 Research Goals

The thesis aims to achieve the following research objectives:

- 1) Develop a parametric design for the upright assembly based on the loads and boundary conditions and the suspension design of the Virginia Tech 2009 Formula SAE car.
- 2) Formulate a nonlinear optimization problem to enhance the upright, focusing on reducing weight while satisfying constraints related to natural frequency, stress, displacement, and fatigue.

- 3) Develop a python script to automate parameter adjustments, remeshing, input file creation, and extraction of analysis results for further examination.
- 4) Identify three design variables from the upright parametric design model based on their sensitivity, impact on the overall objective function and constraints, and qualitative assessment.
- 5) Generate response surfaces, sometimes referred to as surrogate models, for the objective function and constraints to facilitate solving the optimization problem.
- 6) Compare the outputs of the optimized design variables derived from the response surfaces with those from the finite element model.

1.4 Scope

The thesis scope includes the following aspects:

- 1) The finite element (FE) model of the upright focuses on quasi-static loads only, thereby neglecting the inertial effects on the upright assembly.
- 2) The developed python model script can modify parameters specific to a designated Abaqus constrained sketch outlining the FE model's features.
- 3) The developed output extraction script is confined to von Mises stress, deformation, and natural frequency, while strain extraction for fatigue life evaluation is performed manually. Auto-referencing of parameter names based on input from the user is also not used in this thesis.
- 4) The development of response surfaces is demonstrated to showcase their use in the final upright design, aiming to achieve an optimized set of design variables. In this thesis, a single second-order response surface model is presented, with only R^2 analysis employed to assess the model's suitability for solving the optimization problem. However, to obtain more representative response surfaces across the entire design space, extensive statistical analysis and continuous updating of these surfaces are necessary which is beyond the scope of this thesis.
- 5) The FE model consists solely of the upright and bearings as deformable components, while the joints are treated as rigid parts. This assumption is based on the general rigidity of bolts and joints compared to the parts they connect, reducing the overall run time of the FE model. For simplicity,

a constant converged mesh size is adopted for the FE model in this thesis, though future studies may explore adaptive meshing strategies for this model.

1.5 Thesis Outline

The thesis structure comprises several chapters, each addressing specific aspects. Chapter 2 provides a literature review, delving into the suspension system concepts, upright components, structural optimization methods, sequential quadratic programming in a broad context. In Chapter 3, the design inputs and objectives essential for the upright's design and optimization are outlined. Chapter 4 details the development of a parametric finite element model specifically tailored for the upright. The mathematical formulation of the nonlinear optimization problem concerning the upright's design is developed in Chapter 5. Chapter 6 discusses the analysis of parameters within the upright finite element model, focusing on the selection of the three most promising parameters. The process and significant considerations of response surface development are explained in Chapter 7. Chapter 8 presents the results post-optimization and offers a comparative analysis between the response surface and finite element model outcomes. Finally, Chapter 9 provides summary, conclusions drawn from the research, and recommendations for future work.

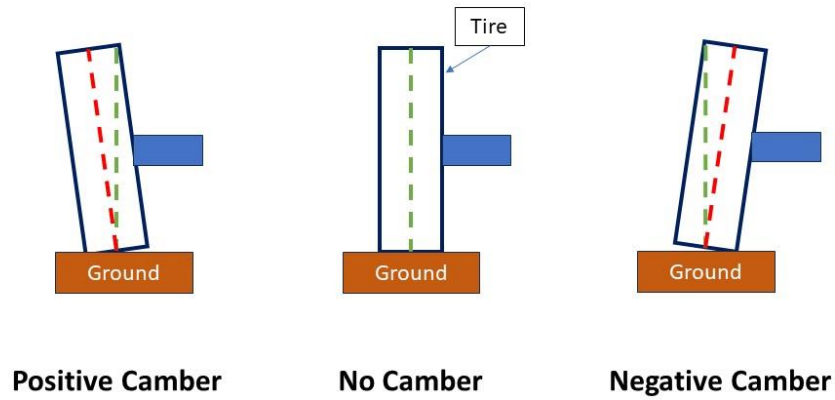
Chapter 2 Literature Review

The background information presented in this section lays the foundation for the rest of the thesis. It encompasses details about the double wishbone suspension system, the upright and its various examples, the structural optimization process.

2.1 Double Wishbone Suspension System

A double wishbone suspension is a type of independent suspension system employed in automobiles. It utilizes two wishbone-shaped arms, known as the upper control arm and lower control arm (sometimes arranged in parallel), to position the wheel. Each wishbone or arm has two attachment points to the chassis and a single attachment point to the upright or steering knuckle (Figure 2-2). The wishbones support the shock absorber and coil spring, managing vertical movement. This design provides engineers with precise control over wheel motion during suspension travel, regulating factors like camber angle, caster angle, toe pattern etc[1]. The design's advantages make it a preferred choice for performance and sports cars. It offers better handling characteristics compared to other suspension types like MacPherson strut systems and is especially great for cars with lower ride height like the Formula SAE cars.

Borg's thesis [6], referenced for the design and optimization of the suspension system upright in this thesis, employs a variation of the double wishbone suspension system. This system features a shorter upper control arm and a longer lower control arm, commonly referred to as the Short Long Arm (SLA) suspension system. Such a suspension setup results in negative camber in the tires. Camber, the inward or outward tilt of the tires when observed from the front of the vehicle, is considered positive if the wheel leans away from the chassis and negative if the wheel leans toward the chassis (Figure 2-1). This slight negative camber in SLA suspension system proves advantageous during turns, as body roll induces positive camber in the lightly loaded tire and negative camber in the heavily loaded outer wheel. This suspension response ensures optimal grip and improved cornering capabilities. However, it is crucial to avoid excessive negative camber, as it could potentially impact the longitudinal traction capabilities of the car.



Tire viewed from the front of the car

Figure 2-1. Camber description.

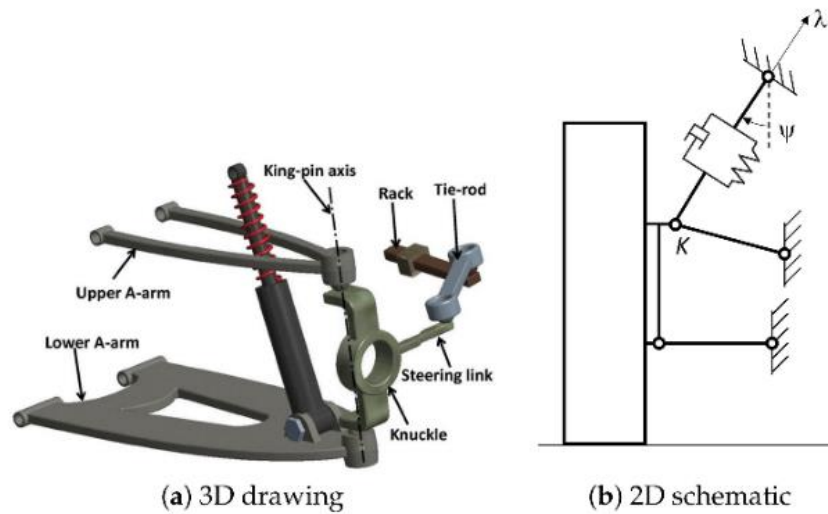


Figure 2-2. Double wishbone suspension system setup[2].

The components in the SLA suspension system used in Borg's thesis[6] are (Figure 2-3):

- 1) Upper Control Arm
- 2) Lower Control Arm

- 3) Upright
- 4) Pull Rod
- 5) Tie Rod
- 6) Rocker Arm
- 7) Spring
- 8) Damper
- 9) Anti Roll Bar

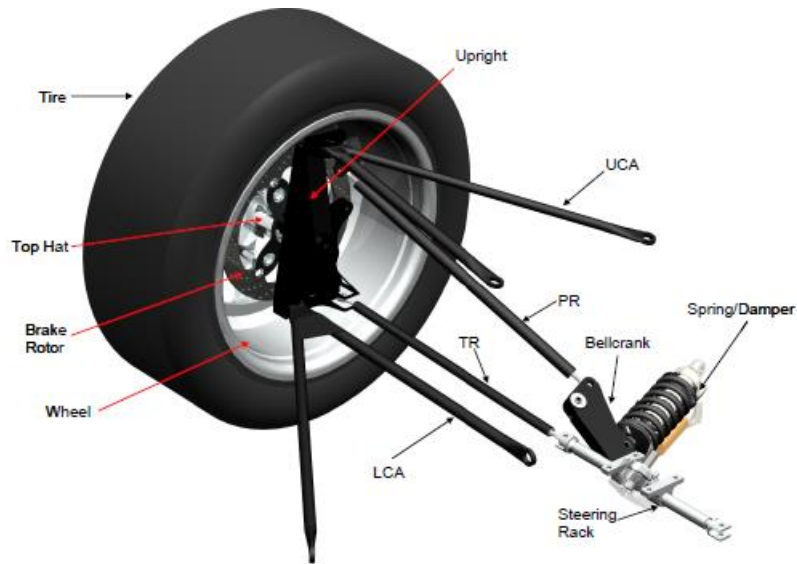


Figure 2-3. SLA suspension system setup [6].

These SLA suspension components must be analyzed and designed to work synchronously and provide optimal performance to improve the ride handling and to an extent the speed of a Formula SAE car. In this thesis as the focus is on designing upright, only the components attached to the upright are considered which are the control arms, brake caliper and tie rod. The exact locations of the points of suspension linkages are given in Chapter 3.

2.2 Upright and some of the examples.

The upright serves as a component of the suspension system, linking the suspension arms to the wheels as shown in Figure 2-2 referred as knuckle. Additionally, it plays a crucial role in the steering and braking systems by transferring braking, acceleration, and steering forces and moments from the wheels to the suspension arms and into the chassis. Due to its impact on driving characteristics, the upright needs to be stiff and lightweight. The upright stiffness is necessary to

ensure that when extreme loads are applied to the upright it doesn't deflect excessively thereby maintaining the steering geometry.

The upright consists of five attachment points for the upper control arm, lower control arm, tie rod and brake calipers, and a central hub to house the bearings and wheel hub for a double wishbone suspension setup. The load transfers from the tire to the chassis through the upright and makes it a critical component. The upright needs to be as stiff and light as practical resulting in research conducted on designing and optimizing the upright.

Bhardwaj et al[14] developed a steering upright for a double wishbone suspension arrangement and implemented five successive design modifications to reduce weight and eliminate stress concentrations through FEA. Following the design modifications, optimal material selection and topology optimization on ANSYS resulted in a 63% and further 18% reduction in weight respectively. However, this study did not extensively consider manufacturability and fatigue.

In contrast, Mesicek et al.[3] focused on the machinability of the upright, providing a comprehensive explanation of considerations for selecting the machining method. They designed a steering upright for a double wishbone setup with a tapered upright from the wheel hub bore to the control arm joints, observable from the car's side. Material selection was based on machinability and weight, and design modifications were made in areas with large factors of safety. This paper also highlights key considerations such as minimum thicknesses during part optimization.

Fidan et al[16] created a rear upright for a Formula SAE car from 2024 Aluminum, adopting a 'Y' shape with a central bore to accommodate the wheel hub and bearings. The design underwent modifications and iterations to minimize weight while ensuring stress and deformation remained within acceptable limits, resulting in an upright weighing 2 lbs. However, the analysis of the control arm pins' impact was omitted in this design, and fixed boundary conditions were employed instead for simplicity. Also, fatigue wasn't taken into consideration.

The research cited above used intuition to change the design typically using a high factor of safety for static design based on yield strength, deformation, but natural frequency and fatigue have not been considered. In this thesis stress, displacement, natural frequency of upright, and fatigue life of upright will be taken into consideration for design and optimization of upright. A nonlinear

programming approach based on a mathematically formulated optimization problem shall be used to optimize the upright in this thesis. Taking inspiration from these previous designs a similar tapered design will be used with different pockets shapes which will be discussed further in the thesis.

2.3 Structural Optimization Methods

There have been many methods to conduct structural optimization, the first analytical work conducted was by Maxwell in 1869, provided theoretical lower bounds on the weights of a truss and insight into the structural optimization design process as described by Vanderplatts[4]. However, it wasn't until Schmit's paper in 1960[15] that the use of a mathematical programming approach was used to solve nonlinear constrained optimization problems which has since continued to evolve. In a nonlinear programming (NLP) approach to get the optimum a mathematical formulation of the optimization problem must be written. The standard format of the NLP constrained optimization is as follows:

$$\begin{aligned} \min \quad & f(x) \\ \text{st.} \quad & g_j(x) \leq 0 \text{ for } j = 1, 2, 3, \dots, J \\ & h_k(x) = 0 \text{ for } k = 1, 2, 3, \dots, K \\ & x_i^L \leq x_i \leq x_i^U \text{ for } i = 1, 2, 3, \dots, N \end{aligned}$$

In the mathematical formulation provided, 'x' represents the design variables in the structure under analysis. The objective function, f(x), is aimed at minimization, while g_j(x) and h_k(x) denote the inequality and equality constraints, respectively. The parameters J, K, and N correspond to the number of inequality constraints, number of equality constraints, and the number of design variables respectively. x_i^L corresponds to the lower bound of the ith design variable, and x_i^U corresponds to the upper bound of the ith design variable. This formulation will be adhered to in the thesis.

Haftka identifies the three most crucial components of a structural optimization solver: 1) sensitivity derivative evaluation, 2) construction of an approximate problem, 3) fine tune the design to adhere to the constraints of the optimization problem and minimize the objective

function. So before delving into methods for solving optimization problems, the critical aspect of design variable selection through sensitivity analysis must be addressed. Numerous design variables are available for selection, and certain variables may prove insensitive, offering limited improvement in the optimization problem. Therefore, a sensitivity analysis, like Mrzyglod's approach[5], is necessary. Mrzyglod's paper discussed the investigation of parametric optimization for structures employing a multiaxial high-cycle fatigue criterion. In this context, the selection of design variables involved evaluating the gradient differences for a small increment in variable values to assess sensitivity. If the sensitivity was deemed too low, the design variable was rejected. In this thesis a similar approach will be employed, but a curve fitting strategy will be used to get the outputs as a function of the design variables to evaluate analytical derivatives for sensitivity analysis.

Once the optimization problem formulation is set there are various ways to solve the optimization problem. The problem will typically have constraints along with the objective function and hence it would be a constrained optimization problem.

The usual categorization of constrained optimization methods includes:

- Methods focusing on optimality, utilizing Lagrange Multipliers.
- Transformation approaches employing penalty functions.
- Constrained direct search strategies, encompassing random search.
- Linearization techniques, such as Sequential Linear Programming (SLP) and Cutting Plane Methods.
- Direct generation methods utilizing linearization, which involve the method of feasible directions, LP Simplex extensions, the Generalized Reduced Gradient method, and Gradient Projection Methods.
- Quadratic Approximation Methods, incorporating Variable Metric Methods and SQP.

Most of these optimization methods like SLP, SQP etc are gradient-based optimization methods where the gradients of the objective function and constraints are used to evaluate vectors to point in the direction of optimality. This method of optimization is extremely beneficial if there are smooth functions with gradients to drive an optimization problem. In contrast some methods are gradient free optimization methods where the objective function and constraint values are searched

inside the constrained space of the design variables to evaluate the optima and don't require evaluation of gradients. Some examples of gradient free optimization algorithms are Genetic algorithm, Simulated annealing, Ant colony optimization etc. In this thesis SQP method is used and the advantages associated with it are:

- 1) SQP is a much faster process than some of the gradient free optimization methods because it is based on a refined representation of the function which includes curvature.
- 2) SQP utilizes a second order approximation of the objective function to find the direction vector towards the optimal solution rather than the linear approximation used in SLP. This is beneficial for a nonlinear objective function as curvature of the function is used in the quadratic approximation.
- 3) SQP is not a feasible point method where neither the initial point nor any subsequent points in the algorithm need to be feasible for the algorithm to run and reach the optimum solution.
- 4) The number of constraints which will be used in the thesis are less, so SQP would be an efficient technique to use.

2.4 Sequential Quadratic Programming (SQP) process

Sequential quadratic programming (SQP) is an iterative approach for constrained nonlinear optimization, based on the quasi-Newton method. The SQP method is best suited for application in mathematical problems characterized by an objective function and constraints that are continuously differentiable. The process is as follows:

- 1) The optimization problem is formulated as per standard NLP formulation shown in Section 2.3.
- 2) The problem then is converted into a quadratic subproblem with linear constraints to find the direction vector for the current iteration towards the optimal solution. The quadratic subproblem to find the optimal direction vector is as follows:

$$\begin{aligned} \min q(\mathbf{d}^k) &= \frac{1}{2} \mathbf{d}^{kT} \mathbf{H} \mathbf{d}^k + \mathbf{c}^T \mathbf{d}^k & (2.1) \\ \text{st. } \mathbf{A}_i \mathbf{d}^k &= \mathbf{b}_i, \quad i = 1, \dots, n \\ (\mathbf{A} \mathbf{i} \mathbf{n} \mathbf{e}_i) \mathbf{d}^k &\leq \mathbf{b} \mathbf{i} \mathbf{n} \mathbf{e}_i, \quad i = 1, \dots, s \end{aligned}$$

In the subproblem described above, the direction vector, denoted as \mathbf{d} , determines the direction for the new iteration of design variables. Here, \mathbf{H} represents the hessian matrix of

the objective function, \mathbf{c} is the gradient vector of the objective function, \mathbf{A}_i is the gradient vector of the i^{th} equality constraint, \mathbf{b}_i is the i^{th} equality constraint value for the current iteration value of design variables, \mathbf{A}_{ine}_i is the gradient vector of the i^{th} inequality constraint, and \mathbf{b}_{ine}_i is the equality constraint value for the current iteration value of design variables. The solution of this subproblem, represented by the direction vector, is utilized to obtain the next iteration value of design variables, as depicted in Eq. 2.2. In Eq. 2.2, \mathbf{x}^{k+1} signifies the subsequent iteration value of design variables, while \mathbf{x}^k denotes the current iteration value of design variables.

$$\mathbf{x}^{k+1} = \mathbf{x}^k + \alpha \mathbf{d}^k \quad 2.2$$

- 3) The convergence criteria of the objective function (Eq. 2.3) and constraint satisfaction will be checked for this new iteration value of design variables. If the design variables have converged and satisfy all the constraints the solution can be considered a local optimum.

$$\|c\| \leq \text{objective function norm convergence value} \quad 2.3$$

Chapter 3 Design Inputs

This chapter outlines the design inputs needed to design the upright parametric finite element model for analysis. These design inputs include the suspension linkage points, and the design objectives for the upright.

3.1 Suspension Linkage Points

The first design input which will dictate the design of the upright is the suspension linkage points. These linkage points were evaluated for the VT 2009 Formula SAE car front right suspension system and are shown in Table 3-1. The focus for upright would be the outboard points (M,P,J,Q) in Figure 3-1 as these points would be connected to the upright.

Table 3-1. Suspension Linkages Outboard Points [6].

	Outboard Points of Suspension Linkage(Upright Joint Points)		
	X	Y	Z
Lower Control Arm	940.5	571.5	-149.9
Upper Control Arm	914.5	539.4	-378.5
Tie Rod	880.9	548.3	-149.9
Pull Rod	908.9	520.4	-352.9
Wheel Center	935.4	609.6	-254

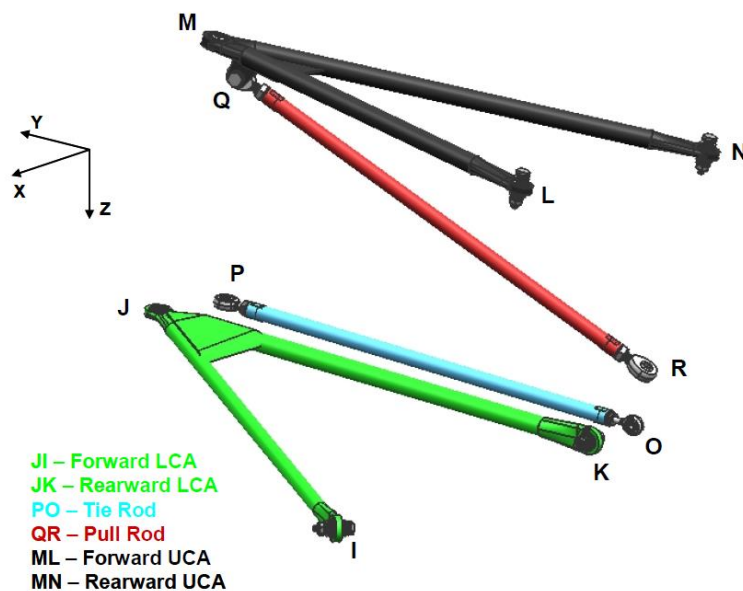


Figure 3-1. Front right suspension system view[6].

The outboard points of the suspension system which are connected to the upright define the working envelope in which the upright needs to be designed. The coordinate system used in Table 3-1 is as per Borg's thesis which is a modification of the SAE coordinate system of the car. Instead of using the conventional SAE car coordinate system shown in Figure 3-2, the coordinates system is such that the reference point for the coordinate system is no longer the center of gravity (CG) but the point of projection of the CG on the road surface.

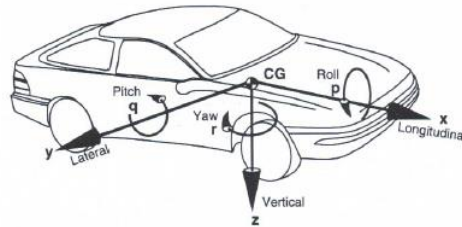


Figure 3-2. SAE car coordinate system[6].

3.2 Design Objectives

The design objectives which the upright would need to achieve are:

- 1) The weight of the upright needs to be minimized to reduce the overall unsprung mass of the car. This, in turn, can enhance the car's speed and reduce downforce.
- 2) Maintaining a high factor of safety (at least 1.2) for stress in the upright, considering the potential high stress areas in the model near the location of wheel hub center.
- 3) Achieving maximum rigidity in the upright, with deformations ideally falling within the range of 0.1 mm to 1 mm.
- 4) In order to avoid resonance and guarantee structural stability, it is imperative that the fundamental natural frequency of the upright as determined by modal analysis surpasses 100 Hz. This criterion is established to ensure that the vertical component's frequency is at least ten times greater than the upper limit of the suspension system's frequency, which is 10 Hz.
- 5) Considering the Formula SAE car's participation in four dynamic events, an approximate estimated minimum of 100 laps on a racetrack must be withstood by the car. If each lap has approximately 15 corners, the upright must then be able to withstand approximately 1500 corner

maneuvers, as represented as a time-dependent loading case in Section 4.6.2. A representation of a corner maneuver is shown in Figure 3-3.

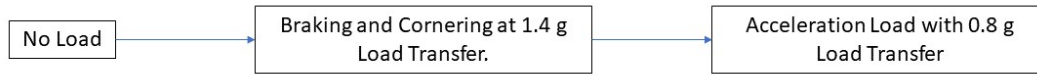


Figure 3-3. Corner Maneuver Loading Scenario.

Chapter 4 Upright Finite Element (FE) Model

4.1 Upright FE Model Data Flow

The Upright parametric finite element model shall be created based on the design inputs available in Chapter 3 and literature review in Chapter 2. This FE model is created on Abaqus CAE 2022 version. The Data Flow Diagram (DFD) for all the steps of creation and submission of Upright FE model in Abaqus is shown in Figure 4-1. The upcoming subsections of this chapter will discuss the steps shown in Figure 4-1.

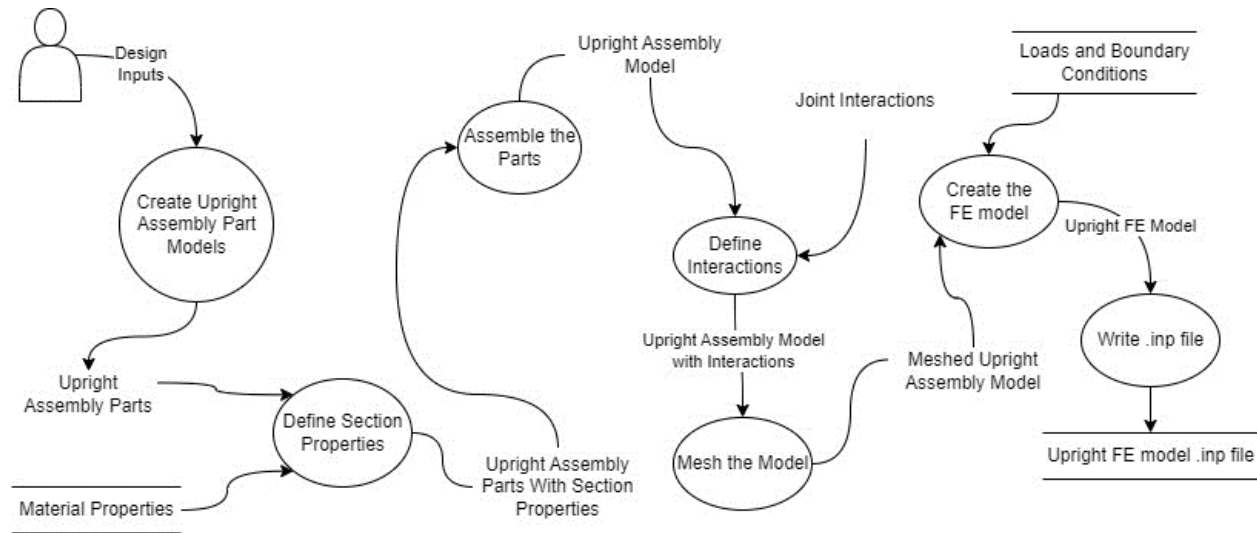


Figure 4-1. DFD of Upright FE model creation.

4.2 Upright Model Part and Assembly Description

Though assembly model development comes after material selection, the assembly and part model have both been described here to justify and finalize the shape of the upright for finite element analysis. The shape of the upright model has been based on the literature studied on the uprights developed, the suspension points locations in Table 3-1, and dominant mechanics. Thus, before getting into the actual shape of the upright, the dominant mechanics needs to be studied.

4.2.1 Dominant Mechanics Identification of Upright.

The upright is an integral component of the vehicle's suspension system, linking the wheels to the chassis through the suspension. It also plays a crucial role in the steering and braking mechanisms

by transmitting the forces generated during braking, acceleration, and cornering from the wheels through the suspension arms and springs to the chassis.

Depending on the type of suspension used, the configuration of the upright's connection to the suspension spring and steering system may vary. The Short Long Arm (SLA) double wishbone suspension is the focus of this thesis, where the upright is designed with three support points: one for the upper control arms, one for the lower control arms, and one for the steering tie rod. The upper control arm joint on the upright will accommodate both the reaction loads of the upper control arm and the push rod, which is connected to it. Additionally, the upright will feature attachments for securing the brake calipers. The setup of the suspension system with the upright is shown in Figure 4-2. In Figure 4-2, the upright component is labeled as 'knuckle' instead of 'upright,' even though they refer to the same part.

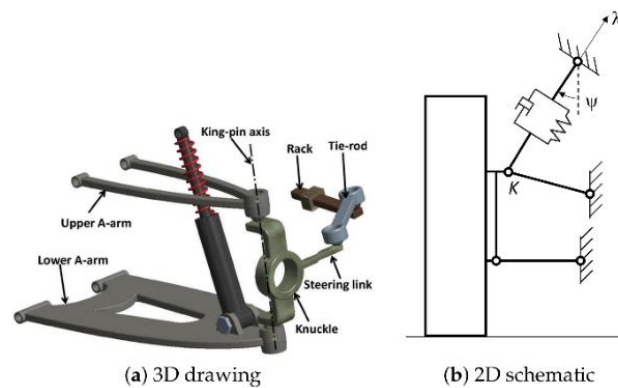


Figure 4-2. Upright for a double wishbone suspension setup[2].

The load path is such where the loads are first generated at the tire contact patch, transferred to the wheel hub bearings, then transferred to the upright which is carried via the suspension control arms through the spring/damper to the chassis.

Based on the load path, the distribution of loads from the wheel hub occurs initially through the bearings fit inside the upright. These loads are dispersed within the upright through the upper control arms, lower control arms, and the tie rod and suspension spring/damper to the chassis.

Typically, automotive suspensions use tapered roller bearings due to their ability to withstand both radial and axial forces originating from the wheel center.

The upright can be idealized as a simply supported 1D beam for the case of cornering and braking separately. The depiction can be seen in Figure 4-3.

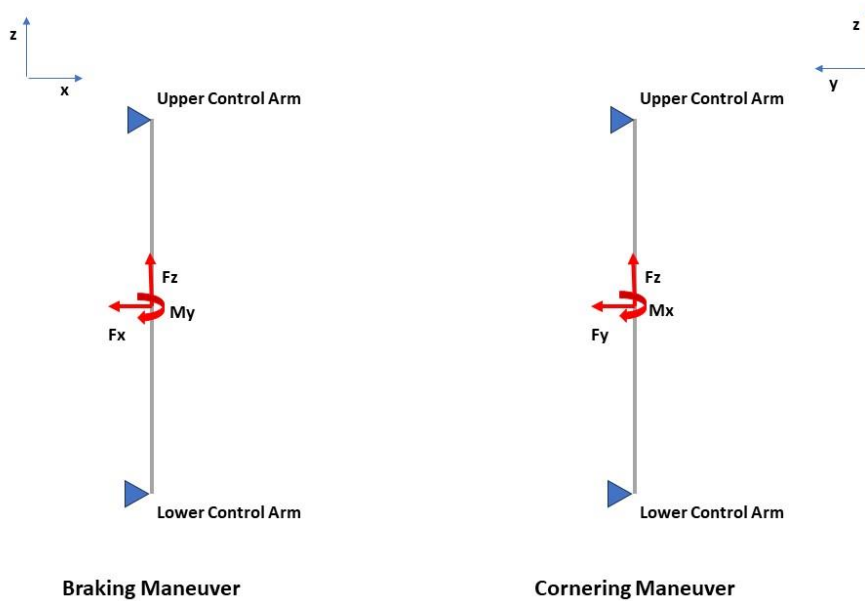


Figure 4-3. 1D beam approximation of upright.

This 1D beam approximation yields significant insights. Firstly, it is evident that the problem results in a multiaxial stress, with substantial bending stresses present in both the XZ and YZ planes during braking and cornering maneuvers respectively. Torsion could come into play due to the combined effects of braking and cornering maneuvers of the car. Secondly, the highest stress and deformation would be developed in the vicinity of the wheel hub area. Reinforcing the wheel hub region with additional material becomes essential to ensure structural integrity.

4.2.2 Initial Assembly Model of Upright

Based on the conclusions in 4.2.1 an initial model of an upright was decided to be a tapered solid block in the XZ plane as per the SAE vehicle coordinate system used in Borg's thesis[6]. The tapered section ensures that greater material would be available near the wheel hub region where

stresses are maximum, and the weight would be less than a rectangular section due to the taper. The first design developed is shown in Figure 4-4.

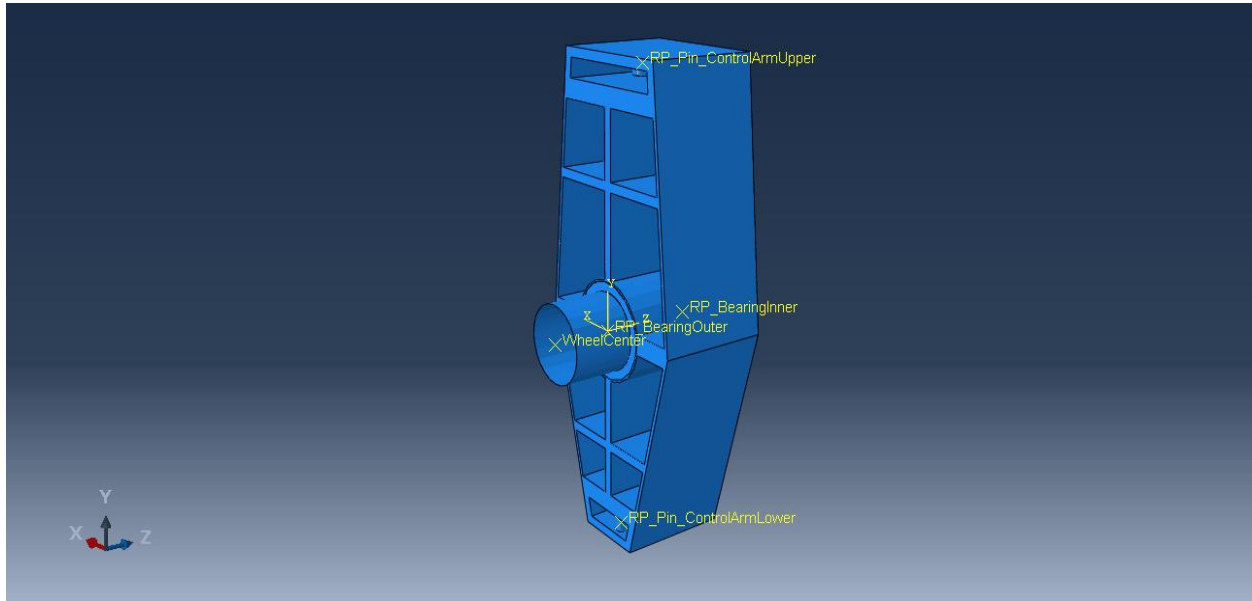


Figure 4-4. Assembly model of initial upright.

Before getting into the characteristics of the upright created it is important to note the change in coordinate system in this model. The change in the coordinate system is described in Table 4-1.

This *Initial Upright Model* possesses several key characteristics:

- 1) It incorporates the crucial components of bearings, wheel hub, and control arm pins.
- 2) The model adopts a straightforward approach, utilizing a deformable cylindrical part to represent the bearing, and rigid analytical pins for the wheel hub and cylindrical pins, as the primary focus lies in designing the upright itself.
- 3) This *Initial upright model* omits the inclusion of tie rod mount and brake caliper mounts. The rationale behind this decision is to initially focus solely on testing the tapered shape of the upright.
- 4) The model consists of horizontal and vertical ribs, which create trapezoidal pockets thereby reducing the weight of the structure. The extrude sketch highlighting these features for the upright is shown in Figure 4-5.

Table 4-1. Coordinate system change description.

Axis Title	Coordinate System used in Lane's Thesis[6]	Coordinate System for the Abaqus models in this thesis
X axis	Along the direction of acceleration	Along the direction of braking starting from inside the upright, at the midpoint of wheel hub cylinder axis.
Y axis	Along the direction of lateral force away from the chassis	Along the direction of axis of bump or weight of the car starting from inside the upright, at the midpoint of wheel hub cylinder axis.
Z Axis	Along the direction of weight of the car.	Along the direction of cornering axis towards the chassis starting from inside the upright, at the midpoint of wheel hub cylinder axis.

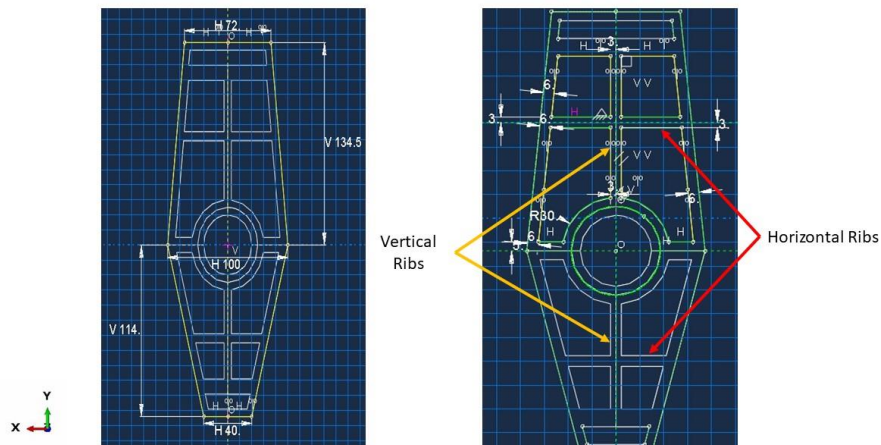


Figure 4-5. Extrude Sketch of First Upright Design.

The initial upright model has a very high fundamental natural frequency (500-1000 Hz), stress levels between 100 - 500 MPa, and deformation in the range of 0.3 mm-0.8 mm. In this model the material used was Aluminum 2024, and as per the objectives outlined in Chapter 3 the results satisfy the constraints by tweaking some parameters. Still some modifications need to be made to reduce weight and intentionally design a direct load path from the wheel hub to the brake caliper mounts when they are added. The new modifications to be added are:

- 1) Addition of asymmetric taper in XY plane of upright part to reduce its weight. This could possibly reduce stiffness thereby reducing the natural frequency, but it should still be greater than the minimum of 100 Hz. Also, once the brake caliper mounts and tie rod mounts are added the stiffness should increase, compensating for the possible decrease in stiffness by the asymmetric tapers.
- 2) Extra diagonal ribs shall extrude from the bearing cage created in the upright to create a load path to the brake caliper mounts, and the angle and thickness of these ribs can be used as parameters for further testing and optimization if required.

4.2.3 Final Upright Parametric Model

Based on the new modifications discussed in [Section 4.2.2](#) a new assembly model of the upright was made as shown in Figure 4-6.



Figure 4-6. Assembly Model of Final Upright.

The key features of the final upright model which incorporates several significant design features that enhance its design and functionality are:

1) Addition of Tie Rod mount: A Tie Rod mount has been integrated into the upright assembly at the specified out-board location of tie rod, indicated in Table 3-1.

2) Introduction of Secondary Angular Ribs: To further strengthen the upright and add a load path to the brake calipers when added, additional angular ribs have been introduced into the design. The thickness and angle of these ribs can be conveniently adjusted through the parameter manager and scripting for further optimization. These ribs shall be named as the secondary angular ribs for further references and are shown in Figure 4-8.

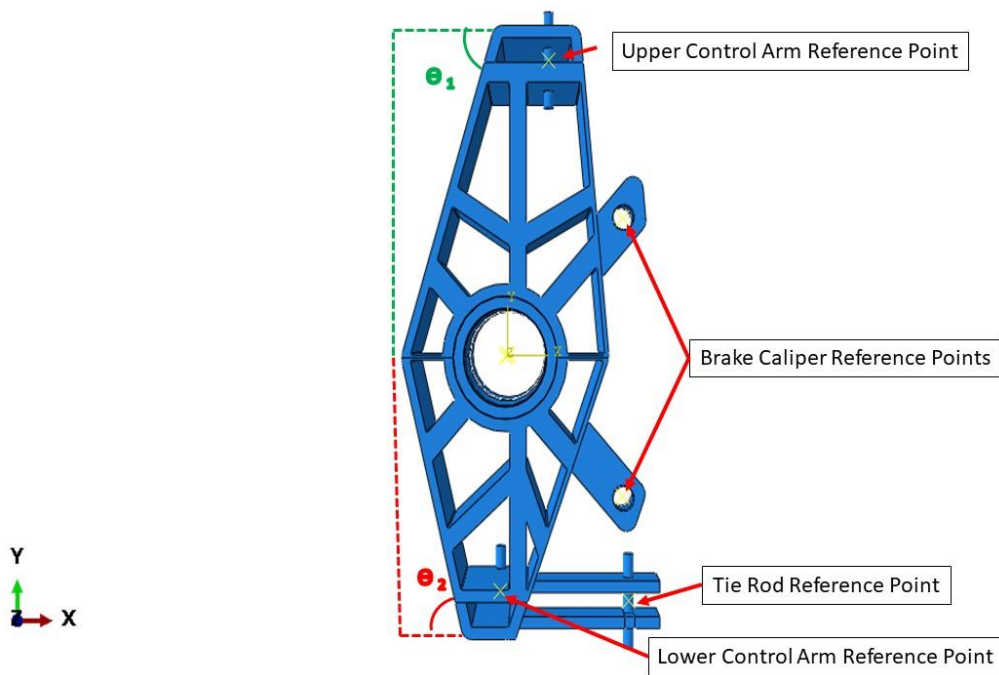


Figure 4-7. Asymmetric tapers in *Final upright model*.

3) Asymmetric Tapers in the XY Plane: To further reduce the weight of the upright the taper angles are increased and kept asymmetric in the XY plane on the top half and bottom half of the upright as shown in the Figure 4-7.

4) Primary Angular Ribs:

The horizontal ribs in the Initial upright model have been modified such that the angle of these ribs can be changed to further refine the design to meet the requirements. These ribs shall be referenced as the primary angular ribs and are shown in Figure 4-8.

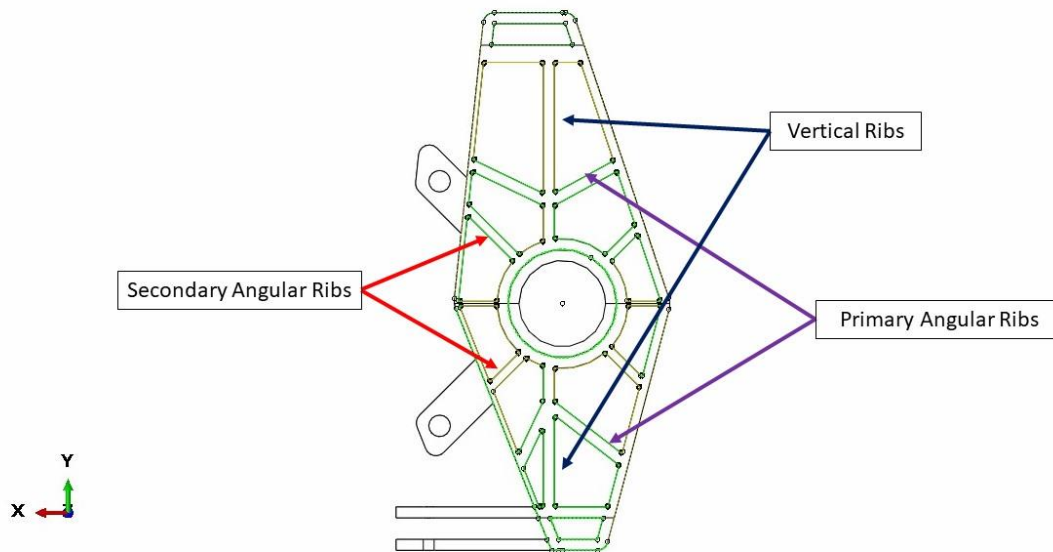


Figure 4-8. New features in *Final upright model*.

The different parts in the complete assembly are described in Table 4-2.

A comparison of the results of the *Initial upright model* and the *Final upright model* is shown in Table 4-3. The *Final upright model* has proven to be promising, providing valuable insights for further development. One observation is that the natural frequency of the *Final upright model* has increased compared to the *Initial upright model*. This can be attributed to several factors: firstly, the inclusion of the tie rod mount and brake caliper mounts have introduced new supports and boundary conditions, thereby enhancing the overall stiffness of the system. Secondly, the natural frequency is influenced by the stiffness-to-weight ratio, and it's observed that the displacements have reduced which means that stiffness has increased, and weight has also reduced, increasing the natural frequency. Additionally, the presence of diagonal ribs contributes to increased stiffness, further impacting the natural frequency.

In terms of stress and deflection, the final design has stresses in the range of 50-600MPa, deformations between 0.1-0.5 mm, and lower weight than the *Initial Upright Model*. This opens

opportunities for testing different pocket shapes and rib thicknesses to fine-tune these parameters. Along with the increase in stress levels, new stress points have emerged in the updated design, necessitating a closer examination to ensure structural integrity. The description of the loads and boundary conditions causing these stresses will be discussed in depth in Section 4.6.

Table 4-2. Final upright assembly parts description.

Sr No	Part name	Type	Dimensions
1	Upright	Deformable	Overall Dimensions=250*120*60 mm ³
2	Inner Bearing	Deformable Cylinder	Outer diameter(do)=50 mm, Thickness(t) =10 mm
3	Outer Bearing	Deformable Cylinder	Outer diameter(do)=50 mm, Thickness(t) =10 mm
4	Tie Rod Pin	Analytical Rigid Pins	Diameter (d _{tr})=10 mm
5	Upper Control Arm Pin	Analytical Rigid Pins	Diameter (d _{uca})=10 mm
6	Lower Control Arm Pin	Analytical Rigid Pins	Diameter (d _{ica})=10 mm
7	Wheel Hub	Analytical Rigid Pins	Diameter(D _{wh}) = 40 mm
8	Brake Caliper Mounts	Analytical Rigid Pins	Diameter (d _{bc})=10 mm

Table 4-3. Comparison of results between *Initial upright model* and *Final upright model*.

Output	Initial Upright Model	Final Upright Model
Stress range (MPa)	100-500	50-600
Maximum displacement range (mm)	0.3-0.8	0.1-0.5
First Natural Frequency (Hz)	509.93-1000	950-1200
Weight Range(gms)	868-1680	838-1500

4.3 Upright Material and Section Properties

The upright part must have three critical characteristics: high stiffness, low weight, and high fatigue strength. The materials considered for the part are:

- 1) Aluminum 2024-T6

2) 4340 Steel

The physical properties of these materials are described in Table 4-4. The material properties are assigned to the model in section properties. It is essential to note the units used, as mass density can easily be described incorrectly in the material properties section. The upright and bearing parts are specified as homogenous solid sections with Aluminum 2024-T6 as the material in section properties. If the parts need two different materials, two different sections need to be created, and associated with the respective part or region of a part.

Table 4-4. Materials tested for upright.

Sr No	Material	Tensile Properties			Strain Life Curve Properties			
		Yield Strength(MPa)	Mass Density(N-s ² /mm ⁴)	Youngs Modulus (MPa)	σ_f (MPa)	b	ϵ_f	c
1	2024-T4 Al	303	2.78E-09	73100	1294	-0.142	0.327	-0.645
2	AISI 4340	1371	7.85E-09	200000	1879	-0.0859	0.64	-0.636

The weight of the part was reduced from 3.5 kgs while using 4340 Steel to less than 1.5 kgs when Aluminum 2024-T6 was used. Also, the stresses developed in the Upright part are ranging from 50 MPa-600 MPa, so a material with very high yield strength (greater than 1000 MPa) is unnecessary. Aluminum 2024-T6 has been chosen as the material for the model as it has lower mass density, good yield strength, comparable stiffness, and good fatigue strength.

The material and section properties used in Abaqus model are shown in Figure 4-9.

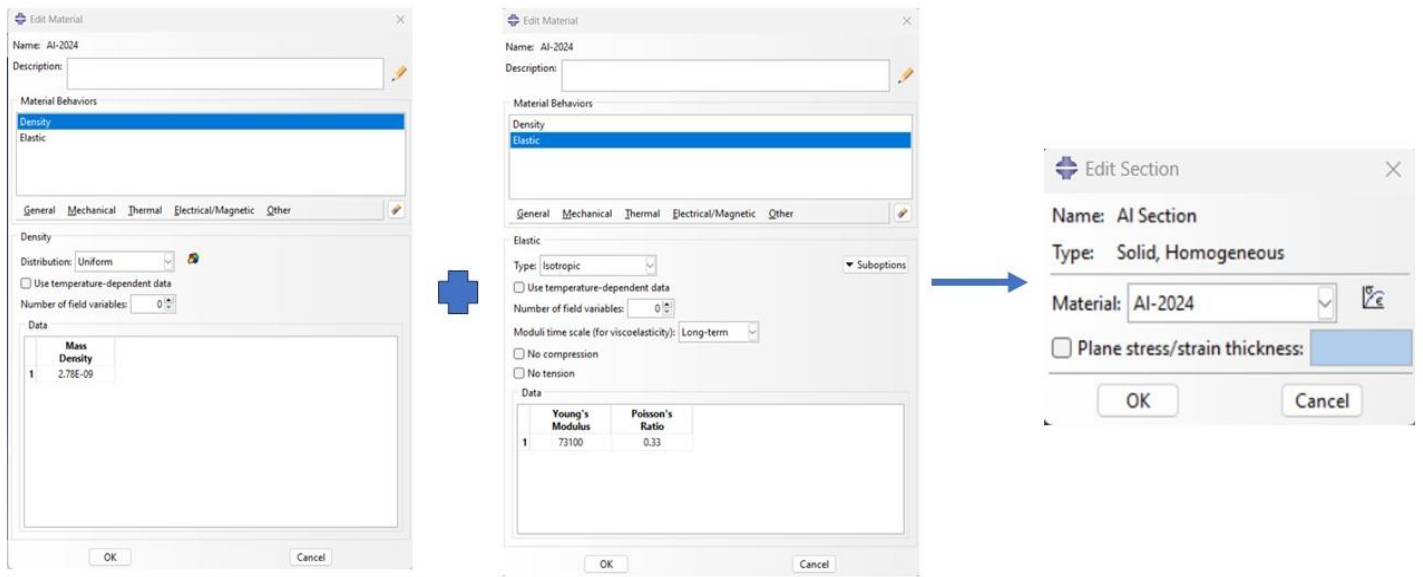


Figure 4-9. Material and section properties given to upright.

4.4 Step Manager

In the Abaqus environment, different analyses are conducted by creating specific analysis "steps" based on the applied loading conditions. The step manager allows for the creation of multiple steps for various analyses. The steps used to conduct the analysis in this thesis are outlined below:

1) Static, General:

This step investigates the influence of loads and boundary conditions, as described in Section 4.5, on the overall structure. It enables the observation of stresses developed and deformation in the upright under quasi-static conditions. This step is preferred over the simpler "Static Linear Perturbation" step because the upright is subjected to several contact conditions with the control arm pins and "Static, General" can handle these contact interactions between multiple parts in the assembly. The parameters used in the "Static General" step are shown in Table 4-5. The parameters in Table 4-5 don't have units as the time-period assigned for a complete load step is a pseudo-time from 0 to 1, and the increment values are just fractions of the time period of the step.

Table 4-5. Static General Step Parameters.

Sr No	Parameter Name	Description/Value
1	Time Period	1
2	Incrementation Scheme	Automatic
3	First Time Increment Value	0.05
4	Minimum Time Increment Value	0.001
5	Maximum Time Increment Value	0.2

2) Frequency Step:

The Frequency step is a linear eigen-value solution used to evaluate the natural frequencies of the model. These values are evaluated to compare the stiffness of the upright for further optimization. In the frequency step Abaqus can provide multiple frequencies, but for this thesis the fundamental frequency is most important. To reduce time and avoid loss of convergence, only the first five frequencies are requested from the frequency step. Another thing to note is that this frequency step

is carried out after the static general step, so this frequency step is carried out with the upright in the strained condition from the Static General step.

4.5 Upright Assembly Joint Interactions

The upright assembly model as described in Section 4.2.1 has a lower control arm pin, upper control arm pin, tie rod, and brake caliper which transfer the wheel loads developed for each load case to the suspension and chassis. These different parts have surface interactions with the upright and need to be given as input to the upright model in the interaction and constraints manager. There are two different surface interactions used, which are described below.

4.5.1 General Surface to Surface Interaction

This interaction is specifically employed to model the combined surface interactions involving contact between the upper control arm pin with the upright, lower control arm pin with the upright, tie rod pin with upright, and brake caliper mounting pins with upright shown in Figure 4-11. This interaction defines the relative motion and load transfer between these joints and the amount of friction that affects the movement of the pins. Moreover, it permits the joints to separate when required after contact.

Typically, TIE constraints are utilized to bond surfaces together, with no relative motion between the surfaces in contact. The TIE constraints don't accurately represent the actual behavior of the joints. A TIE constraint effectively “glues” the pins to the upright, preventing any relative motion, which isn't representative of the behavior in pinned joints. The TIE constraint can develop tension forces in the region where separation should occur. The joints should naturally separate if the reaction forces necessitate it, and the area where the pins rest against the hole experiences compressive forces. A depiction of the same is shown in Figure 4-10.

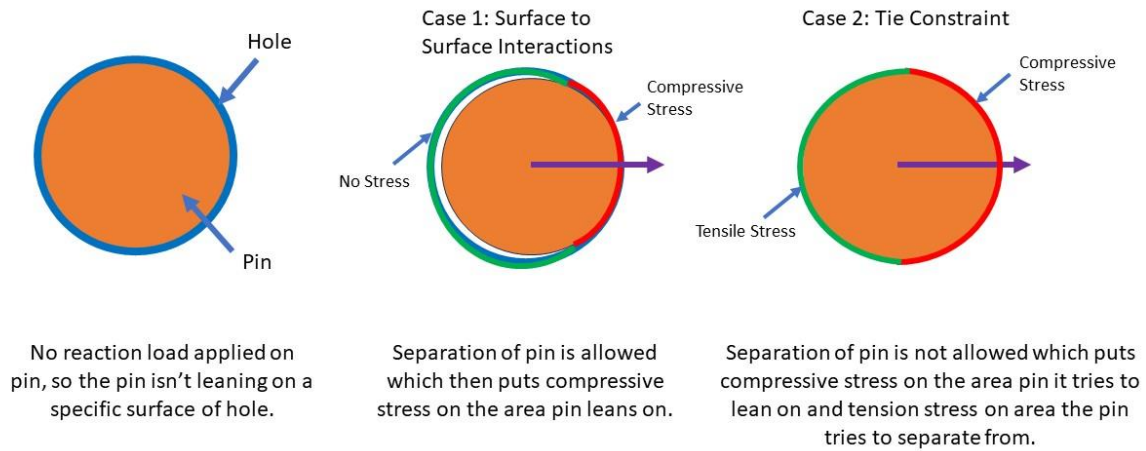


Figure 4-10. Tie constraint and General Surface to Surface interaction distinction.

The parameters input for surface-to-surface interactions for the upright model is shown in Table 4-6.

Table 4-6. Surface to surface interaction contact properties.

Sr No	Contact Property Option	Parameter	Value
1	Tangential Behavior	Coefficient of Friction	0.45[7]
2	Normal Behavior	Separation after contact	Allowed
		Contact Stiffness behavior	Non-Linear
		Pressure Overclosure	Hard Contact

In these interactions the main surface to be selected shall be the outer surface of the pins and the secondary surface of interaction are the internal surfaces of the holes in the upright.

4.5.2 TIE constraints

This interaction is specifically employed to model the combined surface interactions involving: the bearings inner surface contact with the wheel hub outer surface, bearings outer surface contact with upright holes inner surface, and wheel hub outer surface with upright holes inner surface. These interactions are more like constraints to the movement of the respective components. The TIE constraint essentially glues the two components at the surface input given by the user. The TIE constraints have been used in this study to ensure that the load applied at the wheel center is transferred completely through the bearings to the upright.

The summary of all the interactions and constraints has been described in the Table 4-7 and Figure 4-11:

Table 4-7. Interaction and constraints summary.

Sr. No	Main Surface of Contact	Secondary Surface of Contact	Interaction Type
1	Upper Control Arm Pin Outer Surface	Inner Surface of the hole in upright for upper control arm	Surface to Surface Interaction
2	Lower Control Arm Pin Outer Surface	Inner Surface of the hole in upright for lower control arm	Surface to Surface Interaction
3	Tie Rod Pin Outer Surface	Inner Surface of the hole in upright for tie rod	Surface to Surface Interaction
4	Brake Caliper Mounting Pins Outer Surface	Inner Surface of the hole in upright for brake caliper mounts	Surface to Surface Interaction
5	Wheel Hub Outer Surface	Bearings Inner Surface, and Inner Surface of central hole in upright to house the wheel hub	Tie Constraint
6	Bearings Outer Surface	Inner Surface of central hole in upright to house the bearings	Tie Constraint

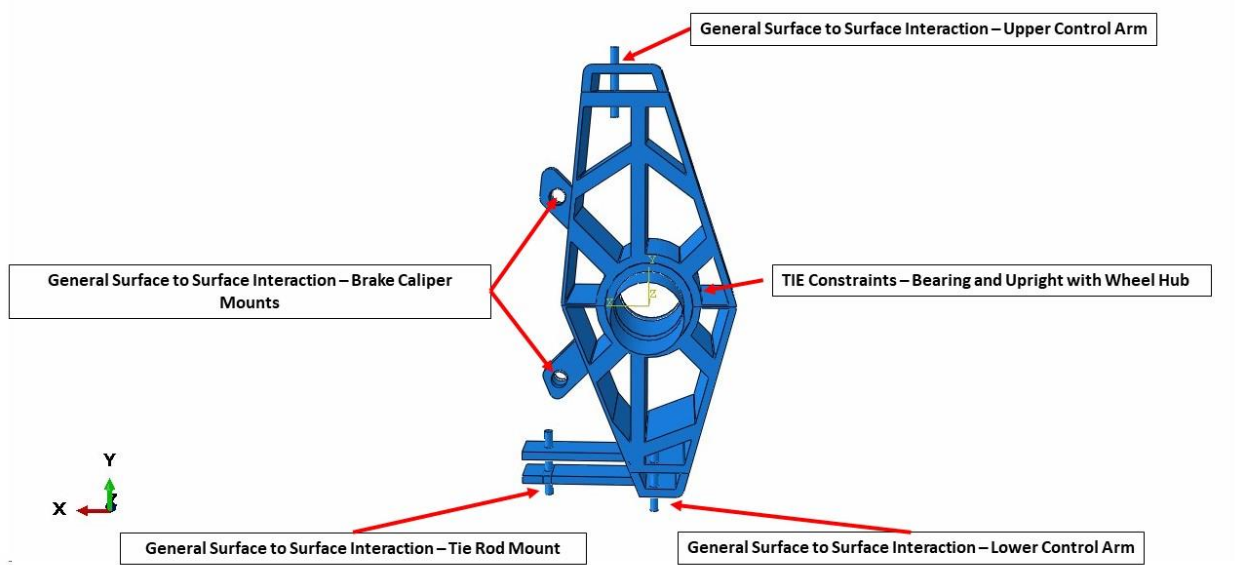


Figure 4-11. Interactions and constraints summary in *Final upright model*.

4.6 Loads and Boundary Conditions

4.6.1 Defining Loads

The loads can be divided into two main categories: the first category includes the forces that are applied, and the second category pertains to the moments that are applied. This thesis encompasses an examination of both a quasi-static singular load scenario, representing the case of combined braking and turning, and a scenario involving time-dependent loading, representing a corner maneuver.

In the case of the singular load scenario, the worst-case scenario which the car may face in terms of loading, involves both braking and cornering with full load transfer. Table 4-8 displays the force values at the wheel center considered for this specific case.

Table 4-8. Load case for a quasi-static single load.

Sr. No	Load Type	Value
1	Force in x direction (CF1)	2236 N
2	Force in y direction (CF2)	1891 N
3	Force in z direction (CF3)	1343 N
4	Moment about x axis (CM1)	-480400 N mm
5	Moment about y axis (CM2)	30600 N mm
6	Moment about z axis (CM3)	567900 N mm

Regarding the time-dependent load scenario, we are analyzing a situation in which a car approaches a corner on a circuit. The sequence of events considered in this scenario is depicted in Figure 4-12. The loads are referred from Borg's thesis[6].

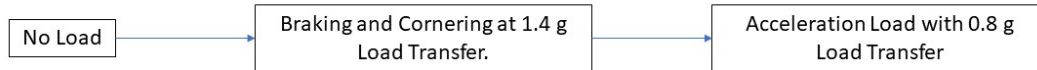


Figure 4-12. Sequence of loading for a corner.

Furthermore, Figure 4-13 and Figure 4-14 provide details of the time dependent forces and moments applied at the wheel center of the upright model's wheel hub rigid pin for fatigue analysis. In the curves in Figure 4-13 and Figure 4-14, the F_x force represents braking force, F_y represents normal direction force, F_z represents cornering force, M_x denotes the moment around the braking axis, M_y denotes the moment around the normal axis, and M_z represents the moment around the lateral or cornering axis.

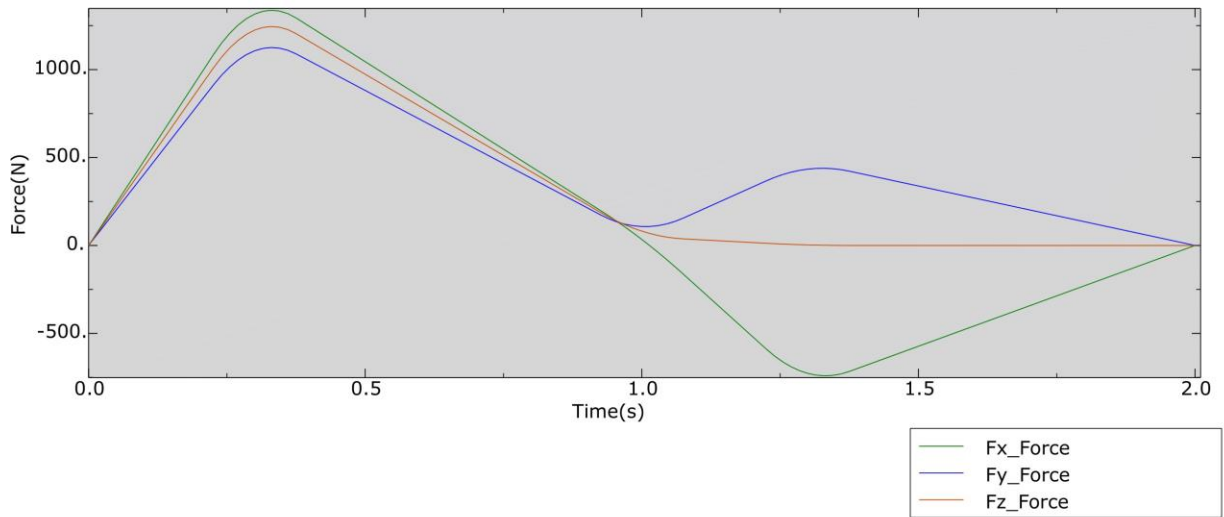


Figure 4-13. Forces at wheel center vs time.

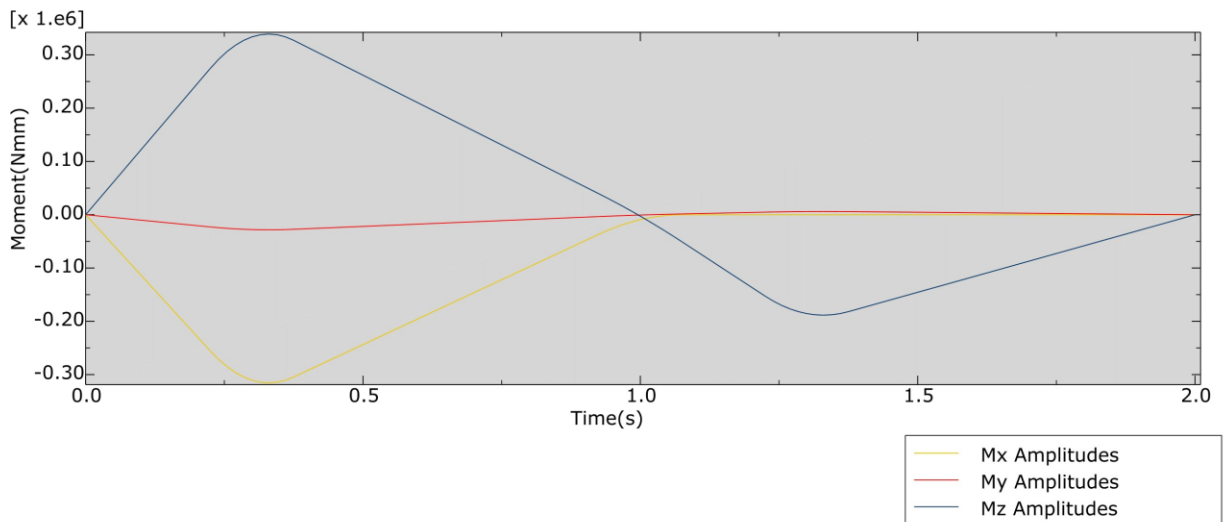


Figure 4-14. Moments at wheel center vs time.

4.6.2 Defining Boundary Conditions

The displacement boundary conditions represent the physical displacement constraints applied to the assembly. In case of the upright assembly model, the Encastre boundary condition is exclusively employed at specific reference points: the upper control arm reference point, lower control arm reference point, tie rod reference point, and brake caliper mounting pins reference points. The Encastre condition mimics a pinned boundary condition, where all displacements in the X, Y, and Z directions are effectively prevented ($U_1=U_2=U_3=0$), where 1, 2, 3 denote the X,

Y, Z directions respectively, and U represents translational displacement). While the interactions detailed in Section 4.5 already restrict a substantial part of the motion, they do not inherently inhibit the free rotation of the pins around their own axes. The implementation of this Encastre boundary condition will ensure that such free rotation is effectively prevented.

The summary of the boundary condition used in the upright model is described in Table 4-9.

Table 4-9. Summary of boundary conditions on upright.

Sr. No	Location of Boundary Condition	Type of Boundary Condition
1	Upper Control Arm Reference Point	Encastre
2	Lower Control Arm Reference Point	
3	Tie Rod Reference Point	
4	Brake Caliper Pins Reference Points	

The loads and boundary conditions applied on the upright model are shown in Figure 4-15.

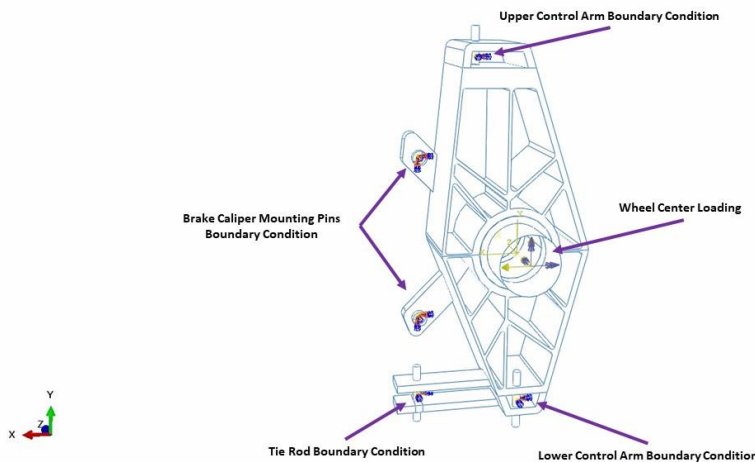


Figure 4-15. Loads and boundary conditions on *Final upright model*.

4.7 Meshing and Element Selection

Meshing is quite dependent on the complexities of the geometry of the design, and meshing strategy and its size can be detrimental towards having a good mesh and a bad mesh. The elements which will be used in the mesh are further dependent on the type of loading and the stresses expected from the model. Thus, proper meshing and element selection is necessary. There are typically two ways a model is meshed:

- 1) Mesh by part, a part-dependent mesh.
- 2) Mesh by assembly instance, a part-independent mesh.

The *mesh by part* strategy is used so that different mesh and element controls can be provided for different parts. The meshes used in each part has been described in subsections below:

4.7.1 Mesh and Element Types for Upright Part

The meshing strategy for the upright part is critical as it's the main load carrying part in the assembly and it has some complex geometric pocket features, where large stress concentrations can be developed, and value discontinuities. The upright part is divided into three regions by partitioning also shown in Figure 4-17:

- 1) Upright main body

In the case of the Upright main body, tetrahedral free meshing becomes the preferred choice due to the intricate geometry, making other meshing strategies impractical. A global mesh size of 1.6 mm was determined through a mesh convergence study conducted on the entire upright. The von Mises stress value, deformation magnitude, and fundamental natural frequency are evaluated in a mesh convergence study, decreasing mesh size from 1.9 mm. At 1.6 mm the error in the new values with respect to the previous ones is less than 2% and selected as the global mesh size for the parts. The % error for quantitative mesh convergence study is evaluated using Eq. (4.1). The summary of the mesh convergence results for fundamental natural frequency is shown in Figure 4-16 and Table 4-10. For all the mesh convergence results please refer the Appendix Section A.

$$\% \text{ Error} = \frac{\text{Current Mesh Size Output Value} - \text{Previous Mesh Size Output Value}}{\text{Current Mesh Size Output Value}} * 100 \quad (4.1)$$

Table 4-10. Quantitative mesh convergence study for fundamental natural frequency.

Sr. No	Mesh Size(mm)	Number of Elements	Fundamental Natural Frequency(Hz)	% Error
1	0	0	0	
2	1.9	415210	1344	100
3	1.75	502850	1344.8	0.059
4	1.6	642352	1345.5	0.052

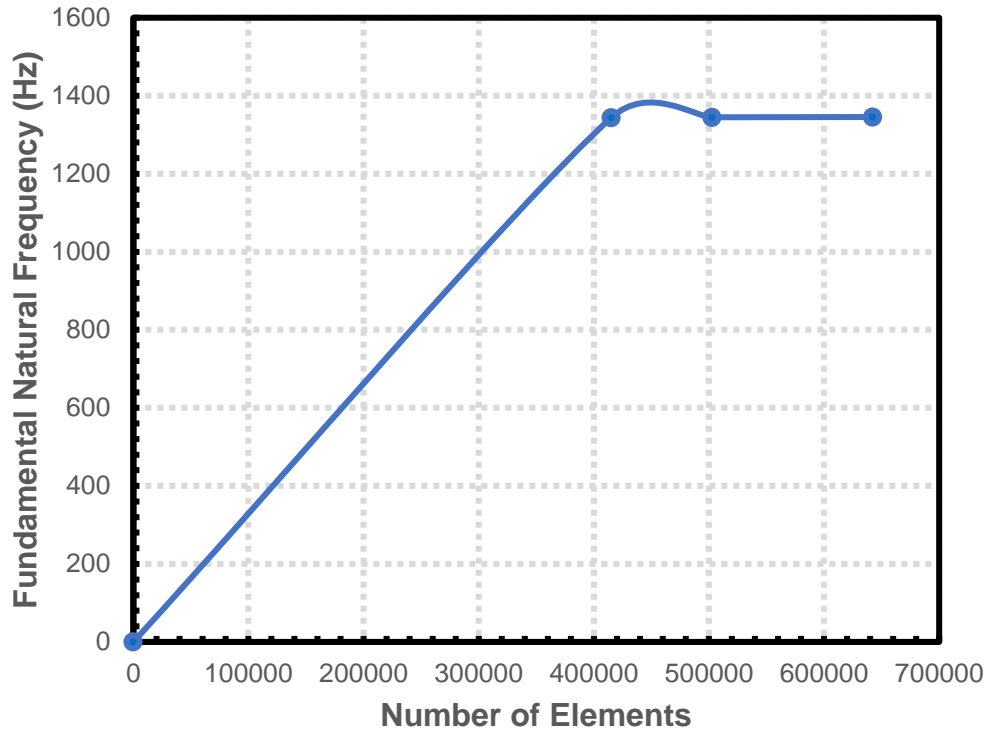


Figure 4-16. Qualitative mesh convergence study for fundamental natural frequency.

Accurate results for bending stresses necessitate the use of quadratic elements from the 3D stress family, specifically the C3D10 element type in Abaqus, as linear elements are inadequate for this purpose. To enhance accuracy and minimize irregularly deformed elements, an additional 94-element seeding is applied around the edges of the hole that supports the contact interaction between the upper control arm and lower control arm pins.

- 2) Arm extension for tie rod and brake caliper mounting arm extension

For the remaining regions, namely "Arm extension for tie rod" and "Brake Caliper Mounting Arm Extension," the geometry exhibits simplicity. Consequently, quadratic hexahedral elements (Abaqus C3D20 elements) are generated using a sweep mesh technique approach. The decision regarding the mesh size, again set at 1.6 mm, is based on the findings of the mesh convergence study presented in Figure 4-16, Table 4-10. The hex mesh reduces the number of elements required for analysis thus reduces computational load. The meshed upright part model is shown in Figure 4-17.

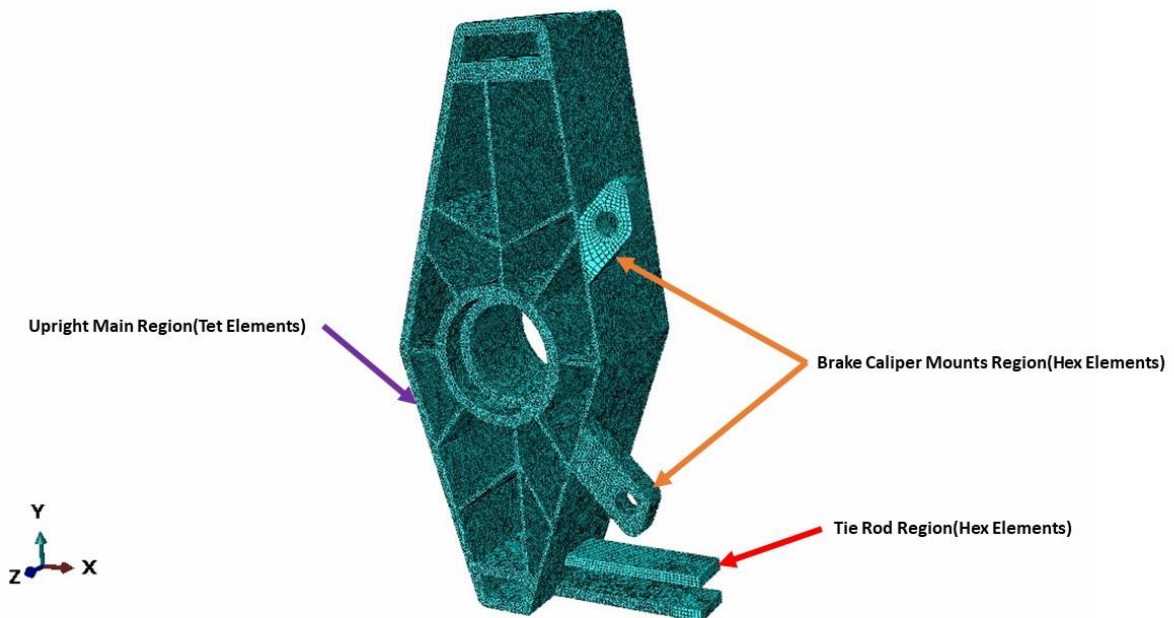


Figure 4-17. Meshed upright part with partitioning.

4.7.2 Mesh and Element Type for Bearings

Bearings used for the analysis have cylindrical shape, so the geometry isn't complex and consequently, quadratic hexahedral elements (Abaqus C3D20 elements) are generated using a sweep mesh technique approach. The element type chosen is quadratic to ensure that the curvature of the bearings is properly represented with lesser elements. The global mesh size is set to 1.6 mm.

The meshed bearing model is shown in Figure 4-18. A summary of the number of elements required for the whole assembly model is given in Table 4-11.



Figure 4-18. Bearing part meshed model.

Table 4-11. Number of nodes and elements in parts of upright.

Sr. No	Part Name	Number of Nodes	Number of Elements
1	Upright	950,000-1,500,000	600,000-950,000
2	Inner bearing	6192	1080
3	Outer Bearing	6192	1080

4.8 Job Creation

After completing the meshing process, the FE model is finalized, enabling the initiation of a job to assess the FE model. To do this, a .INP file is initially generated. This file essentially serves as a text input document containing all the model information needed to describe the finite element model for the Abaqus solver to perform finite element analysis. The Abaqus job subsequently conducts the analysis using this .INP file.

The results of stresses, strains, frequency and displacements are stored in an output database file ('ODB' file) which can be accessed through Abaqus CAE or through python scripting. The parameters chosen for optimization and a detailed explanation of the process of semi-automating the creation of multiple jobs for different parameters and response surface development using Python scripting is discussed in the following chapters.

Chapter 5 Mathematical formulation of the Optimization Problem

In Chapter 4, the finite element model of the upright was made with numerous adjustable features shown in Figure 4-8. These features defined for the parametric FE model will serve as the design variables for optimization of the upright. Figure 5-1 illustrates the DFD for this process. The optimization process will utilize sequential quadratic programming described in Section 2.4 to get the optimized design variables.

The optimization problem's mathematical formulation involves functions related to the objective function and constraints which are then further optimized. As discussed in Section 2.4, sequential quadratic programming utilizes the gradients of the objective function and constraints to get the optimized solution. Different approaches can be applied to use a finite element (FE) model and design variables to get the gradients for optimization. One possible approach involves integrating the FE model into the optimization algorithm. This integration allows for obtaining values from the FE model and gradients for the functions through various methods such as finite differencing, direct differentiation method, and adjoint variable method.

Commonly finite difference method is used to integrate finite element model with the optimization algorithm as its one of the simplest, but adjoint is more computationally efficient if the number of active constraints are less than the number of design variables. In finite difference method it's essential to recognize that using very small step sizes in finite difference differentiation methods for gradient evaluation, particularly in finite element models, may lead to minimal variation in output values. Consequently, this can present challenges for gradient-based optimization algorithms like sequential quadratic programming and hence greater step sizes are utilized. This method though is very useful in FE models with smaller run times.

In this thesis, an alternative method is employed based on response surface methodology (RSM) to create approximate analytical functions for both objective functions and constraints. These response surfaces are approximate or surrogate models that utilize various mathematical and statistical techniques to establish relationships between input variables (referred to as factors) and the corresponding response. These response surfaces ensure that the number of evaluations required from the FE model are limited to the specific design used for constructing the response surface. Also, there won't be an issue of the step size as analytical derivatives would be evaluated through these functions. Though RSM allows the use of analytical derivatives, it is important to

note that continuous refinement and improvement of the representation of the RSM is necessary to obtain accurate results.

Thus, in the sequential quadratic programming algorithm, response surfaces will be developed for the optimization problem's objective function and constraints as shown in Figure 5-1.

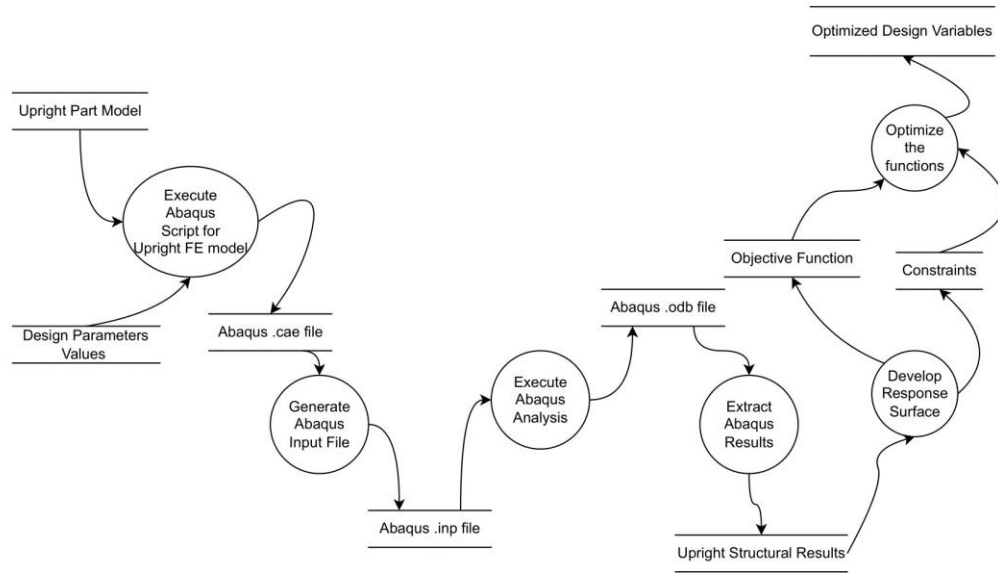


Figure 5-1. DFD of the optimization process.

In this upright there will be three stress constraints at three different points on the upright, and a single displacement constraint at the maximum displacement point. These points are shown in Table 5-2 and Figure 5-2. The mathematical formulation of the optimization problem based on the NLP standard formulation and the objectives in Section 2.3 and Section 3.2 respectively is detailed below:

$$\min f_{weight}(x_1, x_2, x_3)$$

subject to:

$$g_1(x_1, x_2, x_3) = \frac{f_{stress\ point\ VR}(x_1, x_2, x_3)}{\sigma_{yield}} - \frac{1}{FOS_{stress}} \leq 0$$

$$g_2(x_1, x_2, x_3) = \frac{f_{stress\ point\ HR}(x_1, x_2, x_3)}{\sigma_{yield}} - \frac{1}{FOS_{stress}} \leq 0$$

$$g_3(x_1, x_2, x_3) = \frac{f_{\text{stress point AR}}(x_1, x_2, x_3)}{\sigma_{\text{yield}}} - \frac{1}{FOS_{\text{stress}}} \leq 0$$

$$g_4(x_1, x_2, x_3) = \frac{f_{\text{deformation}}(x_1, x_2, x_3)}{u_{\text{allowed}}} - 1 \leq 0$$

$$g_5(x_1, x_2, x_3) = 1 - \frac{f_{\text{fundamental frequency}}(x_1, x_2, x_3)}{f_{\text{minimum natural frequency}}} \leq 0$$

$$g_6(x_1, x_2, x_3) = 1 - \frac{N_{\text{cycles to failure}}(x_1, x_2, x_3)}{N_{\text{minimum cycles}}} \leq 0$$

Table 5-1. Optimization problem variable description.

Variable Name	Description
x_1, x_2, x_3	Three design variables chosen after parameter sensitivity analysis.
FOS_{stress}	Factor of Safety for Stress =1.2
u_{allowed}	Maximum Allowable Deformation of Upright= 0.3 mm
σ_{yield}	Yield stress of Al- 2024 = 303 MPa
$f_{\text{minimum natural frequency}}$	Minimum Allowable First Natural Frequency= 100 Hz
$N_{\text{minimum cycles}}$	Minimum Number of Cycles to Fatigue Failure= 1500 cycles.
$f_{\text{stress point VR}}(x_1, x_2, x_3)$	Response surface of stress for the three design variables at vertical rib root.
$f_{\text{stress point AR}}(x_1, x_2, x_3)$	Response surface of stress for the three design variables at angular rib root.
$f_{\text{stress point HR}}(x_1, x_2, x_3)$	Response surface of stress for the three design variables at horizontal rib root.
$f_{\text{fundamental frequency}}(x_1, x_2, x_3)$	Response surface of fundamental frequency for the three design variables.
$f_{\text{deformation}}(x_1, x_2, x_3)$	Response surface of deformation for the three design variables at displacement point.
$N_{\text{cycles to failure}}(x_1, x_2, x_3)$	Response surface of number of cycles to fatigue failure for the three design variables.

Table 5-2. Stress and displacement points in the upright.

Set Short Name	Set Name
SP-VR	Stress Point at Vertical Rib Root
SP-AR	Stress Point at Angular Rib Root
SP- HR	Stress Point at Horizontal Rib Root
DP	Displacement Point

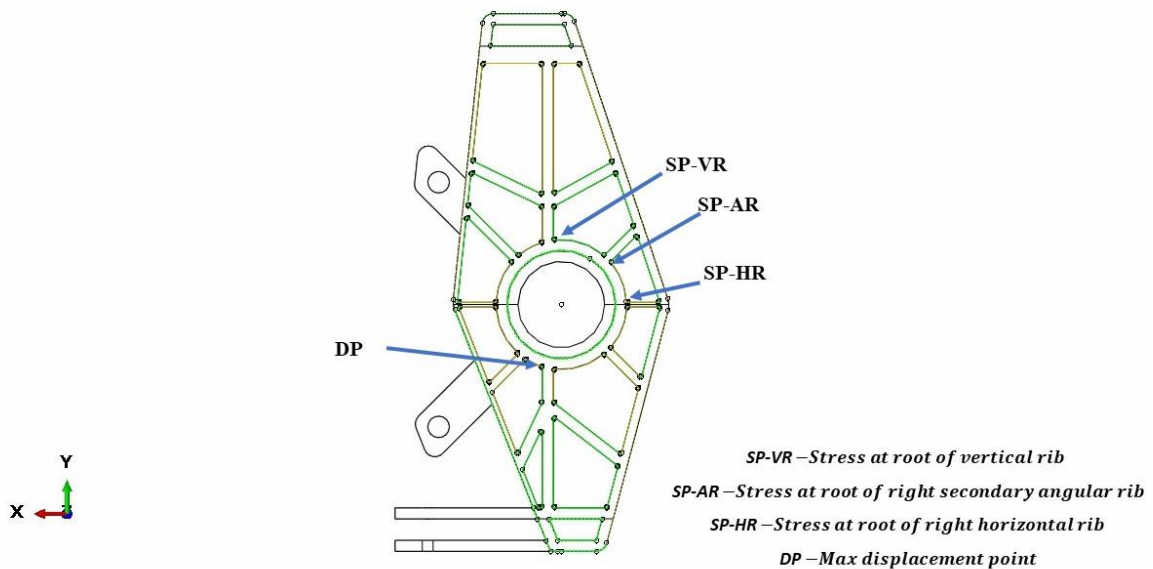


Figure 5-2. Stress and displacement points in the upright.

Chapter 6 and 7 will discuss further on the parameter selection through sensitivity analysis, and the process of development of response surfaces and the specific surfaces developed for optimization of the design variables respectively.

Chapter 6 Parameter selection for optimization

In Chapter 4, the *Final Upright Model* comprises five adjustable features and parameters (Figure 4-8). Modifying these elements can influence the weight of the upright assembly, as well as the stress, deformation, and natural frequency developed in the upright structure. It is imperative to test these structural responses and assess their sensitivity to determine which three parameters to choose for the optimization problem in Chapter 5.

6.1 Upright Baseline Model Chosen for Parameter Sensitivity Analysis

The upright baseline model chosen for parameter sensitivity analysis is like the *Final Upright Model* in Chapter 4, but there is a change in interaction of joint pins in this upright model. Instead of using the general surface to surface interactions for contact, TIE constraints (Section 4.5) shall be used for all the interaction between the upright and pins defined in Section 4.5. These changes were made to reduce the time taken for simulations for the parameter sensitivity analysis.

To evaluate the error in results between tie and surface to surface contact interaction, stresses and displacement magnitude are evaluated at four critical points shown in Figure 5-2 and Table 5-2 respectively using Eq. (6.1) shown in Table 6-1. In both these models with different interactions, the mesh size was kept the same at 1.6 mm for the upright. Though the joint behavior isn't exactly representative of the actual behavior, the results of stress, deformation and first natural frequency have error of less than 10%, justifying the changes with a reduction in analysis time by more than an hour. This upright FE model will be referenced in this chapter as the '*PS_upright*' model.

$$\% \text{ Error} = \frac{\text{Output with only TIE Constraints} - \text{Output with Surface to Surface Interactions}}{\text{Output with Surface to Surface Interactions}} * 100 \quad (6.1)$$

Table 6-1. Comparison of interactions results.

Interaction Type	Tie	General Surface to Surface Interaction	% Error
Stress at Vertical Rib Root(MPa)	413.52	420.1	1.59
Stress at Angular Rib Root(MPa)	448.16	473.99	5.764
Stress at Horizontal Rib Root(MPa)	500.21	512.44	2.447
Displacement Point(mm)	0.41	0.44	6.536
Natural Frequency(Hz)	1121.1	1059.7	5.477
Weight(gms)	840.14	838.63	0.181

6.2 Design Parameters Chosen for the Analysis

There are various design feature parameters which could be tested to selected as design variables. Five design feature parameters were tested within the scope for this thesis. These parameters were limited to changes in the *Cut-extrude* sketch of the upright defining the primary and secondary angular ribs, and the vertical ribs in the upright shown in Figure 6-1 and Figure 6-2. The parameters and their samples for sensitivity analysis are shown in Table 6-2.

Table 6-2. Design parameters to be tested.

Sr. No	Parameter Name	Samples
1	Vertical ribs thickness (t_1)	2 mm, 5 mm, 8 mm
2	Primary angular ribs thickness (t_2)	2 mm, 6 mm, 10 mm
3	Secondary angular ribs thickness (t_3)	2 mm, 6 mm, 10 mm
4	Secondary angular ribs angle (t_4)	20 degrees, 35 degrees, 70 degrees
5	Primary angular ribs angle changer (t_5)	45 mm, 62.5 mm, 80 mm

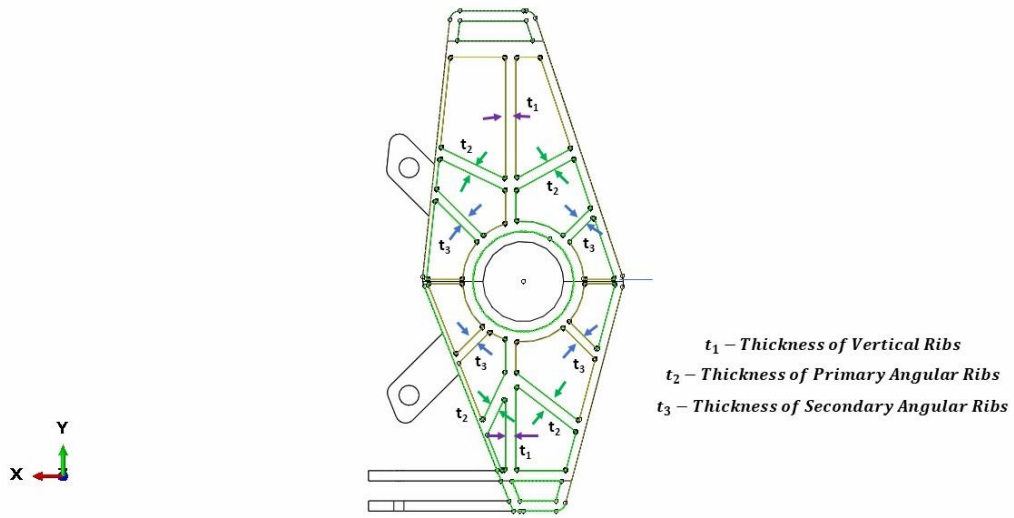


Figure 6-1. Sizing design variables.

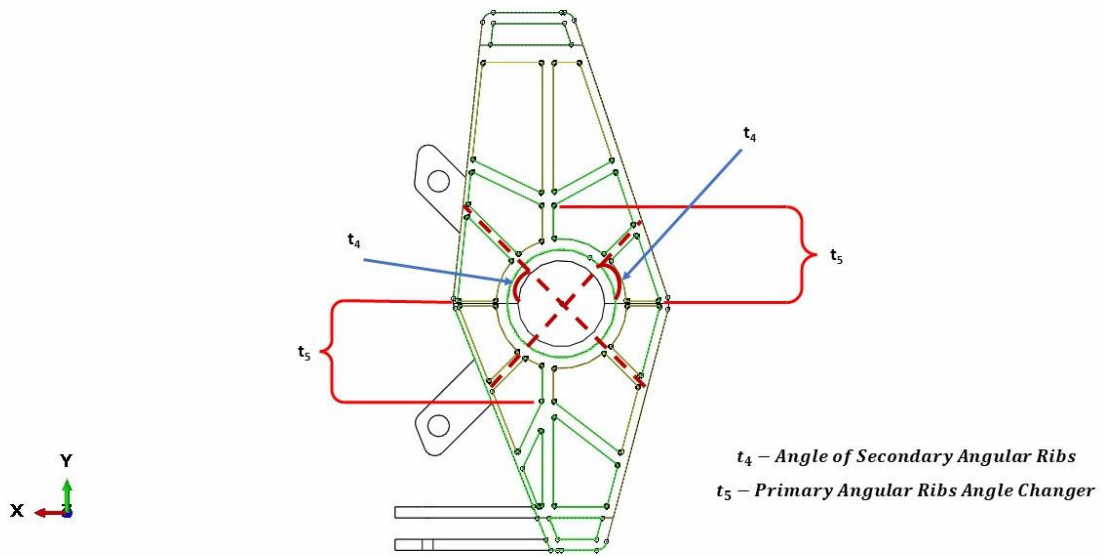


Figure 6-2. Shape design variables.

For the sensitivity analysis different performance indicators were used to test the parameters. The key performance indicators (KPI's) used for the sensitivity analysis are:

1) von Mises Stress: The von Mises stresses at three set points 'SP-VR', 'SP-AR', 'SP-HR' shown in Figure 5-2.

2) Displacement Magnitude: Displacement magnitude at set point 'DP' shown in Figure 5-2 is used for sensitivity analysis.

3) First Natural Frequency: The first natural frequency from the history outputs from frequency step will be extracted and used for sensitivity analysis.

To evaluate the sensitivities the concerned outputs shall be curve fit on a quadratic curve shown in Eq. 6.2:

$$y = ax^2 + bx + c \quad (6.2)$$

In Eq. (6.2), y is the specific output's value; a , b , c are the coefficients of the quadratic curve and x is the design variable value. There could be multiple ways to curve fit, but generally the variable terms are quadratic or linear in nature for stresses and deformations in ribs, and these curve fits are just to see if the parameters are sensitive enough to be used as design variables in the optimization study to follow, so a quadratic estimation is appropriate.

6.3 Script for creating job files and extracting output.

The parameter sensitivity will be conducted using the results extracted by a python script developed to create input files for different samples of the parameter to be tested and extract results for checking sensitivity (*PSanalysis*). This file will use '*input_file_creator*' and '*ODB_extractor*' function modules respectively. The whole '*PSanalysis*' script can be divided into two parts:

1) Job File Creation

2) Results extraction

6.3.1 Job file Creation for Parameter Sensitivity Analysis

The process of creating a job file starts with opening a comma separated variable (CSV) file to store the results for a specific parameter's values. Next, specific values for the design variable to

be analyzed are stored in an array, each with ‘s’ dimensions. Here, ‘s’ signifies the number of samples for the design variable. Then, a new folder is created within the main directory, named after the respective parameter sample value. The working directory is changed to this newly created folder. The current design feature parameter values are given as input to the ‘*input_file_creator*’ module individually. The Data Flow Diagram (DFD) for the ‘*input_file_creator*’ module is shown in Figure 6-3.

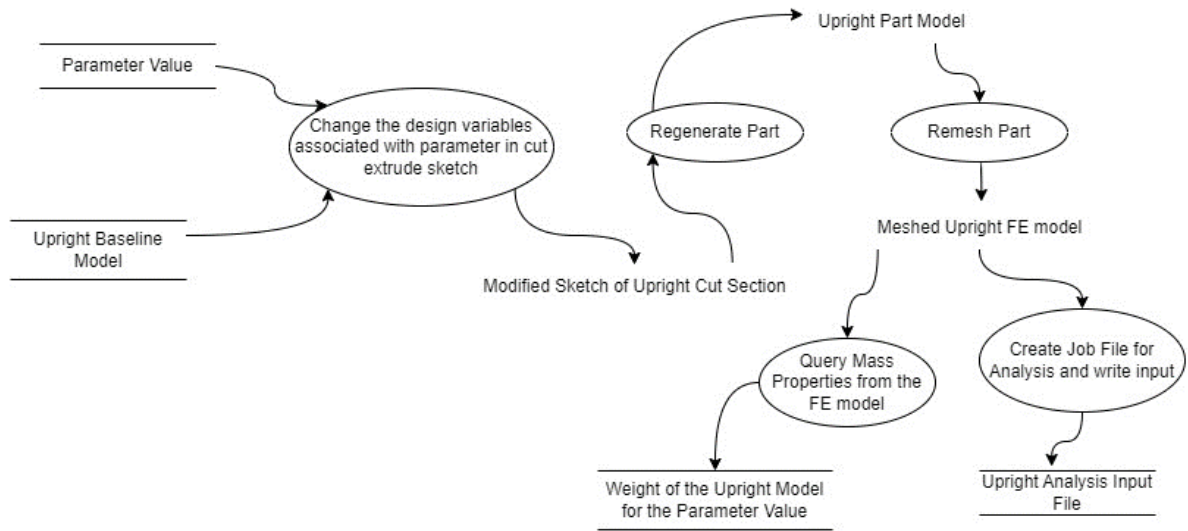


Figure 6-3. DFD for *input_file_creator* module.

In the *input_file_creator* module, firstly the Upright FE model to be used from the main CAE file is accessed (in this chapter *PS_upright*), and the parameter sample values are input. For every sample value associated with the design variable, specific adjustments are applied to the corresponding design variable in the parametrized sketch of the upright part using python scripting functions given by Abaqus [8]. For different parameters the design variable name must be changed in this module. In future work, a data structure could be created which would access all the design variables to be changed and choose the design variable corresponding to the parameter input, instead of changing the design variable manually in the module for each parameter.

As the loads, boundary conditions, and interactions remain constant, the model undergoes remeshing based on the existing mesh criteria after the parameter changes are made to the model. The updated input file is written in this new folder, and the job is submitted for analysis. Once the

job analysis is completed, the module outputs the mass properties. The weight of the upright model is given as output from this module in the *PSanalysis* script.

6.3.2 Results Extraction for Parameter Sensitivity Analysis

Once the analysis has been completed for the specific sample of a parameter to be tested, the results stored in output database files (ODB) will be extracted into the CSV file for further analysis. The results extraction process is performed using the *odbextractor* module within the *PSanalysis* script. The DFD for the *odbextractor* module is shown in Figure 6-4.

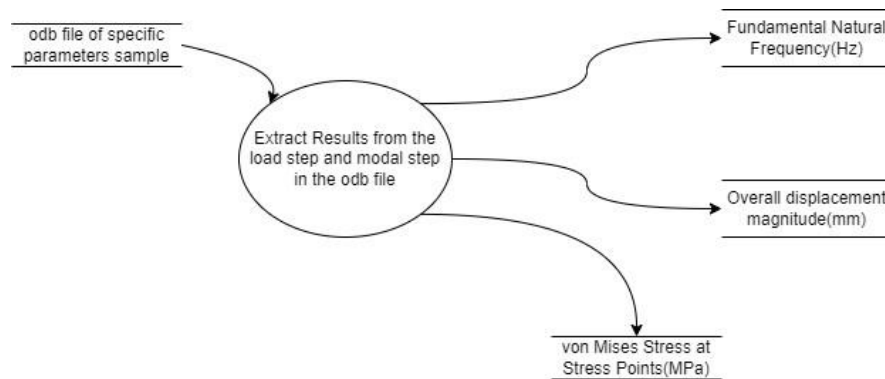


Figure 6-4. DFD for *odbextractor* module.

The extraction procedure commences by opening the ODB file generated following the completion of the analysis for the specific parameter being changed. Subsequently, the user provides the names of sets defined in the *PS_upright* model, where stress, deformation, and frequency need to be evaluated, as input. The module then proceeds to extract stress, deformation, and natural frequency data at these specified points from the static general step and frequency step. This extraction includes von Mises stress, overall deformation magnitude, and first natural frequency, and is carried out using the scripting functions documented in Abaqus[8]. These extracted results, along with the values of the parameter sample, are appended to the CSV file, along with the relevant mass properties extracted in 6.3.1 by the *input_file_creator* module.

Once the analysis and results extraction are completed for all the parameters and their respective samples the script ends. The flowchart for the *PSanalysis* script is provided in Figure 6-5.

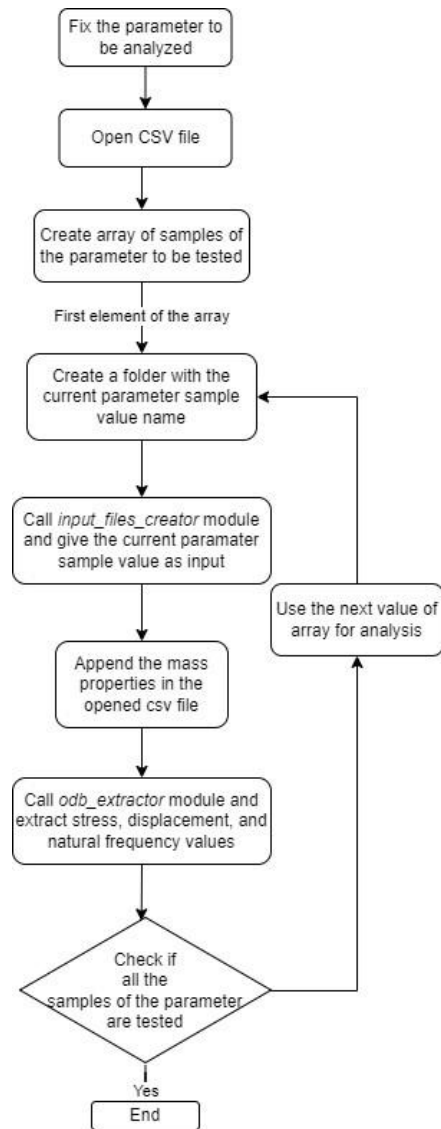


Figure 6-5. Flowchart for '*PSanalysis*' script.

6.4 Parameter Sensitivity Analysis Results

As outlined in Section 6.2, the evaluation of sensitivities for the parameters involves extracting results from three stress points, one displacement point (Figure 5-2), and the first natural frequency from history outputs. There would be qualitative and quantitative analysis conducted for sensitivity analysis. In quantitative analysis the parameters will undergo testing based on two criteria: the percentage change in output values resulting from a variation in parameter values (Eq. 6.3), and the sensitivity of the outputs concerning the parameters. The representation of sensitivity for specific parameter value in the curve fit equation is shown in Eq. (6.4). In Eq. (6.4) the terms a and b are referred from Eq. (6.2).

$$\% \text{ Change} = \frac{\text{Current Parameter Output Value} - \text{Previous Parameter Output Value}}{\text{Previous Parameter Output Value}} * 100 \quad (6.3)$$

$$\text{Sensitivity of output} = \frac{dy}{dx} = 2ax + b \quad (6.4)$$

The sensitivity would be evaluated for the objective function and constraints described in Chapter 5, to check if the design variables are sensitive enough to be used in the optimization problem. To plot the outputs for qualitative analysis, given the diverse scales of displacements, stresses, weight, and natural frequency, normalization is necessary. Stresses are normalized by the allowable stresses, converting to their respective factors of safety (FOS) using Eq. (6.5), while displacements are normalized by allowable displacements leading to computing their FOS using Eq. (6.6). Normalization of both natural frequency and weight is achieved by dividing them by the 1000 shown in Eq. (6.7) and Eq. (6.8) respectively. This process for qualitative analysis will be followed for all other parameters too.

$$FOS_{stress} = \frac{\sigma_{yield} (MPa)}{\sigma_{stress\ point} (MPa) * FOS_{allowed}} \quad (6.5)$$

where $FOS_{allowed} = 1.2 \text{ MPa}$ and $\sigma_{stress\ point}$ – stress at the specific stress point

$$FOS_{displacement} = \frac{u_{max} (mm)}{u_{displacement\ point} (mm)} \quad \text{where } u_{max} = 0.3 \text{ mm} \quad (6.6)$$

$$\text{Normalized First Natural Frequency} = \frac{\text{First Natural Frequency (Hz)}}{1000} \quad (6.7)$$

$$\text{Normalized Weight} = \frac{\text{Weight (gms)}}{1000} \quad (6.8)$$

6.4.1 Vertical Ribs Thickness Sensitivity Results

Table 6-3, Table 6-4, and Figure 6-6 present the quantitative and qualitative analyses of stresses, displacements, first natural frequency, and sensitivity results for various vertical rib thicknesses.

Table 6-3. Outputs and percentage change in outputs for varying vertical rib thickness.

Parameter Value (mm)	Vertical Rib Thickness			Total % Range from 2mm to 8mm
	2	5	8	
Stress at Vertical Rib Root(MPa)	259.946	264.997	209.021	
Stress at Angular Rib Root(MPa)	539.498	346.910	247.316	
Stress at Horizontal Rib Root(MPa)	634.403	374.802	231.484	
Displacement Point(mm)	0.469	0.300	0.210	
First Natural Frequency(Hz)	1107.300	1185.300	1235.900	
Weight(gms)	869.393	939.065	1008.920	
% Change in Stress at Vertical Rib Root	-	1.94	-21.12	-19.591
% Change Stress at Angular Rib Root	-	-35.70	-28.71	-54.158
% Change in Stress at Horizontal Rib Root	-	-40.92	-38.24	-63.512
% Change in Displacement Point	-	-36.06	-29.97	-55.226
% Change in First Natural Frequency	-	7.04	4.27	11.614
% Change in Weight	-	8.01	7.44	16.049

Table 6-4. Sensitivity of outputs for varying vertical rib thickness.

Parameter Value(mm)	Vertical Rib Thickness		
	2	5	8
Stress Constraint Sensitivity of Vertical Rib Root	0.021	-0.010	-0.042
Stress Constraint Sensitivity at Angular Rib Root	-0.267	-0.157	-0.047
Stress Constraint Sensitivity at Horizontal Rib Root	-0.357	-0.214	-0.071
Displacement Constraint Sensitivity at Displacement Point	-0.236	-0.140	-0.044
First Natural Frequency Constraint Sensitivity	0.320	0.200	0.081
Weight Objective Function Sensitivity(gms)	26.694	19.754	12.814

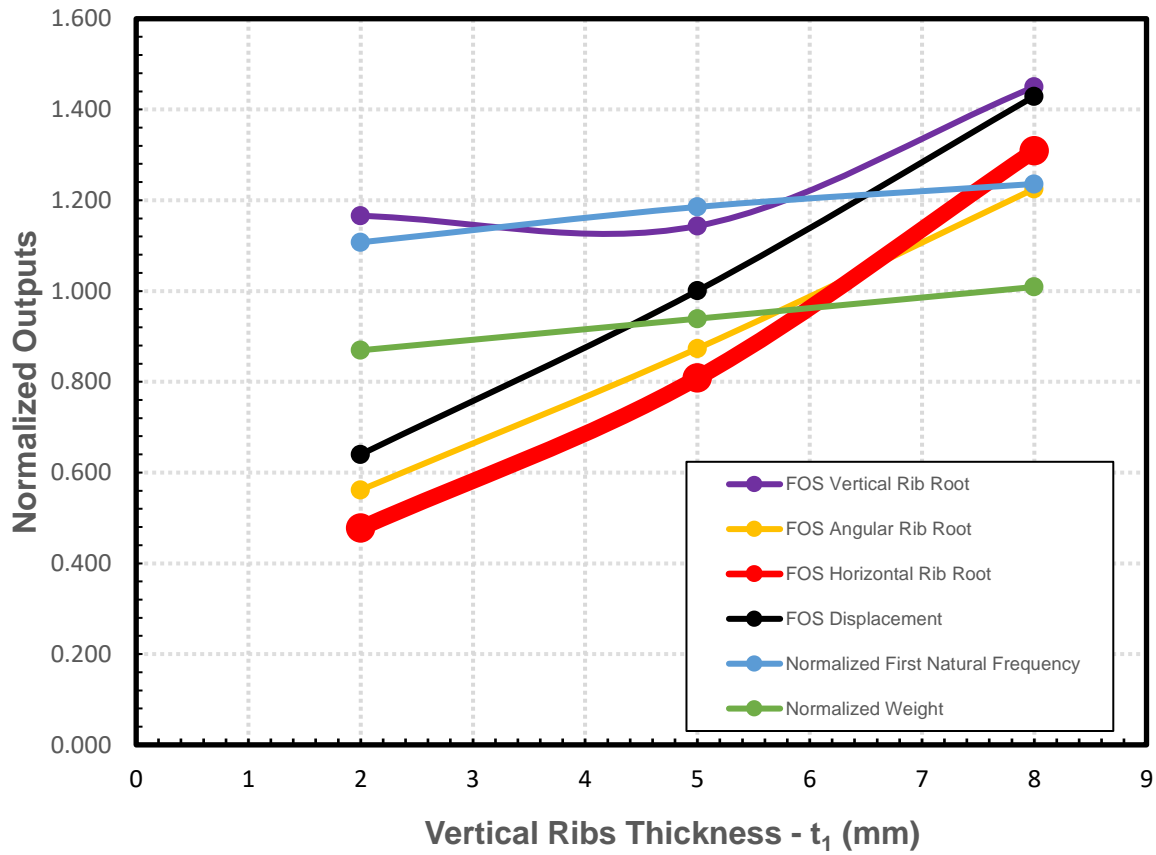


Figure 6-6. Qualitative analysis plot of varying vertical rib thicknesses.

The coefficients of the curve-fit equations as per Eq. (6.2) for vertical rib thickness as design variables are given in Table 6-5.

Table 6-5. Curve fit coefficients of outputs for varying vertical rib thickness.

	a	b	c
Stress at Vertical Rib Root	-1.610	12.953	240.480
Stress at Angular Rib Root	5.535	-102.939	723.237
Stress at Horizontal Rib Root	7.234	-137.170	879.808
Displacement Point	0.005	-0.090	0.630
First Natural Frequency	-1.985	39.895	1035.450
Weight	-1.157	31.320	811.379

The results indicate a maximum 8% change in weight when vertical rib thickness increased from lowest to highest value, and a maximum 41 % and 36% change in stresses and displacements respectively when the vertical ribs thickness value increases from 2 mm to 10 mm. The impact of this design feature parameter on stresses and displacements is critical and would impact the design.

The sensitivity analysis of constraints reveals that stress at the angular rib root and horizontal rib root, as well as displacement constraints at the lowest thicknesses, exhibit sensitivities of -0.267, -0.357, and -0.236 respectively. As the thickness increases, these sensitivities reduce to -0.047, -0.071, and -0.044. These sensitivity values are crucial because, for the Sequential Quadratic Programming (SQP) algorithm, flat constraints with near-zero sensitivity from lower to higher parameter values can disrupt proper functioning. Although the sensitivity values may appear small, the magnitudes are small due to constraint normalization.

6.4.2 Primary Angular Ribs Thickness Sensitivity Results

Table 6-6, Table 6-7, and Figure 6-7 present the quantitative and qualitative analyses of stresses, displacements, first natural frequency, and sensitivity results for various primary angular thicknesses.

Table 6-6. Outputs and percentage change in outputs for varying primary angular rib thickness.

Parameter Value(mm)	Primary Angular Rib Thickness			Total % Range from 2mm to 10mm
	2	6	10	
Stress at Vertical Rib Root(MPa)	239.668	266.730	280.294	
Stress at Angular Rib Root(MPa)	539.847	516.370	581.636	
Stress at Horizontal Rib Root(MPa)	618.311	641.446	628.940	
Displacement Point(mm)	0.479	0.460	0.447	
First Natural Frequency(Hz)	1116.900	1099.200	1086.100	
Weight(gms)	832.621	905.361	975.125	
% Change in Stress at Vertical Rib Root	-	11.291	5.085	
% Change Stress at Angular Rib Root	-	-4.349	12.639	7.741
% Change in Stress at Horizontal Rib Root	-	3.742	-1.950	1.719
% Change in Displacement Point	-	-3.889	-2.970	-6.744
% Change in First Natural Frequency	-	-1.585	-1.192	-2.758
% Change in Weight	-	8.736	7.706	17.115

Table 6-7. Sensitivity of outputs for varying primary angular rib thickness.

Parameter Value(mm)	Primary Angular Rib Thickness		
	2	6	10
Stress Constraint Sensitivity of Vertical Rib Root	0.028	0.017	0.006
Stress Constraint Sensitivity at Angular Rib Root	-0.056	0.017	0.090
Stress Constraint Sensitivity at Horizontal Rib Root	0.034	0.004	-0.025
Displacement Constraint Sensitivity at Displacement Point	-0.018	-0.013	-0.009
First Natural Frequency Constraint Sensitivity	-0.050	-0.039	-0.027
Weight Objective Function Sensitivity(gms)	18.557	17.813	17.069

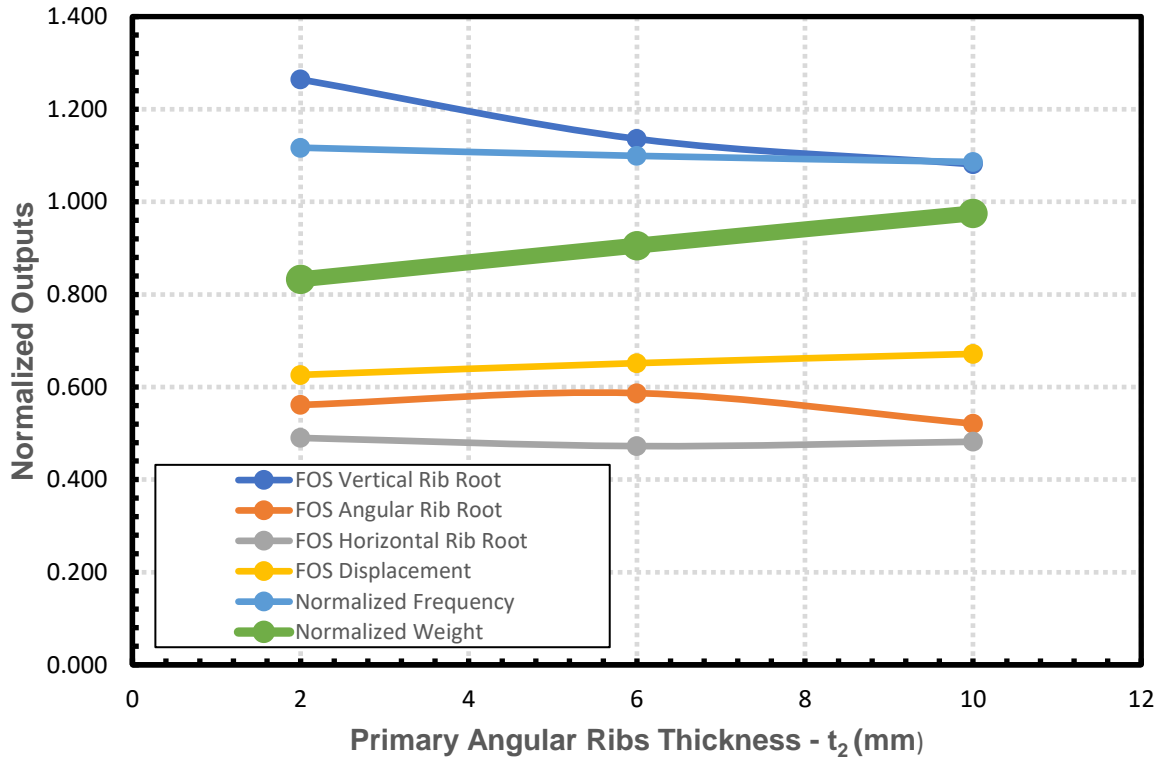


Figure 6-7. Qualitative analysis plot of varying primary angular rib thicknesses.

The coefficients of the curve fit equations as per Eq. (6.2) for primary angular rib thickness as design variables is given in Table 6-8.

Table 6-8. Curve fit coefficients of outputs for varying primary angular rib thickness.

	a	b	c
Stress at Vertical Rib Root	-0.422	10.140	221.075
Stress at Angular Rib Root	2.773	-28.055	584.864
Stress at Horizontal Rib Root	-1.114	14.694	593.378
Displacement Point	0.000	-0.006	0.490
First Natural Frequency	0.144	-5.575	1127.475
Weight	-0.093	18.929	795.135

The results indicate a weight change of approximately 8% in relation to the thickness of primary angular ribs. The impact on stress is smaller compared to the vertical rib thicknesses with maximum change of 12% in stresses. The change in deformation magnitude is also minimal as compared to changes caused due to vertical rib thickness. The interesting point to note is that stress increases marginally when the thickness of the primary angular ribs increases. The sensitivity analysis and the qualitative analysis plots also show that the constraint surfaces are nearly flat, but the objective function sensitivity is similar to that shown by vertical rib thickness and could be useful to minimize weight.

While the primary rib thickness's dependency on angle remains beyond the current scope of this work, exploring the two-factor interactions between primary rib thickness and its angle could offer better insights on the current minimal impact of the primary angular rib thickness on stresses and displacement. Given the limited impact on constraints but a similar impact as the vertical rib thickness, it may be advisable to combine this design variable with vertical rib thickness to leverage the advantageous impact on weight.

6.4.3 Secondary Angular Ribs Thickness Sensitivity Results

Table 6-9, Table 6-10, and Figure 6-8 present the quantitative and qualitative analyses of stresses, displacements, first natural frequency, and sensitivity results for various secondary angular thicknesses.

Table 6-9. Outputs and percentage change in outputs for varying secondary angular rib thickness.

Parameter Value(mm)	Secondary Angular Ribs Thickness			Total % Range from 2mm to 10mm
	2	6	10	
Stress at Vertical Rib Root(MPa)	229.766	91.686	67.098	
Stress at Angular Rib Root(MPa)	536.022	199.693	106.072	
Stress at Horizontal Rib Root(MPa)	631.086	119.482	41.681	
Displacement Point(mm)	0.496	0.173	0.120	
First Natural Frequency(Hz)	1117.400	1138.900	1139.200	
Weight(gms)	834.233	894.050	954.404	
% Change in Stress at Vertical Rib Root	-	-60.096	-26.817	-70.797
% Change Stress at Angular Rib Root	-	-62.745	-46.882	-80.211
% Change in Stress at Horizontal Rib Root	-	-81.067	-65.115	-93.395
% Change in Displacement Point	-	-65.057	-30.736	-75.797
% Change in Natural Frequency	-	1.924	0.026	1.951
% Change in Weight	-	7.170	6.751	14.405

Table 6-10. Sensitivity of outputs for varying secondary angular rib thickness.

Parameter Value(mm)	Secondary Angular Ribs Thickness		
	2	6	10
Stress Constraint Sensitivity of Vertical Rib Root	-0.161	-0.067	0.027
Stress Constraint Sensitivity at Angular Rib Root	-0.378	-0.177	0.023
Stress Constraint Sensitivity at Horizontal Rib Root	-0.601	-0.243	0.115
Displacement Constraint Sensitivity at Displacement Point	-0.381	-0.157	0.020
First Natural Frequency Constraint Sensitivity	0.080	0.027	-0.026
Weight Objective Function Sensitivity(gms)	14.887	15.021	15.156

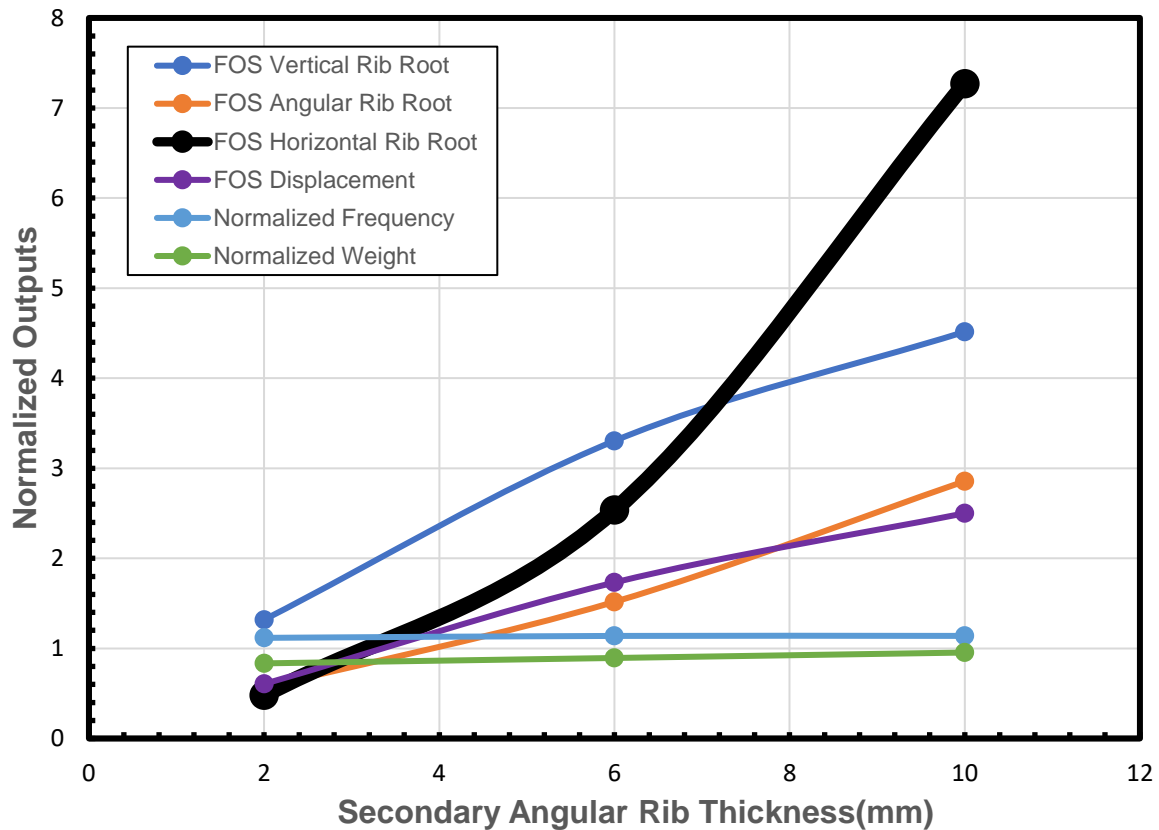


Figure 6-8. Qualitative analysis plot of varying secondary angular rib thicknesses.

The coefficients of the curve fit equations as per Eq. (6.2) for secondary angular rib thickness is given in Table 6-11.

Table 6-11. Curve fit coefficients of outputs for varying secondary angular rib thickness.

	a	b	c
Stress at Vertical Rib Root	3.547	-62.893	341.366
Stress at Angular Rib Root	7.585	-144.759	795.202
Stress at Horizontal Rib Root	13.556	-236.352	1049.564
Displacement Point	0.008	-0.148	0.758
First Natural Frequency	-0.663	10.675	1098.700
Weight	0.017	14.820	804.526

The percentage change and sensitivity results indicate that the thickness of secondary angular ribs exerts significant influence on both stresses and displacements, exhibiting maximum reduction in stress of 81% and displacement of 65%, respectively. This may be attributed to its reinforcing

effect on the upright, particularly in mitigating bending stresses induced by both cornering and braking due to it being angular. Consequently, optimizing this variable holds substantial potential for enhancing overall performance. The impact of the secondary angular ribs thickness on weight is similar to that of vertical rib thickness and primary angular rib thickness, and its impact on natural frequency also remains minimal.

6.4.4 Secondary Angular Ribs Angle Sensitivity Results

Table 6-12, Table 6-13, and Figure 6-9 present the quantitative and qualitative analyses of stresses, displacements, first natural frequency, and sensitivity results for various secondary angular ribs angles values.

Table 6-12. Outputs and percentage change in outputs for varying secondary angular rib angles.

Parameter Value(degrees)	Secondary Angular Ribs Angle			Total % Range from 20 degrees to 50 degrees
	20	35	50	
Stress at Vertical Rib Root(MPa)	174.217	229.960	239.134	
Stress at Angular Rib Root(MPa)	552.859	591.484	510.306	
Stress at Horizontal Rib Root(MPa)	411.849	516.736	689.059	
Displacement Point(mm)	0.409	0.422	0.544	
First Natural Frequency(Hz)	998.060	1072.000	1124.400	
Weight(gms)	827.974	829.959	837.584	
% Change in Stress at Vertical Rib Root		31.996	3.989	37.262
% Change Stress at Angular Rib Root		6.986	-13.724	-7.697
% Change in Stress at Horizontal Rib Root		25.467	33.348	67.309
% Change in Displacement Point		3.313	28.805	33.073
% Change in First Natural Frequency		7.408	4.888	12.659
% Change in Weight		0.240	0.919	1.161

Table 6-13. Sensitivity of outputs for varying secondary angular rib angles.

Parameter Value	Secondary Angular Ribs Angle		
	20	35	50
Stress Constraint Sensitivity of Vertical Rib Root	0.017	0.007	-0.003
Stress Constraint Sensitivity at Angular Rib Root	0.022	-0.005	-0.031
Stress Constraint Sensitivity at Horizontal Rib Root	0.016	0.030	0.045
Displacement Constraint Sensitivity at Displacement Point	-0.009	0.015	0.039
First Natural Frequency Constraint Sensitivity	0.056	0.042	0.028
Weight Objective Function Sensitivity(gms)	-0.056	0.320	0.696

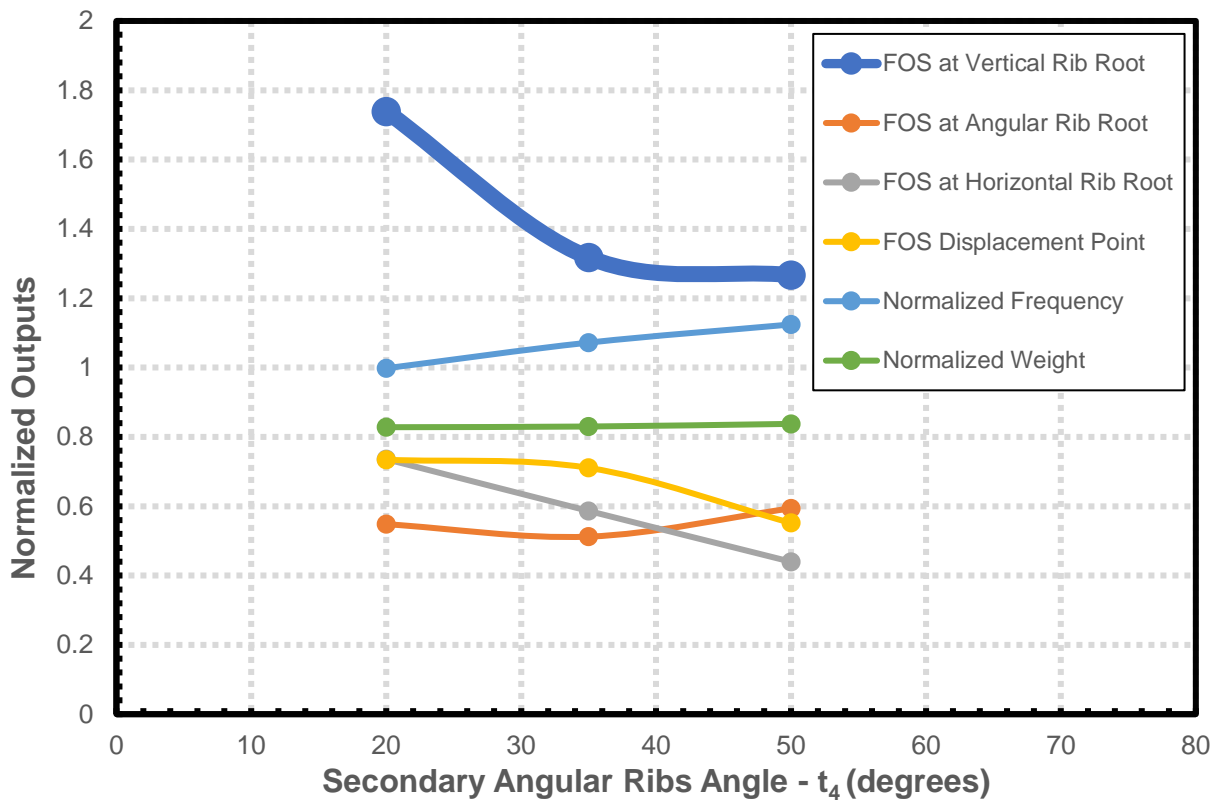


Figure 6-9. Qualitative analysis plot of varying secondary angular ribs angles.

The coefficients of the curve fit equations as per Eq. (6.2) for varying secondary angular ribs angle is given in Table 6-14.

Table 6-14. Curve fit coefficients of outputs for varying secondary angular rib angles.

	a	b	c
Stress at Vertical Rib Root	-0.103	9.408	27.452
Stress at Angular Rib Root	-0.266	17.218	314.999
Stress at Horizontal Rib Root	0.150	-1.250	376.900
Displacement Point	0.000	-0.012	0.559
First Natural Frequency	-0.048	7.562	865.967
Weight	0.013	-0.557	834.101

The key findings from sensitivity analysis of secondary angular ribs angle are:

- 1) The angle of secondary angular ribs have an impact on the stresses, with maximum 32% increase and 34% increase in stress at vertical rib root and horizontal rib root respectively.
- 2) There is an impact on the displacement too with an increasing trend and a maximum 29% increase in displacement when angle of secondary ribs is increased.
- 3) Though % change shows the impact of the thickness of the secondary angular ribs on stress and displacement but in the sensitivity analysis the values are less than 0.1.
- 4) Though these trends are promising, these ribs could be used to create a direct load path from the wheel hub to the brake caliper mount distributing the load better in the upright.

6.4.5 Primary Angular Ribs Angle Changer Sensitivity Results

Table 6-15, Table 6-16, and Figure 6-10 present the quantitative and qualitative analyses of stresses, displacements, first natural frequency, and sensitivity results for various primary angular ribs angle changer values. The qualitative analysis for the outputs has been conducted as explained in section 6.4.1.

Table 6-15. Outputs and percentage change in outputs for varying primary angular ribs angle changer values.

Parameter Value(mm)	Primary Angular Ribs Angle Changer			
	45	62.5	80	
Stress at Vertical Rib Root(MPa)	413.521	227.647	148.518	Total % Range from 45 mm to 80 mm
Stress at Angular Rib Root(MPa)	448.161	538.901	566.615	
Stress at Horizontal Rib Root(MPa)	500.205	620.146	661.300	
Displacement Point(mm)	0.414	0.496	0.512	
First Natural Frequency(Hz)	1121.100	1117.800	1126.300	
Weight(gms)	840.142	834.233	842.590	
% Change in Stress at Vertical Rib Root		-44.949	-34.760	-64.085
% Change Stress at Angular Rib Root		20.247	5.143	26.431
% Change in Stress at Horizontal Rib Root		23.978	6.636	32.206
% Change in Displacement Point		19.812	3.304	23.771
% Change in First Natural Frequency		-0.294	0.760	0.464
% Change in Weight		-0.703	1.002	0.291

Table 6-16. Sensitivity of outputs for varying primary angular ribs angle changer values.

Parameter Value(mm)	Primary Angular Ribs Angle Changer		
	45	62.5	80
Stress Constraint Sensitivity of Vertical Rib Root	-0.045	-0.025	-0.005
Stress Constraint Sensitivity at Angular Rib Root	0.023	0.011	-0.001
Stress Constraint Sensitivity at Horizontal Rib Root	0.030	0.015	0.000
Displacement Constraint Sensitivity at Displacement Point	0.022	0.009	-0.003
First Natural Frequency Constraint Sensitivity	-0.005	0.001	0.008
Weight Objective Function Sensitivity(gms)	-0.745	0.070	0.885

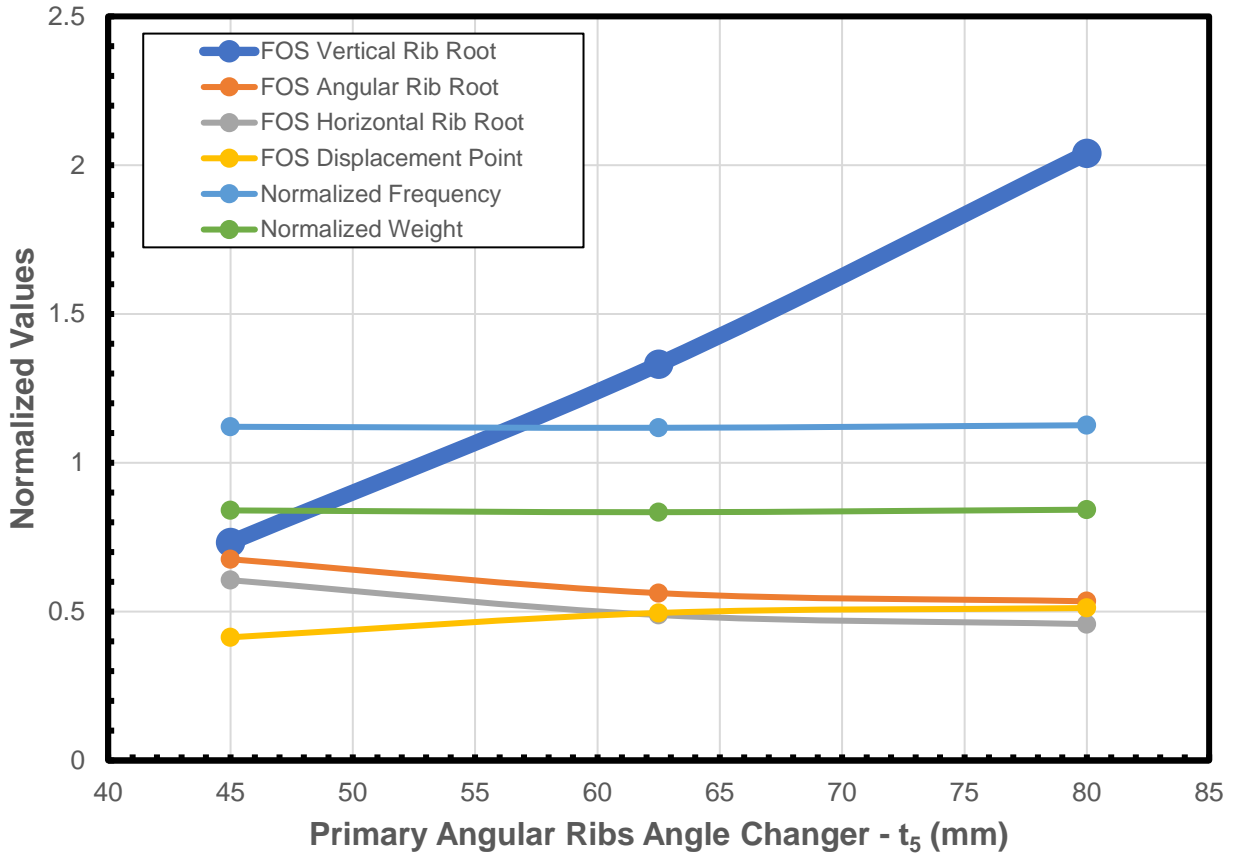


Figure 6-10. Qualitative analysis plot of varying primary angular ribs angle changer values.

The coefficients of the curve fit equations as per Eq. (6.2) for primary angular ribs angle changer is given in Table 6-17.

Table 6-17. Curve fit coefficients of outputs for varying primary angular rib angle changer values.

	a	b	c
Stress at Vertical Rib Root	0.174	-29.356	1381.638
Stress at Angular Rib Root	-0.103	16.247	-74.576
Stress at Horizontal Rib Root	-0.129	20.682	-169.992
Displacement Point	0.000	0.016	-0.098
Natural Frequency	0.019	-2.260	1183.769
Weight	0.023	-2.841	920.844

The key findings from the sensitivity analysis of primary angular ribs angle changer are:

- 1) The primary angular ribs angle changer value has a impact on the stress levels at the vertical rib root, resulting in a notable 44% reduction in stresses with increase in the values of the primary ribs' angle changer. This suggests that configuring the ribs at an angle away from the wheel hub contributes to a reduction of stresses at the vertical rib root. Conversely, for the angular rib root and horizontal rib root stresses, an elevation in the primary angular rib angle changer value leads to an approximate 20% increase in stresses, indicating a contrasting trend compared to that observed for the vertical rib root.
- 2) The displacement, weight, and first natural frequency have minimal changes. The angle of primary angular ribs could be helpful in deciding an optimal configuration to ensure stresses are below the maximum stress value allowed, but its impact on weight, displacement would be very low.

6.5 Final Design Parameters Chosen

The final parameters chosen for further optimization (Figure 6-11) are:

1. Thickness of vertical and primary angular ribs (x_1):

The integration of the thicknesses of vertical and primary angular ribs into a singular variable has been chosen to enhance the sensitivity of the upright's weight. This decision is supported by the observation that vertical ribs lower the stresses, and displacement, while primary angular ribs exhibit comparatively less influence on the stress, displacement, and natural frequency examined during the design sensitivity analysis, as detailed in Section 6.4.1 and Section 6.4.2. Another approach might have been to designate the primary angular ribs' thickness at its minimum value. However, this design variable is combined with the thickness of vertical ribs to maintain symmetry, thus simplifying the part parameterization process.

2. Thickness of Secondary Angular Ribs (x_2):

The change of thickness of secondary angular ribs had the most impact on the structural responses studied in Section 6.4.3 and hence was chosen for further optimization.

3. Primary Angular Ribs Angle Changer (x_3):

The primary angular ribs' angle had similar impact on the stresses compared to that of the secondary angular ribs, but the angle of the secondary angular ribs was chosen to be fixed to the angle of the brake caliper mounts(45 degrees) to create a direct load path radially from the wheel hub center to the brake caliper when braking and cornering. Hence the primary angular ribs are chosen to be further optimized and secondary angular ribs are fixed to the angle of brake caliper mounts i.e. 45 degrees.

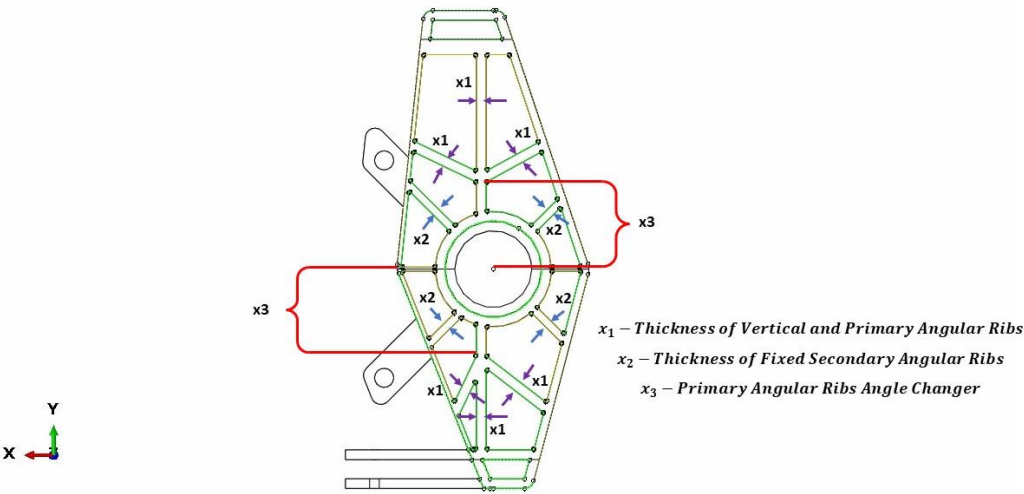


Figure 6-11. Final parameters selected for optimization.

Chapter 7 Response Surface Development

This chapter will explore the development of response surfaces for the three design variables chosen in Chapter 6 for stress, displacement, first natural frequency and fatigue constraints to be utilized in the mathematical formulation of the optimization problem described in Chapter 5.

A few characteristics of the response surface model which will be used in this thesis are as follows:

- 1) Based on the scope of the thesis, a second order model limited to two factor interactions is used to generate the response surface and a three-level factorial design is used for the same.
- 2) The goodness of fit of the response surfaces will be tested by evaluation of the coefficient of determination (R^2) value for each response surface (Section 7.1.4). The minimum R^2 value is kept as 0.85 before being used in the optimization algorithm.

7.1 Overall Procedure of Response Surface Development

The DFD of the process of response surface development is shown in Figure 7-1. To start the response surface development, the design variables need to be sampled. In this thesis a three-level factorial design is used.

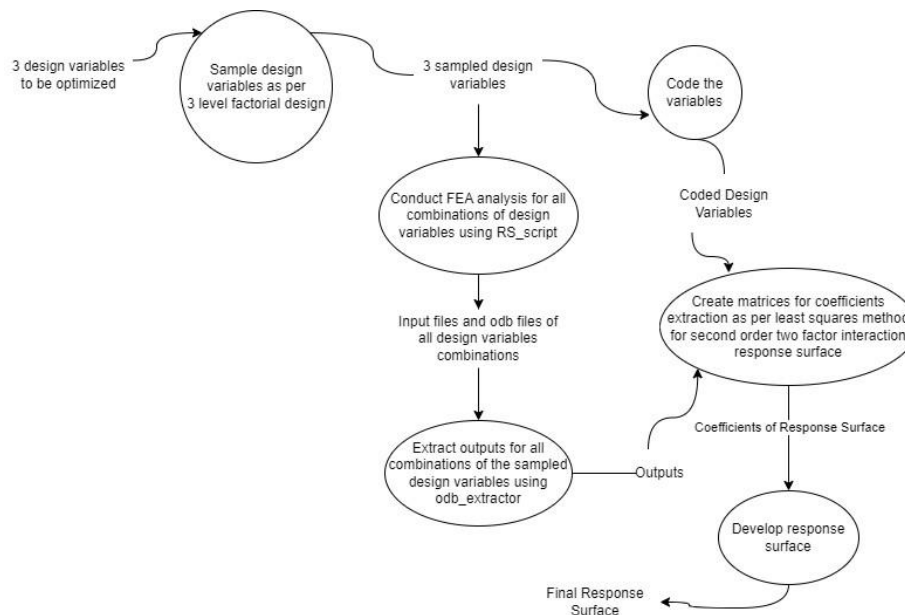


Figure 7-1. DFD of process of response surface development.

7.1.1 Three-Level Factorial Design

A three-level factorial design is a 3^k factorial design where all the combinations of k factors are considered with each factor having three levels. These three levels are low, mid and high levels. The factors are the input, or the design variables and levels are the samples used for the factor in a specific design. A pictorial representation of a three-level factorial design is shown in Figure 7-2.

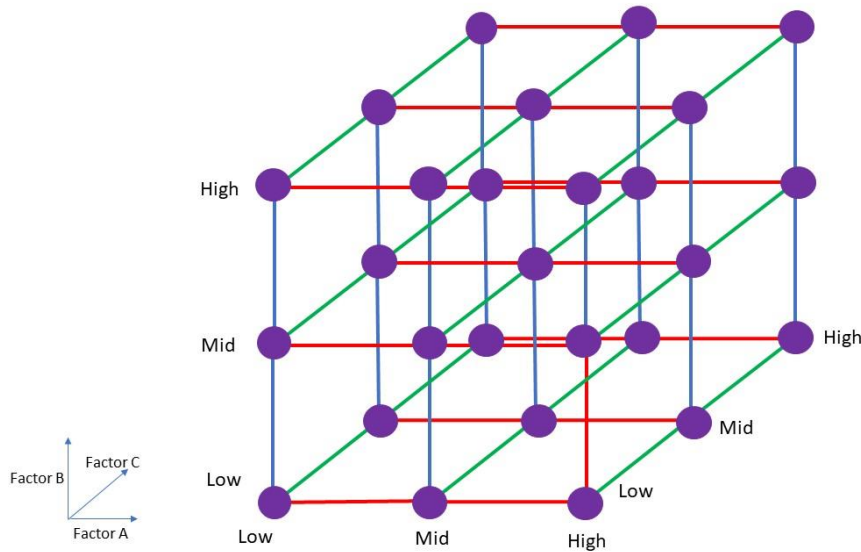


Figure 7-2. Three-level factorial design graphical representation.

A three-level factorial design is employed to capture the curvature of the response model using the center or midpoints for each factor. To enhance model fit, increasing the number of points through the three-level factorial design, as opposed to a two-level factorial design, is beneficial for capturing more information and improving the R^2 value. Ideally, consideration of three-factor interactions and continuous model updates are recommended to refine the response surface model. However, for this thesis, the focus is restricted to two-factor interactions, and a single response surface model is generated for each output.

For the final design variables described in Section 6.5, the levels for three level factorial design are shown in Table 7-1. These input values for the response surface would be coded such that

lowest level has value -1, mid value has value 0 and highest value has value 1. This conversion for a variable is done using Eq.7.1. In Eq. 7.1 ‘x’ denotes the specific parameter’s actual value or decoded value, x_{max} is the maximum value or the highest value of the parameter and x_{min} is the minimum or the lowest value of the parameter. So, the equations for the three design variables are shown in Eq. (7.2), Eq. (7.3), Eq. (7.4).

$$x_{coded} = \frac{x - \frac{x_{max} + x_{min}}{2}}{\frac{x_{max} - x_{min}}{2}} \quad (7.1)$$

$$x_{1coded} = \frac{x_1 - 5}{3} \quad (7.2)$$

$$x_{2coded} = \frac{x_2 - 6}{4} \quad (7.3)$$

$$x_{3coded} = \frac{x_3 - 62.5}{17.5} \quad (7.4)$$

Table 7-1. Three level factorial design for final design variables.

Parameter Name	Three-Level Factorial Design Levels		
	Low	Mid	High
Thickness of Vertical and Primary Angular Ribs - x1(mm)	2	5	8
Thickness of Secondary Angular Ribs - x2(mm)	2	6	10
Primary Angular Ribs Angle Changer - x3(mm)	45	62.5	80

7.1.2 Output extraction for all combinations of the design variables

The sampled design variables now will have 3^3 combinations, as there are 3 factors and 3 levels. So, to generate a response surface, finite element (FE) analysis for all these combinations needs to be conducted followed by output extraction from the ODB files, which would finally be stored in a CSV file. To aid this a python script is developed named *RS_script* which uses modules *input_files_creator* and *odbextractor* used in Section 5.3. This script is like *PSanalysis* script used

in Section 5.3 but in this case instead of evaluating for a single design variable at time, all the combinations of sampled design variables are considered. The modules *input_files_creator* and *odb_extractor* are adapted to take three variables as input and to provide the respective output.

7.1.3 Response Surface Development

Once all the outputs are evaluated, the response surface for a second order model limited to two factor interactions can be created. The equation representing this second order model is shown in Eq. (7.5).

$$y = a_1 + a_2 * x_1 + a_3 * x_2 + a_4 * x_3 + a_5 * x_1^2 + a_6 * x_2^2 + a_7 * x_3^2 + a_8 * x_1 * x_2 + a_9 * x_1 * x_3 + a_{10} * x_2 * x_3 \quad (7.5)$$

To evaluate the coefficients in Eq. 7.5, the least squares method is used. The method of least squares chooses the coefficient values such that the sum of squares of the errors between the observations and the values from equations are minimized. The process for extracting the coefficient values using least squares method is as follows:

- 1) Eq. (7.5) is written in a standardized format as shown in Eq. (7.6). In Eq. 7.6, y_n represents the n th observation output, and the variables in Eq. (7.5) are converted as x_{ni} which represents the n th observation value of the i th variable in the equation. As observed in Eq. (7.5), there are a total of 10 variables consisting of different combinations of the three variables shown in Eq. (7.5). The coefficients are now represented as ‘ β ’ in Eq. (7.6) instead of ‘ a ’ as given in Eq. (7.5). The error is the additional term which will be minimized.
- 2) The equations for all the 27 observations in matrix form as shown in Eq. (7.7). To ensure that the sum of the least squares of the error is minimized the coefficients shall be evaluated using Eq. (7.8). This equation is derived through analytically evaluating the sum of squares of error using Eq. (7.7) and minimizing it. Using these coefficients, the final response surface for a specific output is constructed.

$$y_n = \beta_0 + \beta_1 * x_{n1} + \beta_2 * x_{n2} + \dots + \beta_9 * x_{n9} + \varepsilon_n \quad (7.6)$$

$$y = X\beta + \varepsilon \quad (7.7)$$

Where, $y = [y_1 \ y_2 \ \dots \ y_{27}]^T$, $X = \begin{matrix} 1 & x_{11} & x_{12} & \dots & x_{19} \\ 1 & x_{21} & x_{22} & \dots & x_{29} \\ \vdots & \vdots & \vdots & \dots & \vdots \\ 1 & x_{271} & x_{272} & \dots & x_{279} \end{matrix}$, $\beta = \begin{matrix} \beta_0 \\ \beta_1 \\ \vdots \\ \beta_9 \end{matrix}$, $\varepsilon = \begin{matrix} \varepsilon_0 \\ \varepsilon_1 \\ \vdots \\ \varepsilon_{27} \end{matrix}$

$$\beta = (X^T X)^{-1} X^T y \quad (7.8)$$

Where, X^T denotes the transpose of X matrix.

7.1.4 R² value determination of the response surfaces

To estimate the goodness of fit R² value will be evaluated for the response surfaces and would need to be greater than 0.85 to be accepted. Typically, the coefficient of determination (R²) is determined using Eq. (7.9). In this equation RSS is the residual sum of squares (Eq. 7.10) and TSS (Eq. 7.11) is the total sum of squares. This is a good measure of how well the outputs are replicated by the response surface model.

$$R^2 = 1 - \frac{RSS}{TSS} \quad (7.9)$$

$$RSS = \sum_{i=1}^n (y_i - \hat{y}_i)^2 \quad (7.10)$$

$$TSS = \sum_{i=1}^n (y_i - \bar{y})^2 \quad (7.11)$$

Where,

- i is the changing index of observations.
- n is the total number of observations.
- \hat{y}_i is the predicted value of output for the i^{th} observation.
- y_i is the actual output value for the i^{th} observation.

- \bar{y} is the mean of the actual outputs.

Though this function of R^2 is good, with the addition of extra variables its value will always increase. So, a second order model may have a higher R^2 than that of a first order model, but that result could be misleading as a second order model has a greater number of terms. To counter this an adjusted formula is used to evaluate R^2 shown in Eq. 7.12.

$$R_{adj}^2 = 1 - \frac{n-1}{n-p}(1 - R^2) \quad (7.12)$$

Where,

- n is the number of observations.
- p is the number of coefficients in the response surface.

This new estimate of R^2 is now model dependent and would depend on the form of the model used to fit the data. This adjusted formula will also ensure that the value of R^2 decreases if unnecessary terms are added.

7.2 Response Surfaces for Stress, Displacement, Natural Frequency and Weight

Using the process described in Section 7.1 response surfaces were developed for the three stress points (SP-VR, SP-HR, SP-AR), Displacement Point (DP) and the first natural frequency described in Chapter 5.

The coefficients of the response surfaces for the weight, three stress points, displacement point and first natural frequency, and their coefficient of determination values are shown in Table 7-2 and Table 7-3. The coefficient notation in Table 7-2 is as per Eq. (7.5).

Table 7-2. Response surface coefficients for different stress points equations.

Coefficients	Stress Results			Displacement at Displacement Point	First Natural Frequency	Weight
	At Horizontal Rib Root	At Vertical Rib Root	At Angular Rib Root			
a ₁	125.218	173.200	227.728	0.154	1133.699	1018.842
a ₂	-88.961	-11.185	-78.996	-0.074	44.460	125.827
a ₃	-226.026	-114.666	-185.443	-0.115	10.587	62.409
a ₄	37.146	-47.816	25.506	0.015	16.338	-2.535
a ₅	21.056	-40.589	15.273	0.020	-5.156	-4.448
a ₆	139.236	68.735	84.892	0.069	-9.567	0.246
a ₇	-1.810	17.067	-2.453	-0.008	11.209	16.464
a ₈	114.869	21.226	80.654	0.060	-6.469	0.000
a ₉	-15.549	55.009	-4.267	-0.007	8.303	-3.685
a ₁₀	-41.968	15.011	-12.524	-0.017	0.043	-0.288

Table 7-3. Adjusted Coefficient of determination values of different stress points equations.

	R² value
Stress Point at Horizontal Rib Root(SP-HR)	0.9428
Stress Point at Vertical Rib Root(SP-VR)	0.8646
Stress Point at Angular Rib Root(SP-AR)	0.9655
Displacement Point	0.9561
First Natural Frequency	0.9848
Weight	0.9985

The results in Table 7-3 shows that two stress equations at points horizontal rib root and angular rib root have a fit with a R² value exceeding 0.9, but the stress equation at vertical rib root has a lower R² value but it is still acceptable as it is above 0.85. The equations for displacement, weight, and first natural frequency also have a fit beyond 0.95, with weight having the highest R² value of all. These R² values are evaluated using the adjusted R² formula so the second order model is taken into consideration in it.

To understand the nature of these equations and to check if the equations make sense, contour plots of these functions are developed for the three variables. The contour plots are displayed in Figure 7-3, Figure 7-4, and Figure 7-5. The constraint equation contours (g₁, g₂, g₃) for stresses, displacement, and first natural frequency from Chapter 5 are used for plotting the contours,

alongside different contours for the objective function i.e. weight ($f(x)$). In the contour plots with varying variables x_1 and x_2 in Figure 7-3, the value of x_3 is set to -1 where it is at its lower bound 45 mm. Similarly, for varying variables x_1 and x_3 in Figure 7-4, the value of x_2 is maintained at -0.5 ie at midpoint (5 mm), and for varying variables x_2 and x_3 in Figure 7-5, the value of x_1 is held at -1 ie at lower bound (2mm). The third parameter's constant value in 2D contour plots is chosen as the closest approximate to where the weight is at its minimum, just before constraints begin to be violated. It is essential to emphasize that the variables employed during contour plotting remain in coded form to ensure uniformity across the graphs.

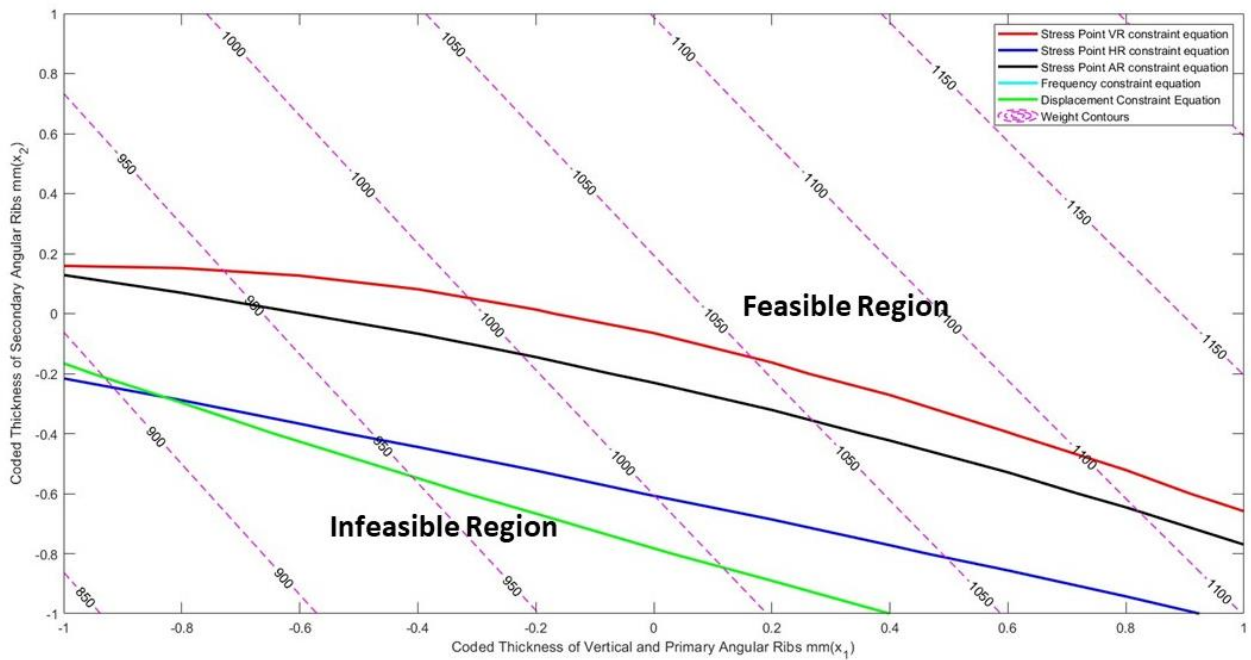


Figure 7-3. Contour Plots for varying x_1 and x_2 .

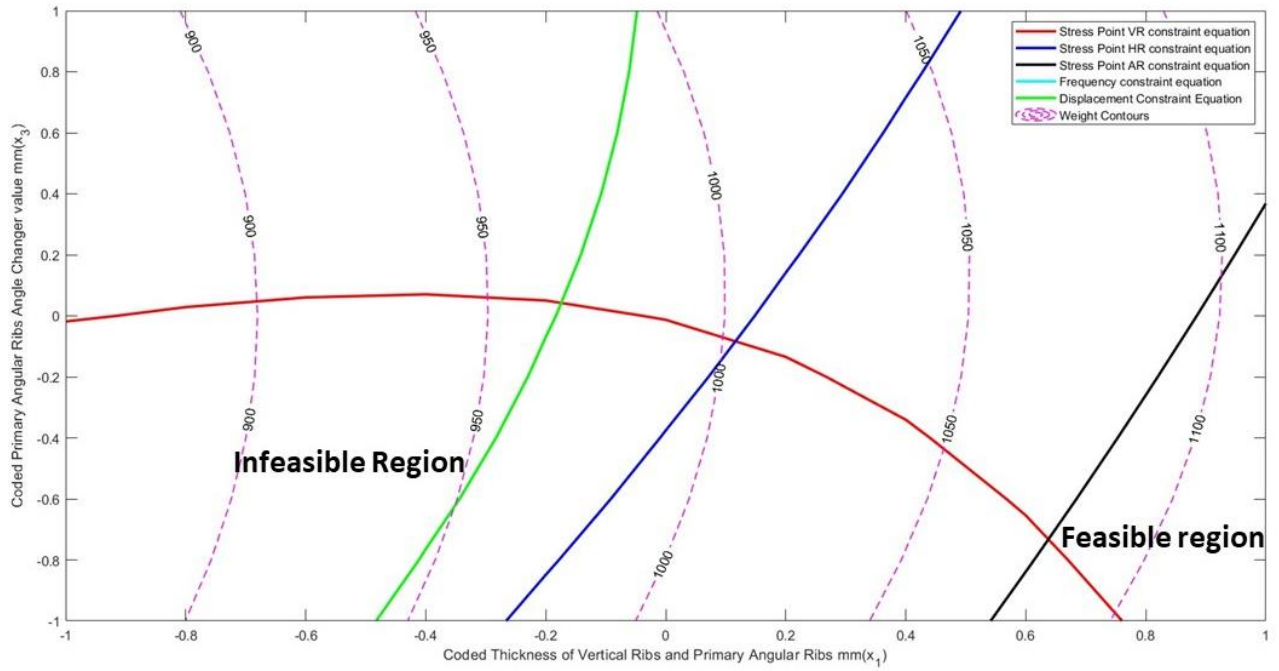


Figure 7-4. Contour plots for varying x_1 and x_3 .

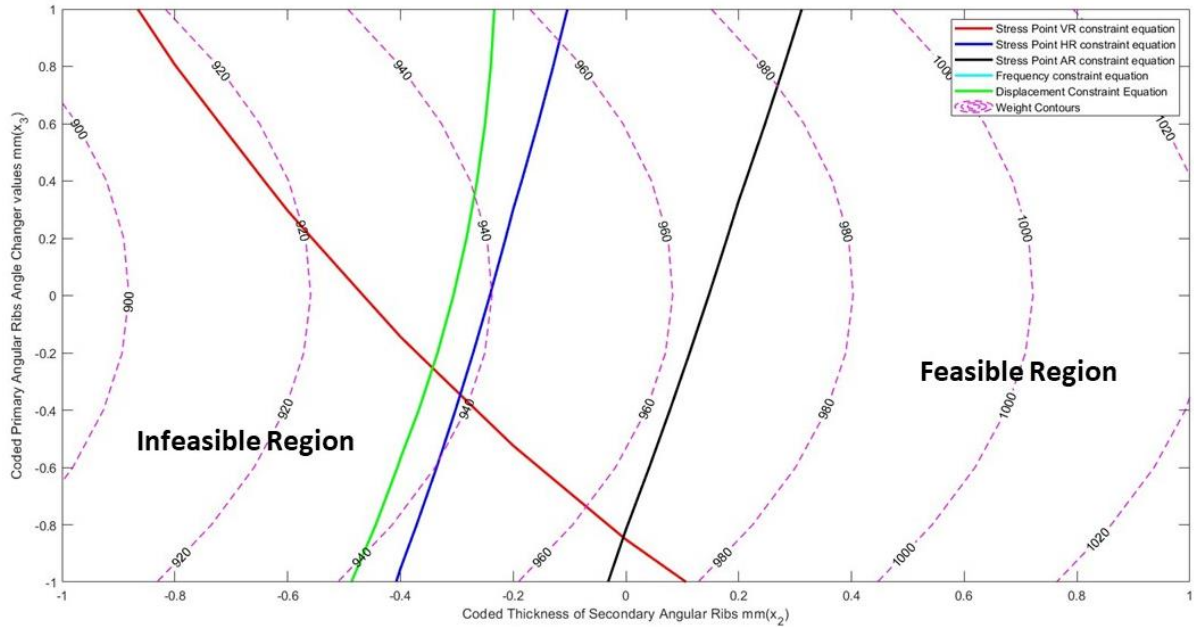


Figure 7-5. Contour plots for varying x_2 and x_3 .

The key characteristics of the contour plots are as follows:

- 1) The contour plots depicting variations in x_1 and x_2 reveal that when both x_1 and x_2 values are below 0 (in decoded form, indicating values below the midpoint), there exists a likelihood that the region is infeasible due to violation of stress point at vertical rib root constraint. It is evident that for any x_2 value below 0, the region becomes feasible only if the x_1 value exceeds 0.6, well beyond the midpoint for x_1 . The identification of infeasible regions at smaller thickness values for x_1 and x_2 is in line with findings from the parameter sensitivity analysis for vertical rib thicknesses and angular rib thicknesses. In those analyses, stresses and displacement are highest at the lowest thickness, gradually decreasing thereafter.
- 2) The frequency equation is absent in all three contour plots. This is logical since the first natural frequency surpasses 1000 Hz for every combination of the three variables. Given that the lower limit is set at 100 Hz, the frequency constraint is consistently satisfied and remains inactive. Consequently, it is permissible to remove this frequency constraint during the optimization process.
- 3) The weight contours exhibit a predictable pattern: an increase in thicknesses x_1 and x_2 results in a higher weight, and when x_3 is altered, the weight experiences a slight decrease until reaching the midpoint and again increases when it reaches near x_3 's extremities. This pattern is illustrated by the subtle curvature observed in the weight contours in both Figure 7-4 and Figure 7-5.
- 4) The stress equations pertaining to stress points at the vertical rib root and angular rib root exhibit a more uniform behavior, in contrast to the distinct behavior observed at the stress point on the horizontal rib root. Additionally, the contour plot in Figure 7-4 indicates the presence of a very limited feasible region. While this might appear unusual, a closer examination in Figure 7-3 reveals that for any value less than 0 for x_2 , the feasible region is inherently small. In the contour plot with varying variables x_1 and x_3 , the value of x_2 was deliberately set as -0.5, thereby justifying the small feasible region depicted in Figure 7-4.

7.3 Fatigue Life Constraint Deletion

In Section 7.1.3, the development of the response surface for frequency revealed that frequencies consistently surpassed the lower frequency limit, rendering it inactive.

Before delving into the development of the response surface for the upright's life before fatigue failure, it is essential to analyze if the fatigue life constraint would be active in the optimization problem. The number of cycles to fatigue failure is calculated for a specific design of the upright. The upright chosen for evaluation represents the minimum weight design, maintaining the final design parameters from Section 6.5 at their minimum values.

The selection of the minimum weight upright for evaluation is based on the observation that stresses and strains are highest when the upright has the lowest thickness. Fatigue life is inversely proportional to stresses and strains, meaning that greater stresses and strains would lead to a reduction in fatigue life. If the fatigue life significantly exceeds the minimum required (i.e., 1500 cycles), the fatigue life constraint remains inactive, and the constraint function is unnecessary.

The variable loading condition for the upright is represented in Section 4.6.1, where there are majorly two loads being applied in a cycle of repeated loading. These two loads are the braking and cornering load, and the acceleration load representing a corner maneuver, the values of these loads are given in Table 7-4.

Table 7-4. Corner Scenario Loads Value.

	Braking and Cornering	Acceleration
Force in x direction(N) - Fx	1443	-802.261
Force in y direction(N) - Fy	1214	473.255
Force in z direction(N) - Fz	1343	0
Moment about x axis(Nmm) - Mx	-341000	0
Moment about y axis(Nmm) - My	366500	6520
Moment about z axis(Nmm) - Mz	-30600	-203774

There are various ways in which multiaxial fatigue failure life could be evaluated, but in this thesis the Multiaxial Brown-Miller Fatigue Failure Criterion is used. This fatigue failure method is one

of the critical plane theories for strain-based fatigue failure and is considered a best practice for low cycle fatigue.

Brown and Miller introduced a multiaxial fatigue criterion, positing that the damage from multiaxial fatigue arises from the interplay between normal and shear components[9]. The critical plane on which fatigue failure occurs is the one where the shear strain attains its highest value, with γ_{max} representing the maximum shear strain amplitude and ε_N denoting the normal strain on the same critical plane.

The Brown-Miller method utilizes the principal strains for the two points in the cycle, and follows a process as described below:

1) Evaluate the maximum values of the three principal strains at the instant of peak load of braking and cornering, and acceleration from Abaqus CAE for the loading described above. Let these three principal strains be $\varepsilon_1, \varepsilon_2, \varepsilon_3$ where ε_1 is the maximum principal strain, ε_2 is the middle principal strain and ε_3 is the minimum principal strain.

2) Evaluate the maximum shear strain range and maximum normal strain range. For each point in the cycle, calculate the shear strain and normal strain values using Equation 7.13 and Equation 7.14, respectively. Subsequently, determine the range of these values for the two points in the cycle.

$$\gamma_{max}(\text{Maximum Shear Strain}) = \varepsilon_1 - \varepsilon_3 \rightarrow \Delta\gamma_{max} \quad 7.13$$

$$\varepsilon_N(\text{Normal Strain}) = \varepsilon_1 + \varepsilon_3 \rightarrow \Delta\varepsilon_N \quad 7.14$$

3) Using the Brown-Miller Fatigue criteria equations, the number of cycles to failure for this cycle range can be evaluated using Eq. 7.15

$$\frac{\Delta\gamma_{max}}{2} + \frac{\Delta\varepsilon_N}{2} = C_1 \frac{\sigma_f'}{E} (2N_f)^b + C_2 \varepsilon_f' (2N_f)^c \quad 7.15$$

Where,

$$C_1 = (1 + \nu_e) + \frac{(1-\nu_e)}{2} \text{ and } C_2 = (1 + \nu_p) + \frac{(1-\nu_p)}{2}$$

During the cycle encompassing braking and cornering loads, as well as acceleration loads, the evaluation of the number of cycles to failure was conducted using the described process, and the corresponding results are presented in Table 7-5. The number of cycles to failure in the braking and cornering driving scenario is 1.33×10^6 cycles, significantly surpassing the minimum requirement of 1500 cycles. For any alternative design, the stresses and strains would be lower, leading to an increase in the number of cycles to failure. Consequently, the number of cycles to failure will always exceed the minimum requirement, rendering the fatigue life constraint inactive. As a result, the constraint equation for fatigue can be disregarded until it is evaluated at the optimal solution, as a result there is no need to assess its response surface.

Table 7-5. Brown Miller fatigue life evaluation for Corner Maneuver cycle.

	Corner Maneuver Cycle	
	Braking and Cornering	Acceleration
Maximum Principal Strain($\mu\epsilon$)	7240	2763
Minimum Principal Strain($\mu\epsilon$)	-5328	-4293
Maximum Shear Strain($\mu\epsilon$)	6284	3528
Normal Strain($\mu\epsilon$)	956	-756
Maximum Shear Strain Range($\mu\epsilon$) - $\Delta\gamma_{\max}$	5512	
Normal Strain Range($\mu\epsilon$) - $\Delta\epsilon_n$	1721	
ϵ_f'	0.327	
σ_f' (MPa)	1294	
b	-0.142	
c	-0.645	
Elastic Poisson's Ratio - ν_e	0.3	
Plastic Poisson's Ratio - ν_p	0.5	
Number of cycles to failure(N_f)	1.33E+06	

Chapter 8 Results after Optimization

This chapter will document the final optimization problem and the results when the optimization problem is run using the SQP algorithm. The results will be compared with the results from the FE model.

8.1 Final Optimization Problem

In chapter 7 it was observed that the natural frequency constraint is always inactive over the range of design variables as the first natural frequency of the upright is always above the minimum target value of 100 Hz. Also, the fatigue life constraint was also determined to be inactive over the range of design variables, as the fatigue life for the minimum weight model was well above the minimum number of cycles of 1500. Thus, these two constraints will be eliminated from the optimization problem formulated in Chapter 5. The final optimization problem is as follows:

$$\min f_{weight}(x_1, x_2, x_3)$$

subject to:

$$g_1(x_1, x_2, x_3) = \frac{f_{stress_point_VR}(x_1, x_2, x_3)}{\sigma_{yield}} - \frac{1}{FOS_{stress}} \leq 0$$

$$g_2(x_1, x_2, x_3) = \frac{f_{stress_point_AR}(x_1, x_2, x_3)}{\sigma_{yield}} - \frac{1}{FOS_{stress}} \leq 0$$

$$g_3(x_1, x_2, x_3) = \frac{f_{stress_point_HR}(x_1, x_2, x_3)}{\sigma_{yield}} - \frac{1}{FOS_{stress}} \leq 0$$

$$g_4(x_1, x_2, x_3) = \frac{f_{deformation}(x_1, x_2, x_3)}{u_{allowed}} - 1 \leq 0$$

$$-1 (2 \text{ mm}) \leq x_1 \leq 1 (8 \text{ mm})$$

$$-1 (2 \text{ mm}) \leq x_2 \leq 1 (10 \text{ mm})$$

$$-1 (45 \text{ mm}) \leq x_3 \leq 1 (80 \text{ mm})$$

Table 8-1. Description of variables of the final optimization problem.

Variable Name	Description
x_1	Thickness of Vertical and Primary Angular Ribs(mm)
x_2	Thickness of Secondary Angular Ribs(mm)
x_3	Primary Angular Ribs Angle Changer(mm)
FOS_{stress}	Factor of Safety for Stress =1.2
$u_{allowed}$	Maximum Allowable Deformation of Upright= 0.3 mm
σ_{yield}	Yield stress of Al- 2024 = 303 MPa
$f_{stress\ point\ VR}(x_1, x_2, x_3)$	Response surface of stress for the three design variables at vertical rib root.
$f_{stress\ point\ AR}(x_1, x_2, x_3)$	Response surface of stress for the three design variables at angular rib root.
$f_{stress\ point\ HR}(x_1, x_2, x_3)$	Response surface of stress for the three design variables at horizontal rib root.
$f_{fundamental\ frequency}(x_1, x_2, x_3)$	Response surface of fundamental frequency for the three design variables.
$f_{deformation}(x_1, x_2, x_3)$	Response surface of deformation for the three design variables at displacement point.
$N_{cycles\ to\ failure}(x_1, x_2, x_3)$	Response surface of number of cycles to fatigue failure for the three design variables.

An important note is that the variables in this optimization formulation are in coded form.

8.2 Optimization Results

The final optimization problem was solved using the 'fmincon' function within MATLAB, a tool designed for solving constrained optimization problems. Within the 'fmincon' function, the SQP algorithm was explicitly selected. Furthermore, rather than relying on the automatic finite difference solver within 'fmincon' to compute gradients, precise analytical gradients were directly provided to the function. The analytical gradients developed from the response surfaces for the objective function and constraints provides an exact representation to the gradient of the response surface, which seeks to reduce the number of function and constraint evaluations.

The results after optimization are presented in Table 8-2. The problem converged in 7 iterations with an overall decrease of weight by 25.3% from the initial assumption of design variables at their upper limit. The objective function history and constraint function history are presented in Figure 8-1 and Figure 8-2 respectively.

Table 8-2. Final Optimization Results

	Final Optimized Results
Thickness of Vertical and Primary Angular Ribs (mm) - (x1)	2
Thickness of Secondary Angular Ribs (mm) - (x2)	7.0084
Angle Changer for Primary Angular Ribs (mm) - (x3)	57.4975
Weight(gms)	905.25

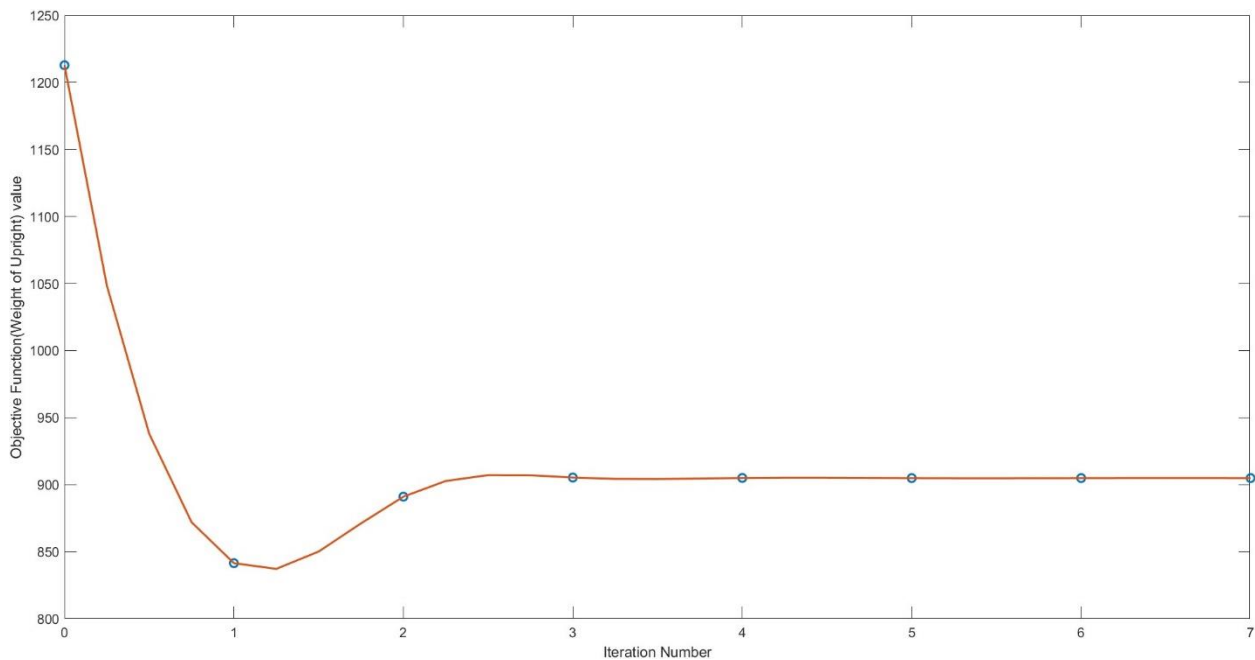


Figure 8-1. Objective function history.

As depicted in Figure 8-1, the weight of the upright initially decreases from the starting value of 1212.8 grams when the design variables are at their upper limits, reaching 840 grams, before rising again to the optimal weight satisfying the constraints at 904.8 grams. This initial decrease to 840 grams and subsequent increase to 904.8 grams can be explained by the direction vector initially guiding the solution towards an infeasibly low weight, before eventually steering the design variables toward a feasible region. This trend is corroborated by Figure 8-2, illustrating the history of constraint values. Initially, the constraints are violated, eventually all constraints are satisfied.

A quicker convergence could have been achieved if the constraint convergence value was set higher than the default value utilized by the 'fmincon' function. The default convergence value of convergence criteria and constraint satisfaction value is 10^{-6} .

The Lagrange multiplier at the final design point is evaluated to examine the sensitivity of the constrained objective function. The Lagrange multiplier for the stress constraint at the Angular Rib Root is the only one available at the final design point. This implies that it is the sole active constraint, as confirmed by the constraint function history in Figure 8-2. The Lagrange multiplier has a value of 86.8151. At a stationary point, the negative gradient direction for the objective function (steepest descent direction) is equal to a linear combination of the gradients of the constraint equations with the Lagrange multipliers as the scalars of the linear combinations of the active constraint gradients[18]. In the case of the current optimization problem, only one constraint is active at the final iteration, so the lagrange multiplier value indicates that an increase of one unit in the constraint value will result in a decrease of 86.815 grams in the objective function at the solution. These values are similar to those observed in the sensitivity analysis, but the values from sensitivity analysis are not exactly representative of the functions in the optimization problem. This is because the sensitivity analysis considered only a single design variable, whereas the actual response surface considered interactions between design variables.

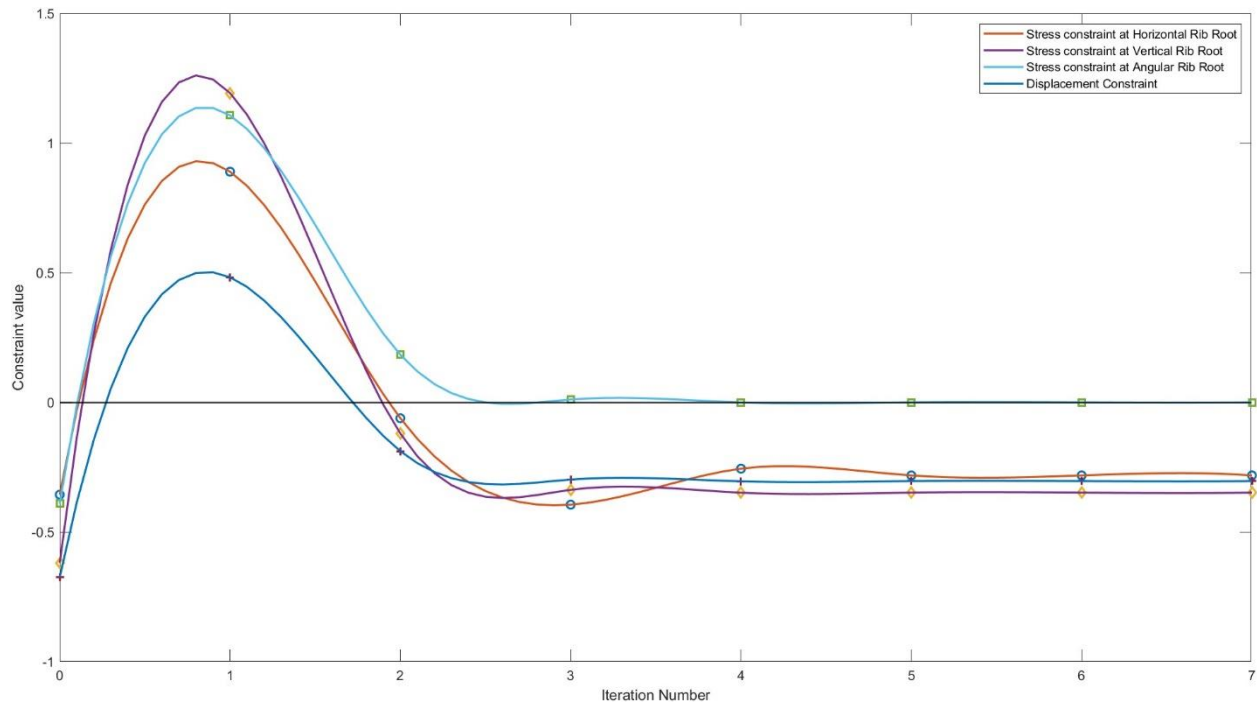


Figure 8-2. Constraint value history.

The results of the outputs from the response surfaces and finite element model for the final design variables evaluated by solving the optimization problem are compared and presented in Table 8-3.

Table 8-3. Comparison of outputs for the final optimized design variables.

	Comparison of outputs for the final optimized design variables.		
	Results from FE model	Results from Response Surface	% error
Displacement(mm)	0.201	0.209	-3.728
Stress at Horizontal Rib Root(MPa)	107.736	146.994	-36.439
Stress at Vertical Rib Root(MPa)	105.451	167.051	-58.416
Stress at Angular Rib Root(MPa)	175.377	252.500	-43.976
Weight of Upright(gms)	908.937	904.888	0.446
Fatigue Life	3.93E+07	-	-
Natural Frequency	1092.400	-	-

The errors in the results exceed 35% for the stresses at all three points, while the errors for the displacement and weight of the upright are below 5%. These deviations align with expectations, the response surface developed for the stress constraints showed a strong correlation with the finite element results for the 27 design variable points used in its creation. Consequently, for points other

than these, the errors could be higher, requiring further development of the stress constraint response surfaces. Future research should be focused on thoroughly analyzing the response surfaces of the constraints and objective function to refine them for more precise results. Additionally, all the outputs fell within the specified constraints in Section 8.1. As detailed in Chapter 7, both fatigue life and natural frequency exceed 1500 cycles and 100 Hz, respectively, as depicted in Table 8-3.

It is evident that the estimates from the response surfaces predict higher stress values compared to the actual values from the finite element model. This suggests an overestimation by the response surfaces, leading to conservative estimations of the design variables. Refining the response surfaces further could lead to optimized design variables with reduced weight. Despite the need for further development of the response surfaces, particularly the stress constraint response surfaces, these methods demonstrate the potential for improved part development through optimization of design variables.

Chapter 9 Summary, Conclusions, and Recommendations

This chapter serves to conclude the thesis with an overall summary of the research, the conclusions obtained from the results, and providing recommendations for future work.

9.1 Summary

The upright plays a critical role in the suspension system as it connects the tire to the suspension spring and manages the steering link. To achieve optimal performance in both suspension and steering, it is essential for the upright to have high stiffness relative to the suspension. Additionally, considering this upright is designed for a Formula SAE car, reducing weight is imperative to decrease the mass of the unsprung part of the vehicle and enable higher speeds and better handling characteristics. This thesis investigates a method of parametric structural optimization using response surfaces to minimize the weight of the upright, while considering constraints such as frequency, stress, displacement, and fatigue. A parametric finite element model of the upright, along with the mathematical formulation of the optimization problem were developed based on the design inputs. Through parameter sensitivity analysis, three design variables were selected from a potential list of five, and response surfaces were created to address the optimization problem using Sequential Quadratic Programming (SQP).

The design inputs play a crucial role in the upright design, acting as the basis for both the design and optimization processes. The Formula SAE upright was created for the SLA double wishbone suspension system of the 2009 Virginia Tech Formula SAE car, as referenced in Borg's thesis [6]. The suspension linkages, including control arms, push rod, and tie rod, are connected to the upright at the outboard points of the suspension system, as detailed in Section 3.1. These points collectively define the working envelope for the upright design. Specific design objectives were established regarding weight, stress, fatigue, displacement, and the first natural frequency, ensuring optimal performance of the Formula SAE car during the event.

A parametric finite element (FE) model was created using the design inputs, which were accessible through scripts developed with the Abaqus scripting library. Static analysis and modal analysis were conducted under a combined load condition of braking and cornering with full load transfer, as well as fatigue analysis under a time-dependent loading condition for a corner on a race circuit. Additionally, a mathematical formulation of the optimization problem for the upright was created.

This problem involves selecting three design variables from the parametric upright finite element model for optimization, a decision informed by parameter sensitivity analysis.

Sensitivity analysis was performed to select three design variables from five potential design variables. The sensitivity of the objective function and the constraints outlined in Chapter 6 was assessed by deriving analytical derivatives of curve fit functions associated with the outputs related to the designated design variables. To streamline the generation of input files and extraction of outputs for parameter sensitivity analysis, a script named *PSanalysis* was created, which was composed of two modules: *input_file_creator* and *odbextraction*.

Finally, response surfaces for the constraints and objective function with respect to the three chosen design variables were created using a three-level full-factorial design to develop a second-order model. The fatigue constraint was eliminated as it was inactive by evaluating the fatigue cycles value to be well above the minimum of 1500 cycles for a minimum weight design where the stresses and strains are highest. The optimization problem with these response surface equations was solved using Sequential Quadratic Programming (SQP), resulting in a 25.3 % weight reduction from the maximum weight design.

9.2 Conclusions

After performing structural optimization of the upright, the optimal design variables were found to be: the thickness of vertical and primary angular ribs $x_1 = 2$ mm, the lower bound on the x_1 design variable, The thickness of secondary angular ribs $x_2 = 6.9$ mm, and the value of the design variable for the angle changer value of primary angular ribs $x_3 = 56.2$ mm. These outcomes were achieved using second-order response surfaces, meeting all constraints with these optimized design variables. The weight of the upright decreased by 25.3% compared to the maximum weight design. From this study, the following insights were gained:

1. The optimization of the upright was executed using a nonlinear programming formulation to state and solve the optimization problem. This approach requires the translation of constraints and objective functions into mathematical expressions, allowing solution by numerical optimization solvers.

2. The parametric modeling of the upright proved to be invaluable. The parametric finite element model enabled geometric adjustments of diverse features within the upright, aiding in the exploration of design features to select the three variables for optimization. This model is now scalable for further exploration and design feature modifications, encompassing not only straight-edged features but also curved features.
3. The simplification of the upright into a simply supported beam within two planes provided a fundamental understanding of the dominant mechanics and their impact on the initial upright design. This approach served as a valuable tool for initiating the development of any parametric design model.
4. The use of scripting was instrumental in altering the design parameters within the finite element model of the upright and extracting results post the completion of finite element analysis runs. This scripting process assisted in parameter selection through extensive study, aiding in the development of response surfaces. Additionally, distinct codes were developed for response surface and optimization, enhancing clarity and error detection within the process. Ideally, unifying parameter sensitivity, response surface development, and optimization would create a comprehensive automated process.
5. The parameter sensitivity analysis conducted in this thesis serves as a foundational platform to assess the impact of different variables on the objective function and constraints. This analysis involved basic curve fits forming a response surface, analytical gradients of the response surface, percent change analysis, and qualitative examination. Moving forward, the interaction of variables with each other must also be considered in the sensitivity analysis before selecting the final design variables for optimization.

9.3 Recommendations

Recommendations include the changes in existing upright design method, scripts for parameter sensitivity analysis, and response surface developments.

9.3.1 Considering the joints characteristics

Joint characteristics have been partially addressed by considering the interactions and omitting tie constraints for surfaces between the joints and the upright, as outlined in Section 4.5. However, there are opportunities for enhancing these characteristics:

1. Enhance the fillets surrounding the joint and upright hole interface and optimize the diameter of the joint cylinders discussed in Section 4. The significance lies in the fillets around the hole reducing stress concentration due to an even and smoother edge where the joint is inserted. Optimizing the diameter of joints such as upper control arms and lower control arms would also be important to avoid these stress concentrations. While this adjustment would not affect the weight, it would impact the stress constraint.
2. Modify joint pins from rigid to deformable. This adjustment allows for a closer examination of joint pin behavior, offering potential avenues for refining the joint design.

9.3.2 Improving the script used for conducting parameter sensitivity analysis and response surface development

The script currently semi-automates the process of input files generation and the extraction of results from the output data base (.odb) file, but there is a room for improvement in these scripts:

1. In the *PSanalysis* script in the input file generation module, the parameter name used for the Abaqus model representing the specific design variable needs to be changed manually once analysis for one variable is completed. Instead of manually changing this variable name, all the design variables to be analyzed can be put in a dictionary data structure in python. Thus, the parameter names can be stored in dictionary as follows:

a. *Parameter_names*= {
 "1": "*Vertical_Rib_Thickness*",
 "2": "*Horizontal_Rib_Thickness*",

"3": "Secondary_Angular_Rib_Angle"

}

- b. These parameter names can be then accessed and automated using a for loop as follows:

For i=1:number of parameters

Parameter_to_be_analyzed=Parameter_names.get(i)

Conduct the analysis for this value of the current parameter

End

2. The existing scripts lack a way to identify/handle errors after executing a job, posing a potential problem for subsequent file runs. A recommended approach could be to employ Python's built-in OS commands to identify any lock files (.LCK). If a .LCK file is found, the CSV outputs will be marked as N/A, and the .LCK file will be removed to facilitate the execution of the next job analysis.

9.3.3 Testing more design variables in the upright

This thesis focused on three design variables, comprising two sizing variables and one shape design variable. Subsequent research could explore the impact of additional shape design variables on the objective function and constraints. Rather than employing exclusively straight-edged ribs, future investigations could introduce additional rib structures as design variables. Additionally, upcoming studies might examine and compare triangular pocket shapes with the trapezoidal pocket shapes employed in this thesis.

Furthermore, a more thorough examination of design variables in various planes of the part could be conducted, testing the taper in the YZ plane revealed minimal impact. Additionally, frequent errors occurred during part regeneration after modifying design variables, leading to the exclusion of this variable from the analysis. Subsequent research could delve into investigating the root cause of this issue and exploring additional design variables.

9.3.4 Response Surface Development

The response surfaces developed in this study were used to demonstrate that a parametric finite element model of the upright could be optimized. In the future, these response surfaces need to be more thoroughly analyzed and continuously refined to get a better representation of the objective function and constraints. There are various ways in which this could be achieved:

- 1) Currently only the output values have been used to construct the response surfaces, but sensitivity information can be used to develop better response surfaces using interpolation function.
- 2) Statistical analysis such as ANOVA needs to be conducted to test the significance of single factor, two factor, and three factor interactions to understand the impact of the variables on the outputs and each other.
- 3) Some variables in the optimization problem could be defined differently by a change of variable to reduce the nonlinearity of the final response surface equations for stresses and displacement, possibly rendering the constraint equations as linear. For stresses and displacement in beams certain thickness variables in the cross-section could be explored using ‘Reciprocal or Exponential Approximation’ based on respective functional representation. These approximation techniques could simplify the functions and may result in reducing the error between results from the response surface and finite element model. A review on some of these methods is presented in Vanderplaats et al[17].

Further research on the upright design and optimization should be prioritized in the following order:

- 1) Improving the joint characteristics of the finite element model.
- 2) Experimenting with additional design variables in the upright.
- 3) Developing more effective response surfaces.
- 4) Improving the script utilized for parameter sensitivity analysis and response surface development.

References

- [1] Metar, M., 2021, “Structural Analysis of Double-Wishbone Suspension System,” *Int J Res Appl Sci Eng Technol*, **9**(12), pp. 1681–1685.
- [2] Reddy, K. V., Kodati, M., Chatra, K., and Bandyopadhyay, S., 2016, “A comprehensive kinematic analysis of the double wishbone and Macpherson strut suspension systems,” *Mechanism and Machine Theory*, **105**, pp. 441–470.
- [3] Mesicek, J., Richtar, M., Petru, J., Pagac, M., and Kutiova, K., 2018, “Complex View to Racing Car Upright Design and Manufacturing,” *Manufacturing Technology*, **18**(3), pp. 449–456.
- [4] Vanderplaats, G. N., 1982, “Structural Optimization-Past, Present, and Future,” *AIAA Journal*, **20**(7), pp. 992–1000.
- [5] Mrzyglod, M., and Zielinski, A. P., 2007, “Parametric Structural Optimization with Respect to the Multiaxial High-Cycle Fatigue Criterion,” *Structural and Multidisciplinary Optimization*, **33**(2), pp. 161–171.
- [6] Borg, L. T., 2009, *An Approach to Using Finite Element Models to Predict Suspension Member Loads in a Formula SAE Vehicle*.
- [7] “Friction- Friction Coefficients and Calculator,” [Online]. Available: https://www.engineeringtoolbox.com/friction-coefficients-d_778.html.
- [8] *Abaqus Scripting Reference Guide ABAQUS 6.14*.
- [9] Brown, M. W., and Miller, K. J., *A THEORY FOR FATIGUE FAILURE UNDER MULTIAXIAL STRESS-STRAIN CONDITIONS*.
- [10] Milliken, W., Milliken, D., *Race Car Vehicle Dynamics*, Society of Automotive Engineers, Inc., 1995
- [11] “fmincon” [Online]. Available: <https://www.mathworks.com/help/optim/ug/fmincon.html>
- [12] “contour” [Online]. Available: <https://www.mathworks.com/help/matlab/ref/contour.html>
- [13] “MATWEB: Material Property Data”[Online].Available: <https://matweb.com/>

- [14] Bhardwaj, S., Ashok, B., Lath, U., and Agarwal, A., 2018, "Design and Optimization of Steering Upright to Reduce the Weight Using FEA," *SAE Technical Papers*, SAE International.
- [15] Schmit, L. A., "Structural Synthesis 1959-1969: A Decade of Progress," *Recent Advances in Matrix Methods of Structural Analysis and Design*, University of Alabama Press.
- [16] Fidan, I., McGough, A. and Foote, J. (2004) 'The development stages of rear upright for Formula Car', *Innovations in Engineering Education: Mechanical Engineering Education, Mechanical Engineering/Mechanical Engineering Technology Department Heads* [Preprint]. doi:10.1115/imece2004-60286.
- [17] Vanderplaats, G. N., Thomas, H. L., & Shyy, Y. K. (1991). 'A review of approximation concepts for structural synthesis'. *Computing Systems in Engineering*, 2(1), pp 17-25.
- [18] Arora, *Introduction to Optimum Design*. Academic Press, 2024.

Appendix

A) Mesh convergence study

The mesh convergence study for fundamental natural frequency, stress and displacement is given below:

1. Quantitative Analysis

Table A-1. Quantitative analysis results of fundamental natural frequency

Sr. No	Mesh Size(mm)	Number of Elements	Fundamental Natural Frequency(Hz)	% Error
1	0	0	0	
2	1.9	415210	1344	100
3	1.75	502850	1344.8	0.059
4	1.6	642352	1345.5	0.052

Table A-2. Quantitative analysis results of stress at vertical rib root

Sr. No	Mesh Size(mm)	Number of Elements	Stress Point Root Pocket 2(MPa)	% Error
1	0	0	0	
2	1.9	415210	292.284	100
3	1.75	502850	299.859	2.526
4	1.6	642352	296.473	1.142

Table A-3. Quantitative analysis results of stress at horizontal rib root

Sr. No	Mesh Size(mm)	Number of Elements	Stress Point Root Pocket 3(MPa)	% Error
1	0	0	0	
2	1.9	415210	233.511	100
3	1.75	502850	228.032	2.4
4	1.6	642352	227.931	0.04

Table A-4. Quantitative analysis results of displacement

Sr. No	Mesh Size(mm)	Number of Elements	Displacement(mm)	% Error
1	0	0	0	
2	1.9	415210	0.390754	100
3	1.75	502850	0.390828	0.019
4	1.6	642352	0.3915	0.172

2. Qualitative Analysis

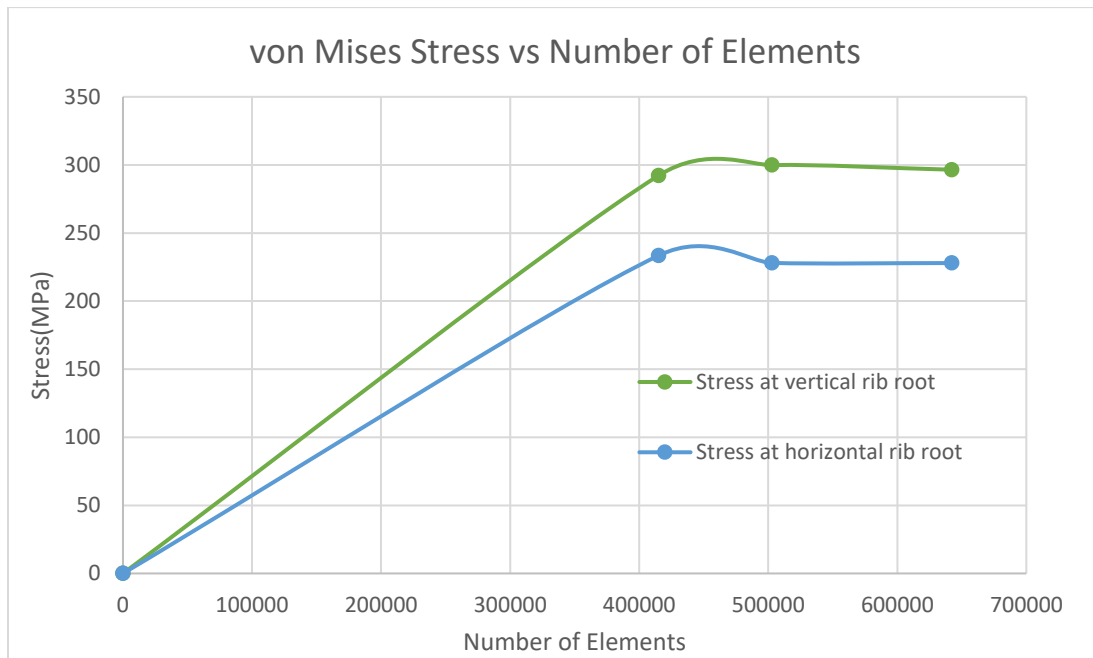


Figure A-1. Qualitative analysis results of stresses

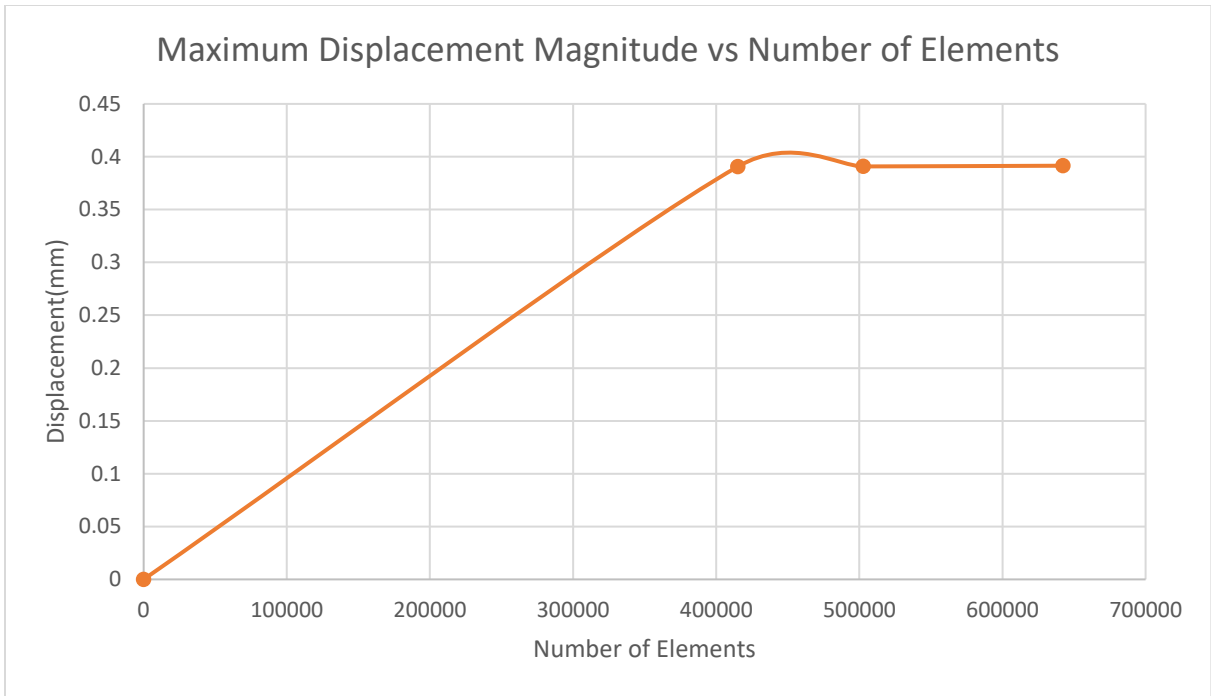


Figure A-2. Qualitative analysis results of displacements.

